GLOBAL CONVERGENCE AND QUASI REVERSIBILITY FOR COEFFICIENT INVERSE PROBLEMS

by

Andrey Kuzhuget

A dissertation submitted to the faculty of
the University of North Carolina at Charlotte
in partial fulfillment of the requirements
for the degree of Doctor of Philosophy in
Applied Mathematics

Charlotte

2011

Approved by:

Dr. Stanislav Molchanov

Dr. Joel Avrin

Dr. Boris Vainberg

Dr. Arindam Mukherjee

ABSTRACT

ANDREY KUZHUGET. Global convergence and quasi reversibility for coefficient inverse problems. (Under the direction of DR. MICHAEL KLIBANOV)

An inverse problem of the determination of an initial condition in a hyperbolic equation from the lateral Cauchy data is considered. This problem has applications to the thermoacoustic tomography, as well as to linearized coefficient inverse problems of acoustics and electromagnetics. A new version of the quasi-reversibility method is described. This version requires a new Lipschitz stability estimate, which is obtained via the Carleman estimate. Numerical results are presented.

A new globally convergent numerical method is developed for a 1-D and 2-D coefficient inverse problem for a hyperbolic partial differential equation (PDE). The back reflected data are used. A version of the quasi-reversibility method is proposed. A global convergence theorem is proven via a Carleman estimate. The results of numerical experiments are presented.

ACKNOWLEDGMENTS

In my way of pursuing this Ph.D. degree in the past years, so many people contributed a lot, in many different ways, to make my success as a part of their own. I am so excited of this moment, the moment I could publicly express my thanks to all of them.

First of all, to my advisor Dr Michael Klibanov, who taught me not only lessons of mathematics but also lessons of life, then to the whole Department of Math of UNCC, including all of the graduate students. And also i would like to thank my parents, for their support and understanding of my desire to study and self improvement.

Research of chapter 2 resulted as [35] and was supported by the U.S. Army Research Laboratory and U.S. Army Research Office under contract/grant number W911NF-05-1-0378.

Research of chapter 3 resulted as [48] and was supported by the U.S. Army Research Laboratory and U.S. Army Research Office under grant number W911NF-05-1-0378. The authors of [48] are grateful to Professor Paul Sacks (Iowa State University) for kindly providing his data for blind testing.

Research of chapter 4 resulted as [49] and was supported by the U.S. Army Research Laboratory and U.S. Army Research Office under grants number W911NF-08-1-0470 and W911NF-09-1–0409.

TABLE OF CONTENTS

LIST OF FIGURES

LIST OF TABLES

CHAPTER 1: INTRODUCTION

1.1 Quasi Reversibility Method and Thermoacoustic Computed Tomography

The Quasi Reversibility Method (QRM) was introduced in the book [20] as an approach for the numerical solution of ill-posed boundary value problems for partial differential equations. The QRM amounts to the minimization of the Tikhonov functional for an Ill-Posed boundary value problem for a Partial Differential Equation (PDE). In such a problem usually one has both Dirichlet and Neumann boundary conditions at a part of the boundary and no conditions at the rest of the boundary. This works for the case of a second order elliptic PDE. In the time dependent case (i.e. parabolic and hyperbolic cases) Dirichlet and Neumann boundary conditions can be assigned at a part of the lateral boundary of the time cylinder and no initial conditions would be given. As a result of the QRM one obtains a weak solution of a fourth order PDE. To practically get this solution we use the Finite Difference Method. Convergence of the QRM is proved via Carleman estimates. It should be pointed out that while the QRM was extensively used in above references for solving linear problems, it was not used before for solving nonlinear problems, such as, e.g. Coefficient Inverse Problems. So, our works in chapters 3, 4 are the first ones in this direction. QRM consists in replacing the ill-posed second order problem with a well-posed fourth order problem, and was previously applied to ill-posed Cauchy problems for elliptic [2,3,10,20], parabolic [9,20] and hyperbolic [13] equations as well as coefficient inverse problems [8,12]. In chapter 2 we present a new version of QRM applied to ill-posed Cauchy problem for a hyperbolic equation, which has application in acoustics, electromagnetics and thermoacoustic tomography.

Many practical problems are concerned with determining the strength and location of sources of disturbances in a medium, when only boundary measurements are available. Examples include medical imaging, seismic observations, geodynamics, or tracing electromagnetic pulses. If the sources can be temporally localized, this problem is equivalent to the determination of the initial conditions in a wave equation. One such application is the medical imaging method of Thermoacoustic Computed Tomography (TCT), where electromagnetic radiation induces a pressure wave in a sample, which is proportional to the varying energy absorption by different types of tissue. From time dependent measurements, one wishes to calculate the absorption coefficient and from this, the tissue distribution (e.g., healthy and cancerous tissue). If it would be possible to completely characterize a final state, then the time reversibility of the wave equation can be employed to calculate the wave field backwards in time to the moment of interest. However, in practical applications, it is usually either not possible to measure a wave field in a complete region, or dissipative terms break the time invariance of the equation. In both cases, the problem is then the reconstruction of initial conditions from boundary measurements only. The problem is known to be ill-posed in general, but under certain conditions observability estimates can be proved, which warrant a unique and stable solution. An additional difficulty appears when the wave propagates in a medium with spatially varying wave speed, as for instance in bone and soft tissue or water. In this case, the wave propagation will no longer happen along straight lines, a fact which increases the difficulties in proving the stability estimates as well as in computing the numerical solution. Previous works on the numerical determination of the initial condition in a hyperbolic equation from lateral Cauchy data were [7] and [13], which only applied to constant coefficients in the principal part of the operator. The variable coefficient case was considered in [14], but no numerical studies were done. For numerical approaches to TCT in a homogeneous medium, see e.g. [5], [47], [7] and [4].

1.2 The Coefficient Inverse Problem in 1D

In chapter 3 a new globally convergent numerical method for a one-dimensional Coefficient Inverse Problem (CIP) for a hyperbolic PDE is presented. We modify here the idea of [27] for our case (also, see follow up publications [28, 29, 31]). This CIP has applications in acoustics and electromagnetics. More specifically, we consider here an application to the problem of imaging of antipersonnel plastic land mines. It is well known that plastic land mines are hard to detect by ground penetrating radars because they do not have a significant metal component in them. So, our idea is to image the spatial distribution of the relative dielectric constant in them. A similar idea was carried out in [39] by the globally convergent numerical method of the first generation, the so-called convexification algorithm [14]. However, [27] represents the second generation of such methods.

The 1-D problem is considered here only as a preliminary step before applying similar ideas to 2-D and 3-D cases. In other words, the goal of the chapter 3 is to develop a methodology for our future studies of 2-D and 3-D problems. Similar 1-D CIPs were studied numerically quite extensively in the past, see, e.g. [36] and references cited there. Those publications were working either in time or in frequency domain. The latter is generated by the Fourier transform of the time domain equation. Since our ultimate goal is to work in several dimensions, then following [27], we work in the "pseudo frequency" domain generated by the Laplace transform of the 1-D hyperbolic equation. In our definition "global convergence" entails: (1) a rigorous convergence analysis that does not depend on the quality of an initial guess for the solution, and (2) numerical simulations confirming the advertised convergence property.

The main difficulties in numerical studies of CIPs are linked to the fact that CIPs are both nonlinear and ill-posed. A conventional way to numerically solve a CIP is via the minimization of a least squares objective functional. However, it is well

known that the phenomenon of multiple local minima and ravines of these functionals represents the major obstacle in this approach. This phenomenon naturally causes local convergence of resulting numerical methods. Following [27], the method of the current work is not using those functionals and relies on a structure of the underlying differential operator instead. First, we reduce the CIP to a boundary value problem for a nonlinear integral differential equation. The numerical solution of this equation is the main difficulty here. The major difference between both our method and the one of [27] is the approach to the solution of the latter equation. While [27] approximates the solution of this equation via the solution of a series of Dirichlet boundary value problems for elliptic PDEs, we use over-determined boundary conditions for these problems, thus, solving them via the Quasi-Reversibility Method (QRM) [14, 20]. The QRM is well suitable to handle over-determined boundary conditions for PDEs [8, 10, 14, 20, 35]. As to CIPs, in the past QRM was used for numerical solutions of 1-D CIPs for parabolic equations via locally convergent numerical methods [8, 33, 37]. However, it was not used for the global convergence.

The reason why we use over-determined boundary conditions is twofold. First, our numerical experience has shown that we cannot get good results without this over-determination. This is because, the one-dimensional case is less informative compared with 2-D and 3-D cases of [27–29, 31]. Second, we want to work only with the back-reflected data in our future 2-D and 3-D cases, and in this case one has Dirichlet and Neumann boundary conditions at the back reflected side. We prove a global convergence theorem for our method. Instead of the Schauder theorem, which was used for this purpose in [27–29, 31], we use Carleman estimate. Since Carleman estimates enable to obtain upper bounds for corresponding constants, we obtain explicit estimates for all constants involved in the convergence analysis. At the same time obtaining an estimate for a certain constant in the Schauder theorem is a quite complicated problem, which was not addressed in [27–29, 31].

1.3 The Coefficient Inverse Problem in 2D

In chapter 4 we extend the recently developed globally convergent numerical method of [27, 31, 40, 41] for a hyperbolic CIP for the case of backscattering data. Note that only the case of the data given at the entire boundary was considered [27, 31, 40, 41]. Just as before, we work with a CIP with the data resulting from a single measurement, i.e. either a single position of the point source or a single direction of the initializing plane wave. Since we have both Dirichlet and Neumann boundary conditions on the backscattering part of the boundary of the domain of interest, we use the Quasi-Reversibility Method (QRM) [20], which was not a part of [27, 31, 40, 41]. We refer to, e.g. [2–4, 14, 35] for some recent publications on the QRM.

The main new analytical result here is the proof of the global convergence theorem in the case when the QRM is used. To do so, we first obtain an analog of *a priori* upper estimate of the QRM solution using a Carleman estimate. Next, the global convergence result is established. Applications of our CIP are in imaging of dielectric constants of explosives, since their dielectric constants are much higher than those of regular materials, see http://www.clippercontrols.com/info/. The target application of this publication is in imaging of plastic land mines. We also mention an important application of CIPs with backscattering data to geophysics.

An independent verification of the technique of [27] was carried out in [44] for the case of experimental data. Computations were conducted for *blind* data only. Comparison of computed refractive indices of dielectric abnormalities with *a posteriori* measured ones has revealed an excellent accuracy of computational results. Because of this accuracy, it was concluded in [44] that the technique of [27, 31] "is completely validated now", regardless on a certain approximation, which is a part of that technique. This conclusion justifies the same approximation of the chapter 4. In our opinion, some approximation like this one are inevitable for such challenging

problems as CIPs are. Indeed, CIPs are both nonlinear and ill-posed.

That approximation is due to the truncation of certain Volterra-like integrals at a high value $\overline{s} > 1$ of the parameter $s > 0$ of the Laplace transform of the original hyperbolic PDE. We call s *pseudo frequency*. This truncation is similar with the truncation of high frequencies. As an analogy, we point out that such truncations are routinely done in engineering without any proofs of convergence, and still those things usually work quite well in practice. The meaning of this approximation was discussed in detail in subsection 3.3 of [44] and in subsection 6.3 of [31], where a new mathematical model was proposed. In particular, it was shown in these references that this model has the same nature as the truncation of divergent asymptotic series in the classical Real Analysis.

We use a two-stage numerical procedure here, the framework of which was developed in [31, 40, 41]. Indeed, because of the above approximation, the global convergence theorem only guarantees that the resulting solution is sufficiently close to the correct one. However, it does not guarantee that this solution can be made infinitely close to the correct one, because the truncation pseudo frequency $\overline{s}$ cannot be made infinitely large in practical computations. On the other hand, the availability of a good first approximation for the correct solution is the *key component* of any locally convergent algorithm. Therefore, our procedure works as follows. On the first stage the globally convergent numerical method provides a good first approximation for the solution. On the second stage this approximation is refined via a locally convergent modified gradient method, which uses the solution of the first stage as its starting point.

More precisely, our numerical experience shows that the first stage provides good locations of mine-like targets. The subsequent application of the second stage, which is a modified gradient method in our case, provides accurate values of the unknown coefficient within those targets. At the same time, it is worthy to note that the modified gradient method being applied without the first stage results in quite

inaccurate images (not shown here), even if the background value of the unknown coefficient is taken as the starting point, see subsection 8.4 of [44] for a similar observation.

CHAPTER 2: QUASI REVERSIBILITY METHOD FOR A HYPERBOLIC PDE

2.1 Problem Formulation

In this chapter we propose a new version of the QRM for the inverse problem of the determination of an initial condition in a hyperbolic equation from the lateral Cauchy data. We discuss applications of this inverse problem to thermoacoustic tomography, as well as to linearized coefficient inverse problems of acoustics and electromagnetics. Using the Carleman estimate, we prove convergence of our version of the QRM. We also present numerical results. In particular, we show that this version of the QRM enables one to image $\delta-$ like functions, i.e., narrow high peaks.

Let $\Omega \subset \mathbb{R}^n$ be a convex domain with a piecewise smooth boundary $\partial\Omega$ and $2R$ be the diameter of $\Omega, 2R = \max_{x,y\in\Omega} |x-y|$. Let $T = const. > R$. Denote $Q_T = \Omega \times (0,T)$. Consider the elliptic operator $L(x,t)$ of the form

$$L(x,t)u = \Delta u + \sum_{j=1}^{n} b_j(x,t)\, u_j + b_0(x,t)\, u_t + c(x,t)\, u,$$

where $u_j := \partial_{x_j} u$. We assume that all coefficients of the operator L belong to $C\left(\overline{Q}_T\right)$. Let the function $u \in H^2(Q_T)$ be a solution of the hyperbolic equation in the cylinder Q_T,

$$u_{tt} = L(x,t)u + F(x,t) \text{ in } Q_T, \tag{2.1}$$

$F \in L_2(Q_T)$ with initial conditions

$$u(x,0) = \varphi(x), u_t(x,0) = \psi(x), \varphi \in H^1(\Omega), \psi \in L_2(\Omega). \tag{2.2}$$

We consider the following

Inverse Problem 1. Let one of functions φ or ψ be known and another one be unknown. Determine that unknown function assuming that the following functions f and g are given

$$u\mid_{S_T}= f(x,t),\ \frac{\partial u}{\partial \nu}\mid_{S_T}= g(x,t),\ S_T=\partial\Omega\times(0,T), \tag{2.3}$$

where ν is the unit outward normal vector at $\partial\Omega$. We call the problem of the determination of the function φ the "$\varphi-$problem" and the problem of the determination of the function ψ the "$\psi-$problem".

In principle, in the case $T>2R$ one should not assume that one of functions φ or ψ is known. This is because for $T>2R$ the following Lipschitz stability estimate takes place (see [4, 11, 12] and Theorem 2.4.1 in [14])

$$\|u\|_{H^1(Q_T)}\leq C\left(\|f\|_{H^1(S_T)}+\|g\|_{L_2(S_T)}+\|F\|_{L_2(Q_T)}\right). \tag{2.4}$$

Here and below C denotes different positive constants depending only on Ω, T and $C\left(\overline{Q}_T\right)$ norms of coefficients of the operator L. However, since numerical studies for the case of the finite domain were conducted in previous publications [4, 13], we are interested here in solving the Inverse Problem 1 in an *unbounded* domain, which was not done before. This leads us to the case $T>R$. Namely, we want to solve an analogue of the Inverse Problem 1 in a quadrant, assuming that the lateral Cauchy data are given only on parts of two coordinate axis. We are motivated by the publication [15], where the Lipschitz stability was proven for an analogue of Inverse Problem 1 for the case of either a quadrant in $\mathbb{R}^2$ or a an octant in $\mathbb{R}^3$, assuming that one of initial conditions (2.2) is zero, and the second one has a finite support.

We now specify conditions of our numerical study. Suppose that equation (2.1) is homogeneous with $F(x,t)\equiv 0$ and it is satisfied in $D_T^3=\mathbb{R}^2\times(0,T)$. Consider

the quadrant $QU = \{x_1, x_2 > 0\}$. And also consider the square $SQ \subset QU$,

$$SQ(a) = \{0 < x_1, x_2 < a\}.$$

Suppose that

$$\varphi(x) = \psi(x) = 0 \text{ outside of } SQ(a). \tag{2.5}$$

Then the energy estimate implies that

$$u(x,t) = 0, \forall (x,t) \in \{x \mid x \in QU, dist(x, SQ(a)) > T\} \times (0,T). \tag{2.6}$$

Denote

$$\Gamma_{1T} = \{x_1 \in (0, a+T), x_2 = 0\} \times (0,T),$$

$$\Gamma_{2T} = \{x_2 \in (0, a+T), x_1 = 0\} \times (0,T),$$

$$\Gamma_{3T} = \{x_1 = a+T, x_2 \in (0, a+T)\} \times (0,T),$$

$$\Gamma_{4T} = \{x_2 = a+T, x_1 \in (0, a+T)\} \times (0,T),$$

see Figure 2.1. Then by (2.6)

$$u = \frac{\partial u}{\partial \nu} = 0 \text{ on } \Gamma_{3T} \cup \Gamma_{4T}. \tag{2.7}$$

Hence, we focus our numerical study on

Inverse Problem 2. Let equation (2.1) be satisfied in D_T^3 with initial conditions (2.2) satisfying (2.4). In this case $\Omega := SQ(a+T)$ .Suppose that one of these initial conditions is zero. Determine the second initial condition, assuming that functions f and g are known, where

$$u\mid_{\Gamma_{1T} \cup \Gamma_{2T}} = f(x,t), \ \frac{\partial u}{\partial \nu}\mid_{\Gamma_{1T} \cup \Gamma_{2T}} = g(x,t). \tag{2.8}$$

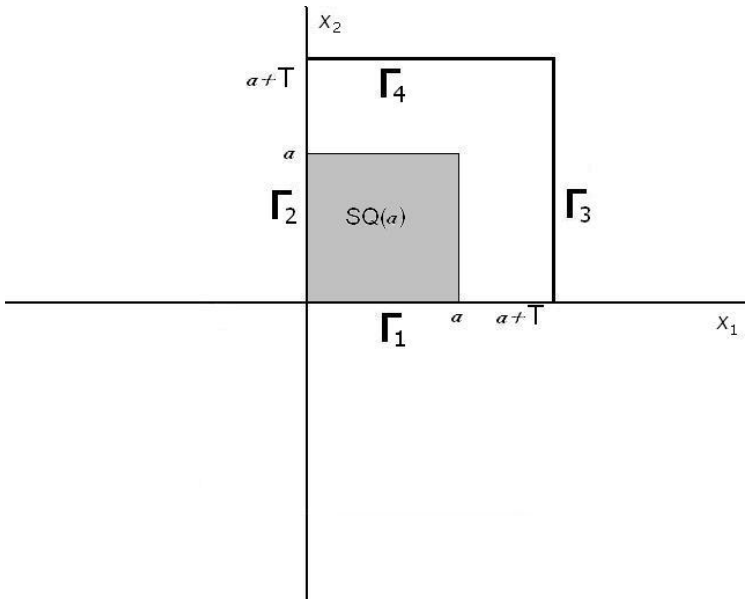

Figure 2.1: Geometry for the Inverse problem 2.

Suppose for a moment that only the function $f(x,t)$ is given. Then one can solve the boundary value problem for equation (2.1) with $F \equiv 0$ outside of the square $SQ(a+T)$ with the following initial and boundary data

$$u(x,0) = u_t(x,0) = 0, x \in R^2 \diagdown SQ(a+T),$$

$$u\mid_{\Gamma_{1T} \cup \Gamma_{2T}} = f(x,t), u\mid_{\Gamma_{3T} \cup \Gamma_{4T}} = 0.$$

This gives one in a *stable way* the normal derivative $g(x,t)$ on $\Gamma_{1T} \cup \Gamma_{2T}$. Thus, we arrive at Inverse Problem 2. It was proven in [15] that if

$$T > \frac{a\sqrt{2}}{2-\sqrt{2}} \tag{2.9}$$

and one of functions φ or ψ equals zero, then the following Lipschitz stability estimate is valid

$$\|u\|_{H^1(G_T)} \leq C\left(\|f\|_{H^1(\Gamma_T)} + \|g\|_{L_2(\Gamma_T)}\right), \tag{2.10}$$

where $\Gamma_T = \Gamma_{1T} \cup \Gamma_{2T}$ and $\|f\|_{H^1(\Gamma_T)} = \|f\|_{H^1(\Gamma_{1T})} + \|f\|_{H^1(\Gamma_{2T})}$. The estimate (2.10) implies a similar estimate for the unknown initial condition [15]. The knowledge of the fact that one of initial conditions was zero was used in [15] for either odd or even extension with respect to t of the function $u(x,t)$ in $\{t < 0\}$, depending on which of initial conditions was assumed to be unknown. The proof of [15] is based on the Carleman estimate. The method of Carleman estimates was first applied in [12] to obtain the Lipschitz stability for the hyperbolic problem with the lateral Cauchy data, also see [11] and Theorem 2.4.1 in [14]. Prior to [12] the Lipschitz stability for the hyperbolic problem with the lateral Cauchy data was obtained in [21] by the method of multipliers, but only for the case when lower order terms in (2.1) are absent. The use of the Carleman estimate enables one to incorporate lower order terms and also to extend to the case of hyperbolic inequalities. Recently the method of [11, 12, 14] was extended to hyperbolic equations with the non-constant principal part, see, e.g. [23–25]. The method of multipliers was recently extended to the case of non-zero lower order terms in Theorem 3.5 of the book [6].

The problems considered above were previously studied and solved numerically in [4, 7, 13, 16]. The work [7] was the first one, where the problem of thermoacoustic tomography was formulated and solved numerically as Inverse Problem 1, i.e., as the hyperbolic Cauchy problem with the lateral data. The QRM for the latter problem was used in [4]. The QRM was first proposed in the book [20] for a variety of ill-posed boundary value problems. Its convergence rates were established in [10, 12] for the cases of Laplace and hyperbolic equations respectively and in section 2.5 of [14] for elliptic, parabolic and hyperbolic equations. In particular, it was shown in [14] that one can work with weak H^2 solutions of QRM instead of strong H^4 solutions of the original book [20]. Also, see [2, 3] for the recent results for the QRM for the elliptic case and [8] for the application of the QRM to linearized coefficient inverse problems for parabolic equations. The main tool of works [4, 8, 10, 12, 14] is the tool of Carleman

estimates.

There are three main differences between the current chapter and the previous works on the QRM for hyperbolic equations. First, we take into account boundary conditions via including them in the Tikhonov regularizing functional J_ε. Unlike this, boundary conditions were made zero in [4] via subtracting off a corresponding function, and they were treated via integration by parts in [13]. Second, we incorporate in J_ε a penalizing term, which reflects our knowledge of one of initial conditions. We show numerically that without this term we cannot image well maximal values of the unknown initial condition inside of narrow peaks. On the other hand, since cancerous tumors can be modeled as narrow peaks, it is interesting to image those peaks in the application to thermoacoustic tomography considered below. These first two ideas for J_ε are taken from [16]. Mainly because of the second difference we cannot apply previously derived convergence results and thus, need to prove convergence of our new version of the QRM. In particular, we need to prove a new Lipschitz stability estimate (Theorem 2.1). Finally, the third difference is that while H^2 finite elements were used in [4, 13], we use finite differences now. Note that while smooth slowly varying functions were reconstructed numerically in [4,13], our numerical experiments reconstruct both those functions and $\delta-$like functions. $\delta-$like functions were also reconstructed in [16] for the Inverse Problem 2. However, the numerical technique of [16] is different from one of the current chapter. The method of [7,16] is based on the representation of the function $u(x,t)$ via truncated Fourier series and minimization of the resulting residual least squares functional.

2.2 Applications

In this section we discuss two applications of above inverse problems

2.2.1 Thermoacoustic tomography

Inverse Problems 1 and 2 arise in thermoacoustic tomography, which is described in [4, 17, 26]. In this case the target is subjected to a short electromagnetic impulse. The electromagnetic energy is absorbed. As a result, temperature is increased and the target is expanded. This causes a pressure wave, which is measured as a change in the acoustic field at the boundary of the sample. Assuming that the absorption of the electromagnetic energy is spatially varying inside the sample, the resulting wave field is carrying the signature of the inhomogeneity. On the other hand, cancerous regions absorb more than surroundings. This leads to applications in medical imaging. Hence, the problem is to calculate the absorption coefficient $\alpha(x)$ of the sample using time dependent measurements at its boundary. Let β be the thermal expansion coefficient, c_p be the specific capacity of the medium and I_0 be the power of the source. Usually β, c_p and I_0 are known. Also, assume that the speed of sound in the medium is constant and equals 1. Let $u(x,t)$ be the pressure wave. It was shown in e.g., [4] that

$$u_{tt} = \Delta u, (x,t) \in \mathbb{R}^3 \times (0,T), \tag{2.11}$$

$$u(x,0) = \alpha(x) I_0 \frac{\beta}{c_p}, \quad u_t(x,0) = 0. \tag{2.12}$$

Suppose that we measure the function $u(x,t)$ at the boundary of the domain Ω and $\alpha(x) = 0$ outside of Ω. Then those measurements give us the boundary value problem for equation (2.11) outside of Ω with zero initial conditions. Solving this problem, we uniquely determine the normal derivative of the function $u(x,t)$ at $\partial\Omega$. Thus, we arrive at the $\varphi-$ problem.

A different approach to the problem of thermoacoustic tomography is currently actively developed in a number of publications. In this approach the solution of the problem (2.11), (2.12) is presented via the Poisson-Kirchhoff formula, which leads to the problem of integral geometry of recovering a function via its integrals over certain

spheres, whose centers run over a surface and radii vary. Then uniqueness theorems are proven for this case and inversion formulas are derived, see, e,g., [1, 5, 17, 18]. In particular, works [1, 17] include the case of a variable speed and [17, 18] include numerical examples. A survey of these developments can be found in [17]. Also, see §1 of Chapter 6 of the book [19] for an example of the ill-posedness of this integral geometry problem for the case when centers of spheres run over a plane in $\mathbb{R}^3$.

2.2.2 Linearized inverse acoustic and electromagnetic problems

There is also another application, in which Inverse Problems 1 and 2 can be considered as linearized inverse acoustic and inverse electromagnetic problems. The idea of this subsection is motivated by §1 of Chapter 7 of [19] and §3 of Chapter 2 of [22]. We present this application now without discussing delicate details about the validity of the linearization. In this setting the point source is running along a surface and time dependent measurements of back-reflected data are performed at the positions of the source. In [12] the Newton-Kantorovich method was presented for the case when the source position is fixed and the time dependent measurements are performed at a surface.

Let the function $\alpha(x) \in C(\mathbb{R}^3)$ be strictly positive, $\alpha(x) \geq const. > 0$. Consider the Cauchy problem for the hyperbolic equation

$$\alpha(x) w_{tt} = \Delta_x w + 4\pi\delta(x - x_0, t), (x, t) \in \mathbb{R}^3 \times (0, T), \tag{2.13}$$

$$w(x, x_0, 0) = w_t(x, x_0, 0) = 0, \tag{2.14}$$

where $x_0 \in \mathbb{R}^3$ is the source position. It is well known that in acoustics $\alpha(x) = c^{-2}(x)$, where $c(x)$ is the speed of sound in the medium, and in some situations of the electromagnetics $\alpha(x) = (\mu\epsilon)(x)$, where μ and ϵ are respectively magnetic permeability and electric permittivity of the medium. We pose the following

Inverse Problem 3. Suppose that the function $\alpha(x) = 1$ outside of the domain

Ω and it is unknown inside of this domain. Determine this function for $x \in \Omega$, assuming that the following function $p(x_0, t)$ is known

$$w(x_0, x_0, t) \mid_{x_0 \in \partial\Omega} = p(x_0, t). \tag{2.15}$$

The full Inverse Problem 3 is difficult to address because of its nonlinearity. Hence, we consider now a linearized problem. Similarly with §3 of Chapter 2 of [22], suppose that the function $\alpha(x)$ can be represented in the form

$$\alpha(x) = 1 - \xi a(x),$$

where $\xi \in (0,1)$ is a small parameter. Hence, the term $\xi a(x)$ is a small perturbation of 1. We assume that this perturbation is unknown, i.e., the function $a(x)$ is unknown. Again, similarly with [22], we can formally set at $\xi \to 0$

$$w(x, x_0, t) = w_0(x, x_0, t) + \xi w_1(x, x_0, t) + O\left(\xi^2\right), \tag{2.16}$$

where functions w_0 and w_1 are independent on ξ. This setting was rigorously justified in §3 of Chapter 2 of [22] for the case of the telegraph equation

$$w_{tt} = \Delta w + (a_0(x) + \xi a_1(x)) w. \tag{2.17}$$

It was also justified in §1 of Chapter 7 of [19] for equation (2.17) without the introduction of the parameter ξ, which is actually introduced here for convenience only. Indeed, instead, one can assume that $\alpha(x) = 1 - a(x)$, where $|a(x)| << 1$.

Substituting (2.17) in (2.13) and (2.15) and dropping the term with $O(\xi^2)$, we obtain that functions w_0 and w_1 are solutions of the following Cauchy problems

$$w_{0tt} = \Delta_x w_0 + 4\pi\delta(x - x_0, t), (x, t) \in \mathbb{R}^3 \times (0, T), \tag{2.18}$$

$$w_0(x,x_0,0)=w_{0t}(x,x_0,0)=0, \tag{2.19}$$

$$w_{1tt}=\Delta_x w_1+a(x)\,w_{0tt}(x,x_0,t),(x,t)\in\mathbb{R}^3\times(0,T), \tag{2.20}$$

$$w_0(x,x_0,0)=w_t(x,x_0,0)=0. \tag{2.21}$$

Consider the function $h(x,x_0,t)$,

$$h(x,x_0,t)=\int_0^t d\tau\int_0^\tau w_1(x,x_0,s)\,ds.$$

Integrating (2.20) with respect to t twice and using (2.19) and (2.21), we obtain

$$h_{tt}=\Delta_x h+a(x)\,w_0(x,x_0,t),(x,t)\in\mathbb{R}^3\times(0,T), \tag{2.22}$$

$$h(x,x_0,0)=h_t(x,x_0,0)=0, \tag{2.23}$$

It follows from (2.18), (2.22), (2.23) and the formula (7.13) of §1 of Chapter 7 of [19] that the function $h(x,x_0,t)$ is

$$h(x,x_0,t)=\frac{1}{2\pi\left(t^2-|x-x_0|^2\right)}\int\limits_{S(x,x_0,t)}|y-x_0|^2\,a(y)\,d\omega_y, \tag{2.24}$$

where $d\omega_y=\sin\theta d\varphi d\theta,(\varphi,\theta)\in[0,2\pi]\times[0,\pi]$ are angles in the spherical coordinate system with the center at $\{x_0\}$ and $S(x,x_0,t)$ is the following ellipsoid with foci at $\{x\}$ and $\{x_0\}$

$$S(x,x_0,t)=\left\{y\in\mathbb{R}^3:|x-y|+|x_0-y|=t\right\}.$$

Setting in (2.24) $x_0:=x$ and denoting $v(x,t)=h(x,x,t)$, we obtain that the function v is the spherical Radon transform of the function a,

$$v(x,t)=\frac{1}{4\pi}\int\limits_{|x-y|=t/2}a(y)\,d\omega_y. \tag{2.25}$$

On the other hand, (2.25) implies that the function $\widetilde{v}(x,t) = v(x,2t)\cdot t$ is the solution of the following Cauchy problem

$$\widetilde{v}_{tt} = \Delta\widetilde{v}, (x,t) \in \mathbb{R}^3 \times (0,2T). \tag{2.26}$$

$$\widetilde{v} \mid_{t=0} = 0, \widetilde{v}_t \mid_{t=0} = a(x). \tag{2.27}$$

Also, using the above linearization one can "translate" the data $p(x_0,t)$ in (2.15) for the Inverse Problem 3 in the following function $\widetilde{p}(x,t)$

$$\widetilde{v} \mid_{S_T} = \widetilde{p}(x,t), t \in (0,2T). \tag{2.28}$$

Since the function $a(x) = 0$ outside of the domain Ω, then solving the initial boundary value problem (2.26)-(2.28) for $(x,t) \in (\mathbb{R}^3 \setminus \Omega) \times (0,T)$, we obtain the normal derivative $q(x,t)$,

$$\frac{\partial\widetilde{v}}{\partial\nu} \mid_{S_T} = q(x,t), t \in (0,2T) \tag{2.29}$$

In conclusion, we have reduced the linearized Inverse Problem 3 to the $\psi-$problem, which consists in the recovery of the function $a(x)$ from conditions (2.26)-(2.29). A similar derivation is valid for a similar inverse problem for the telegraph equation (2.17) at $a_0 \equiv 0$, see [19, 22].

2.3 The Method

We consider Inverse Problem 1, because it is more general than Inverse Problem 2. Denote $Mu = u_{tt} - Lu$. To solve the Inverse Problem 1 numerically, consider the Tikhonov regularizing functional

$$J_\varepsilon(u) = \|Mu - F\|^2_{L_2(Q_T)} + \varepsilon \|u\|^2_{H^2(Q_T)}$$

$$+ \left\|D^\beta u \mid_{S_T} - D^\beta f\right\|^2_{L_2(S_T)} + \|u_\nu \mid_{S_T} - g\|^2_{L_2(S_T)} \tag{2.30}$$

$$+\chi_{\varphi}\left\|u_t(x,0)-\psi\right\|^2_{L_2(\Omega)}+\chi_{\psi}\left\|u(x,0)-\varphi\right\|^2_{H^1(\Omega)},\forall u\in H^2\left(Q_t\right).$$

Here $\varepsilon>0$ is the regularization parameter,

$$u_{\nu}\mid_{S_T}:=\frac{\partial u}{\partial \nu}\mid_{S_T}$$

and $D^{\beta},|\beta|\leq 1$ is the operator of (x,t) derivatives with, where x-derivatives are those, which are taken in directions orthogonal to the normal vector. Also,

$$\chi_{\psi}=\left\{\begin{array}{c}1\text{ for the }\psi-\text{problem}\\ 0\text{ for the }\varphi-\text{problem}\end{array}\right\},\chi_{\varphi}=\left\{\begin{array}{c}1\text{ for the }\varphi-\text{problem}\\ 0\text{ for the }\psi-\text{problem}\end{array}\right\}.$$

Hence, $\chi_{\varphi}\chi_{\psi}=0,\chi_{\varphi}+\chi_{\psi}=1$. In previous works on the QRM terms in the second line of (2.30) were absent because of subtracting off boundary conditions from the original function u. Terms in the third line of (2.30) were absent also, and they are incorporated now to emphasize the knowledge of one of initial conditions.

To find the minimizer of $J_{\varepsilon}\left(u\right)$, we set the Fréchet derivative of this functional to zero and obtain for all $v\in H^2\left(Q_T\right)$

$$\int\limits_{Q_T}MuMvdxdt+\int\limits_{S_T}\left(D^{\beta}vD^{\beta}u+vu\right)\mid_{S_T}dS+\int\limits_{S_T}\left(v_{\nu}u_{\nu}\right)\mid_{S_T}dS$$

$$+\chi_{\psi}\int\limits_{\Omega}\left[\nabla u\nabla v+uv\right](x,0)\,dx+\chi_{\varphi}\int\limits_{\Omega}u_t(x,0)v_t(x,0)dx+\varepsilon\left[u,v\right] \tag{2.31}$$

$$=\int\limits_{Q_T}FMvdxdt+\int\limits_{S_T}\sum_{|\beta|\leq 1}\left(D^{\beta}v\mid_{S_T}\right)D^{\beta}fdS++\int\limits_{S_T}\left(v_{\nu}\mid_{S_T}\right)\cdot gdS$$

$$+\chi_{\psi}\int\limits_{\Omega}\left[\nabla\varphi\nabla v\left(x,0\right)+\varphi v\left(x,0\right)\right]dx+\chi_{\varphi}\int\limits_{\Omega}\psi v_t(x,0)dx.$$

Riesz theorem and (2.31) imply

Lemma 2.1. For any vector function $(F,f,g)\in L_2\left(Q_T\right)\times H^1\left(S_T\right)\times L_2\left(S_T\right)$ there

exists unique solution $u_\varepsilon \in H^2(Q_T)$ of the problem (2.31) and

$$\|u_\varepsilon\|_{H^2(Q_T)} \leq \frac{C}{\sqrt{\varepsilon}} \left(\|F\|_{L_2(Q_T)} + \|f\|_{H^1(S_T)} + \|g\|_{L_2(S_T)} + \chi_\psi \|\varphi\|_{H^1(\Omega)} + \chi_\varphi \|\psi\|_{L_2(\Omega)} \right).$$

Setting in (2.31) $v := u$, we obtain that the unique minimizer of the functional $J_\varepsilon(u)$ satisfies the following estimate

$$\begin{aligned} &\|Mu\|^2_{L_2(Q_T)} + \chi_\psi \|u(x,0)\|^2_{H^1(\Omega)} + \chi_\varphi \|u_t(x,0)\|^2_{L_2(\Omega)} \\ &+ \|u\,|_{S_T}\|^2_{H^1(S_T)} + \|u_\nu\,|_{S_T}\|^2_{L_2(S_T)} \qquad (2.32) \\ &\leq \|F\|^2_{L_2(Q_T)} + \|f\|^2_{H^1(S_T)} + \|g\|^2_{L_2(S_T)} + \chi_\psi \|\varphi\|^2_{H^1(\Omega)} + \chi_\varphi \|\psi\|^2_{H^1(\Omega)}. \end{aligned}$$

To prove convergence of our method, we need to derive from (2.32) the Lipschitz stability estimate for the function u in the $H^1(Q_T)$-norm. This in turn requires a modification of the proofs of [4, 11, 12, 14]. We specifically refer to the proofs of Theorem 2.4.1 in [14] and Theorem 4.4 in [4]. The main difference with previous proofs is that now either $\|u(x,0)\|^2_{H^1(\Omega)}$ or $\|u_t(x,0)\|^2_{L_2(\Omega)}$ can be estimated via the right hand side of (2.32), which was not done before. This is because terms in the third line of (2.30) were not included in the Tikhonov functional for QRM. So, if $\chi_\psi = 0$, then $\chi_\varphi = 1$ and we estimate $\|u(x,0)\|^2_{L_2(\Omega)}$ in the $\varphi-$problem. If, however, $\chi_\psi = 1$, then $\chi_\varphi = 0$ and we estimate $\|u_t(x,0)\|^2_{L_2(\Omega)}$ in the ψ problem. It is because of the incorporation of these terms that we can assume that $T > R$, as it is required in Inverse Problem 2 (see (2.9)), instead of $T > 2R$ of previous works. The required modification is done in the next section.

2.4 Lipschitz Stability Estimate

Theorem 2.1. Let $\Omega \subset \mathbb{R}^n$ be a convex bounded domain with the piecewise smooth boundary and let $T > R$. Suppose that the function $u \in H^2(Q_T)$ satisfies the

inequality

$$\|Mu\|_{L_2(Q_T)} + \chi_\psi \|u(x,0)\|_{H^1(\Omega)} + \chi_\varphi \|u_t(x,0)\|_{L_2(\Omega)} \tag{2.33}$$

$$+ \|u\,|_{S_T}\|_{H^1(S_T)} + \|u_\nu\,|_{S_T}\|_{L_2(S_T)} \leq K,$$

where $K = const. > 0$. Then

$$\|u\|_{H^1(Q_T)} + \chi_\varphi \|u(x,0)\|_{H^1(\Omega)} + \chi_\psi \|u_t(x,0)\|_{L_2(\Omega)} \leq CK. \tag{2.34}$$

Proof. Choose a pair of points x',$y' \in \partial\Omega$ such that $|x' - y'| = 2R$. Put the origin at the point $(x+y)/2$. Choose a constant $\eta \in (0,1)$. Consider the function $p(x,t)$,

$$p(x,t) = |x|^2 - \eta t^2.$$

Consider the Carleman Weight Function (CWF) $\mathcal{C}(x,t)$,

$$\mathcal{C}(x,t) = \exp(2\lambda p(x,t)),$$

where $\lambda > 1$ is a parameter. For any positive number b denote

$G_b = \{(x,t) \mid p(x,t) > b, x \in \Omega, t > 0\}$. Choose a sufficiently small number $c \in (0, R^2)$. Since $T > R$, then in G_c

$$t^2 < \frac{R^2 - c}{\eta} < T^2, \forall \eta \in (\eta_0, 1),$$

where $\eta_0 = \eta_0(T,R) \in (0,1)$. Hence, $G_c \subset Q_T$. Choose $\delta \in (0,c)$ so small that $G_{c+4\delta} \neq \varnothing$. Note that

$$G_{c+4\delta} \subset G_{c+3\delta} \subset G_{c+2\delta} \subset G_{c+\delta} \subset G_c. \tag{2.35}$$

Denote $M_0 u = u_{tt} - \Delta u$. The following pointwise Carleman estimate takes place

$$(M_0 u)^2 \mathcal{C}^2 \geq C\lambda \left(|\nabla_{x,t} u|^2 + \lambda^2 u^2 \right) \mathcal{C} + \nabla \cdot U + V_t \text{ in } G_c, \forall u \in C^2\left(\overline{G}_c\right), \forall \lambda > \lambda_0, \quad (2.36)$$

where

$$|U| + |V| \leq C\lambda \left(|\nabla_{x,t} u|^2 + \lambda^2 u^2 \right) \mathcal{C} \text{ in } G_c \quad (2.37)$$

and $\lambda_0 (G_c, \eta) > 1$ is sufficiently large. In addition, the function V is estimated as

$$|V| \leq C\lambda^3 t \left(|\nabla_{x,t} u|^2 + u^2 \right) \mathcal{C} + C\lambda^3 |u_t| \left(|\nabla u| + |u| \right) \mathcal{C} \text{ in } G_c. \quad (2.38)$$

This Carleman estimate was proven in Theorem 2.2.4 of [14]. It was derived earlier in §4 of Chapter 4 of [19].

Consider the cut-off function $\rho(x,t) \in C^2\left(\overline{G}_c\right)$ such that

$$\rho(x,t) = \left\{ \begin{array}{c} 1 \text{ in } G_{c+2\delta} \\ 0 \text{ in } G_c \diagdown G_{c+\delta} \\ \text{between 0 and 1 otherwise} \end{array} \right\}. \quad (2.39)$$

The existence of such functions is well known. For an arbitrary function $u \in C^2\left(\overline{G}_c\right)$ denote $v = v(u) := \rho u$. Using (2.36)-(2.38), we obtain

$$\int\limits_{G_c} (M_0 v)^2 \mathcal{C} dx dt \geq C\lambda \int\limits_{G_c} \left(|\nabla_{x,t} v|^2 + \lambda^2 v^2 \right) \mathcal{C} dx dt$$

$$-C\lambda^3 \int\limits_{\Omega} \left[|u_t| \left(|\nabla u| + |u| \right) \right](x,0) \exp\left(2\lambda |x|^2\right) dx - C\lambda \int\limits_{S_T} \left[\left(D^\beta u\right)^2 + \lambda^2 u_\nu^2 \right] \mathcal{C} dS.$$

Because by (2.35) $G_{c+2\delta} \subset G_c$, then (2.39) implies that the last inequality can be

rewritten as

$$\int\limits_{G_c} (M_0 v)^2 \mathcal{C} dxdt \geq C\lambda \int\limits_{G_{c+2\delta}} \left(|\nabla_{x,t} u|^2 + \lambda^2 u^2 \right) \mathcal{C} dxdt \tag{2.40}$$

$$-C\lambda^3 \int\limits_{\Omega} \left[|u_t| \left(|\nabla u| + |u| \right) \right] (x,0) \exp\left(2\lambda |x|^2 \right) dx - C\lambda \int\limits_{S_T} \left[\left(D^\beta u \right)^2 + u_\nu^2 \right] \mathcal{C} dS.$$

By (2.39) the left hand side of (2.40) can be estimated from the above as

$$\int\limits_{G_c} (M_0 v)^2 \mathcal{C} dxdt \leq \int\limits_{G_{c+2\delta}} (M_0 u)^2 \mathcal{C} dxdt + C \int\limits_{G_c \setminus G_{c+2\delta}} \left(|\nabla_{x,t} u|^2 + u^2 \right) \mathcal{C} dxdt$$

$$\leq \int\limits_{G_{c+2\delta}} (M_0 u)^2 \mathcal{C} dxdt + C\lambda^3 \|u\|^2_{H^1(Q_T)} \exp\left[2\lambda \left(c + 2\delta \right) \right]$$

$$\leq \int\limits_{G_{c+2\delta}} (Mu)^2 \mathcal{C} dxdt + C \int\limits_{G_{c+2\delta}} \left(|\nabla_{x,t} u|^2 + u^2 \right) \mathcal{C} dxdt + C \|u\|_{H^1(Q_T)} \exp\left[2\lambda \left(c + 2\delta \right) \right].$$

Substituting this in (2.40), recalling that λ is sufficiently large and using (2.35), we obtain

$$\int\limits_{G_{c+2\delta}} (Mu)^2 \mathcal{C} dxdt + \lambda^3 \|u\|^2_{H^1(Q_T)} \exp\left[2\lambda \left(c + 2\delta \right) \right]$$

$$+\lambda \int\limits_{S_T} \left[\left(D^\beta u \right)^2 + \lambda^2 u_\nu^2 \right] \mathcal{C} dS + \lambda^3 \int\limits_{\Omega} \left[|u_t| \left(|\nabla u| + |u| \right) \right] (x,0) \exp\left(2\lambda |x|^2 \right) dx$$

$$\geq C\lambda \int\limits_{G_{c+2\delta}} \left(|\nabla_{x,t} u|^2 + \lambda^2 u^2 \right) \mathcal{C} dxdt \geq C\lambda^3 \exp\left[2\lambda \left(c + 3\delta \right) \right] \int\limits_{G_{c+3\delta}} \left(|\nabla_{x,t} u|^2 + u^2 \right) dxdt.$$

Let $m = \max_{\overline{G}_c} p(x,t)$. Dividing the last inequality by $C\lambda^3 \exp\left[2\lambda \left(c + 3\delta \right) \right]$, we obtain

$$\int\limits_{G_{c+3\delta}} \left(|\nabla_{x,t} u|^2 + u^2 \right) dxdt \leq$$

$$Ce^{2\lambda m} \left(\|Mu\|^2_{L_2(Q_T)} + \|u \mid_{S_T}\|^2_{H^1(S_T)} + \|u_\nu \mid_{S_T}\|^2_{L_2(S_T)} \right) + C \|u\|^2_{H^1(Q_T)} e^{-2\lambda\delta} \tag{2.41}$$

$$+Ce^{2\lambda m}\int\limits_{\Omega}\left[|u_t|\left(|\nabla u|+|u|\right)\right](x,0)\,dx.$$

The last term of (2.41) was not present in previous publications, and we will analyze it now. Consider the $\varphi-$problem first. That is, consider the case $\chi_\varphi = 1, \chi_\psi = 0$. Let $\gamma > 0$ be a small number which we will choose later. We estimate the last term of (2.41) as

$$Ce^{2\lambda m}\int\limits_{\Omega}\left[|u_t|\left(|\nabla u|+|u|\right)\right](x,0)\,dx$$

$$\leq C\gamma\int\limits_{\Omega}\left(|\nabla u|^2+u^2\right)(x,0)\,dx+\frac{Ce^{4\lambda m}}{\gamma}\int\limits_{\Omega}u_t^2\,(x,0)\,dx \tag{2.42}$$

$$\leq C\gamma\left\|u\,(x,0)\right\|^2_{H^1(\Omega)}+\frac{Ce^{4\lambda m}}{\gamma}K^2.$$

We have used (2.33) to estimate the last term in the second line of (2.42). Consider now the $\psi-$problem. Then similarly with (2.42)

$$Ce^{2\lambda m}\int\limits_{\Omega}\left[|u_t|\left(|\nabla u|+|u|\right)\right](x,0)\,dx\leq C\gamma\left\|u_t\,(x,0)\right\|^2_{L_2(\Omega)}+\frac{Ce^{4\lambda m}}{\gamma}K^2. \tag{2.43}$$

Consider now the set

$$F_1\,(c,\delta)=G_{c+3\delta}\cap\left\{t\in(0,\delta)\right\}.$$

Then

$$\left\{(x,t):|x|>\sqrt{c+3\delta+\eta\delta^2},x\in\Omega,t\in(0,\delta)\right\}\subset F_1\,(c,\delta)\,. \tag{2.44}$$

Then (2.41), (2.42) and (2.43) imply that

$$\int\limits_{F_1(c,\delta)}\left(|\nabla_{x,t}u|^2+u^2\right)dxdt\leq\frac{Ce^{4\lambda m}}{\gamma}K^2+C\left\|u\right\|^2_{H^1(Q_T)}e^{-2\lambda\delta}$$

$$+Ce^{2\lambda m}\left(\left\|u\mid_{S_T}\right\|^2_{H^1(S_T)}+\left\|u_\nu\mid_{S_T}\right\|^2_{L_2(S_T)}\right)$$

$$+\chi_\varphi C\gamma \left\| u\left(x,0\right)\right\|^2_{H^1(\Omega)} + \chi_\psi C\gamma \left\| u_t\left(x,0\right)\right\|^2_{L_2(\Omega)}.$$

Hence, by (2.33)

$$\int\limits_{F_1(c,\delta)} \left(\left|\nabla_{x,t} u\right|^2 + u^2\right) dxdt \leq \frac{Ce^{4\lambda m}}{\gamma} K^2 + C\left\|u\right\|^2_{H^1(Q_T)} e^{-2\lambda\delta} \tag{2.45}$$

$$+\chi_\varphi C\gamma \left\| u\left(x,0\right)\right\|^2_{H^1(\Omega)} + \chi_\psi C\gamma \left\| u_t\left(x,0\right)\right\|^2_{L_2(\Omega)}.$$

Choose numbers c and δ so small that $3\sqrt{c+3\delta+\eta\delta^2} < R$. Hence, we can choose $x_0 \in \Omega$ such that $|x_0| = 3\sqrt{c+3\delta+\eta\delta^2}$. Next, we "shift" the function $p\left(x,t\right)$ to the point x_0, thus considering the function

$$p\left(x-x_0,t\right) = \left|x-x_0\right|^2 - \eta t^2.$$

For $b > 0$ let $G_b\left(x_0\right) = \left\{(x,t) \mid p\left(x-x_0,t\right) > b, x \in \Omega, t > 0\right\}$. Similarly with the above denote

$$F_2\left(c,\delta\right) = G_{c+3\delta}\left(x_0\right) \cap \left\{t \in (0,\delta)\right\}.$$

Then

$$\left\{(x,t) : |x-x_0| > \sqrt{c+3\delta+\eta\delta^2}, x \in \Omega, t \in (0,\delta)\right\} \subset F_2\left(c,\delta\right). \tag{2.46}$$

Consider an arbitrary point x such that $x \in \left\{|x| < 2\sqrt{c+3\delta+\eta\delta^2}\right\}$. Then

$$|x_0 - x| \geq |x_0| - |x| \geq 3\sqrt{c+3\delta+\eta\delta^2} - 2\sqrt{c+3\delta+\eta\delta^2} = \sqrt{c+3\delta+\eta\delta^2}.$$

Hence, by (2.46)

$$\left\{(x,t) : |x| < 2\sqrt{c+3\delta+\eta\delta^2}, t \in (0,\delta)\right\} \subset F_2\left(c,\delta\right).$$

Combining this with (2.44), we see that

$$\Omega \times (0,\delta) = Q_\delta \subset F_1(c,\delta) \cup F_2(c,\delta). \tag{2.47}$$

Using function $p(x-x_0,t)$ instead of $p(x,t)$, we obtain similarly with (2.45)

$$\int\limits_{F_2(c,\delta)} \left(|\nabla_{x,t} u|^2 + u^2\right) dxdt \leq \frac{Ce^{4\lambda m}}{\gamma} K^2 + C \|u\|^2_{H^1(Q_T)} e^{-2\lambda\delta}$$

$$+\chi_\varphi C\gamma \|u(x,0)\|^2_{H^1(\Omega)} + \chi_\psi C\gamma \|u_t(x,0)\|^2_{L_2(\Omega)}.$$

Combining this with (2.45) and (2.47), we obtain

$$\|u\|_{H^1(Q_\delta)} \leq \frac{Ce^{4\lambda m}}{\gamma} K^2 + C \|u\|^2_{H^1(Q_T)} e^{-2\lambda\delta}$$

$$+\chi_\varphi C\gamma \|u(x,0)\|^2_{H^1(\Omega)} + \chi_\psi C\gamma \|u_t(x,0)\|^2_{L_2(\Omega)}.$$

Hence, there exists a number $t^* \in (0,\delta)$ such that

$$\int\limits_{\Omega} \left(|\nabla_{x,t} u|^2 + u^2\right)(x,t^*)\, dx \leq \frac{Ce^{4\lambda m}}{\delta\gamma} K^2 + \frac{C}{\delta} \|u\|^2_{H^1(Q_T)} e^{-2\lambda\delta}$$

$$+\frac{1}{\delta}\left[\chi_\varphi C\gamma \|u(x,0)\|^2_{H^1(\Omega)} + \chi_\psi C\gamma \|u_t(x,0)\|^2_{L_2(\Omega)}\right].$$

This inequality combined with (2.33) and the standard energy estimates implies that

$$\|u\|^2_{H^1(Q_T)} + \chi_\varphi \|u(x,0)\|^2_{H^1(\Omega)} + \chi_\psi \|u_t(x,0)\|^2_{L_2(\Omega)} \leq C \|u\|^2_{H^1(Q_T)} e^{-2\lambda\delta}$$

$$+\frac{Ce^{4\lambda m}}{\gamma} K^2 + \chi_\varphi C\gamma \|u(x,0)\|^2_{H^1(\Omega)} + \chi_\psi C\gamma \|u_t(x,0)\|^2_{L_2(\Omega)}. \tag{2.48}$$

Note that δ is independent on λ. Choose sufficiently large λ_0 such that

$$1 - Ce^{-2\lambda_0 \delta} > \frac{1}{2}$$

and set $\lambda := \lambda_0$. Choose γ so small that $C\gamma < 1/2$. Then we obtain (2.34) from (2.48).

□

2.5 Convergence

Theorem 2.1 enables us to prove convergence of our method. Following the Tikhonov concept for ill-posed problems [19], we first introduce an "ideal" exact solution of either φ or ψ problem without an error in the data. Next, we assume the existence of the error in the boundary data f and g and prove that our solution tends to the exact one as the level of error in the data tends to zero. We consider the more general Inverse Problem 1. Let $f^* \in H^1(S_T)$ and $g^* \in L_2(S_T)$ be the exact boundary data (2.3), $F^* \in L_2(Q_T)$ be the exact right hand side of equation (2.1) and φ^* and ψ^* be exact initial conditions. We assume that there exists an exact function $u^* \in H^2(Q_T)$ satisfying

$$u^*_{tt} = L(x,t)u^* + F^*(x,t) \text{ in } Q_T, \tag{2.49}$$

with initial conditions

$$u^*(x,0) = \varphi^*(x), u^*_t(x,0) = \psi^*(x), \varphi^* \in H^1(\Omega), \psi^* \in L_2(\Omega), \tag{2.50}$$

$$u^* \mid_{S_T} = f^*(x,t), \frac{\partial u^*}{\partial \nu} \mid_{S_T} = g^*(x,t), \tag{2.51}$$

where φ^* and ψ^* are exact initial conditions. We assume that the real boundary data in (2.3) have an error, so as the given initial condition. In other words, we assume

that

$$\|f - f^*\|_{H^1(S_T)} + \|g - g^*\|_{L_2(S_T)} + \|F - F^*\|_{L_2(Q_T)} \tag{2.52}$$

$$+\chi_\psi \|\varphi - \varphi^*\|_{H^1(\Omega)} + \chi_\varphi \|\psi - \psi^*\|_{L_2(\Omega)} \leq \delta,$$

where $\delta > 0$ is a small number. The following convergence theorem holds

Theorem 2.2. Suppose that $T > R$. Let $u_{\varepsilon\delta} \in H^2(Q_T)$ be the solution of the QRM problem (2.31), which is guaranteed by Lemma 2.1. Let conditions (2.49)-(2.52) be satisfied. Then the following estimate is valid

$$\|u - u^*\|_{H^1(Q_T)} + \chi_\varphi \|\varphi - \varphi^*\|_{H^1(\Omega)} + \chi_\psi \|\psi - \psi^*\|_{L_2(\Omega)} \leq C\left(\delta + \sqrt{\varepsilon}\right).$$

Proof. Since the functional $J_0(u)$ with the exact data (2.50), (2.51) achieves its minimal zero value at $u := u^*$, then the function u^* satisfies equation (2.31) with $\varepsilon = 0$ and with the exact data (2.50), (2.51). Subtracting that equation for u^* from equation (2.31) for $u := u_{\varepsilon\delta}$, denoting $w = u_{\varepsilon\delta} - u^*$, setting in resulting equation $v := w$ and using (2.52), we obtain similarly with (2.32)

$$\int\limits_{Q_T} (Mw)^2 \, dxdt + \chi_\psi \|w(x,0)\|^2_{H^1(\Omega)} + \chi_\varphi \|w_t(x,0)\|^2_{L_2(\Omega)}$$

$$+ \|w\,|_{S_T}\|^2_{H^1(S_T)} + \|w_\nu\,|_{S_T}\|^2_{L_2(S_T)} \leq 4\delta^2 + \varepsilon.$$

The rest of the proof follows immediately from Theorem 2.1. $\square$

2.6 Numerical Implementation

In our numerical study we have considered the Inverse Problem 2. To generate the data for the inverse problem, we have solved the Cauchy problem

$$u_{tt} = \Delta u, (x,t) \in \mathbb{R}^2 \times (0,T), \tag{2.53}$$

$$u(x,0)=\varphi(x),u_t(x,0)=\psi(x). \tag{2.54}$$

In our numerical experiments $\psi(x)\equiv 0$ for the $\varphi-$problem, and $\varphi(x)\equiv 0$ for the $\psi-$problem. Because of (2.5) and the finite speed of propagation, we use in our solution of the forward problem zero Dirichlet boundary condition at the boundary of the rectangle $(-T,a+T)\times(-T,a+T)$ (Figure 1). Hence, we solve initial boundary value problem inside of this rectangle for equation (2.53) with initial conditions (2.54) at zero Dirichlet boundary condition. In all our calculations we took $a=1$. In Tests 2.1, 2.2 and 2.5, which are concerned with the Inverse Problem 2, we took $T=3$. Hence, condition (2.9) is satisfied. Tests 2.3 and 2.4 are concerned with the Inverse Problem 1 and we have taken different values of T in these tests. The square $SQ(a)$ is $SQ(a)=SQ(1)=(0,1)\times(0,1)$, the domain Ω in tests 2.1, 2.2 and 2.5 is

$$\Omega:=(0,4)\times(0,4) \tag{2.55}$$

and in all tests

$$\varphi(x)=\psi(x)=0 \text{ for } x\notin SQ(1). \tag{2.56}$$

We have solved the Cauchy problem (2.53), (2.54) via finite differences using the uniform grid. We set

$$u(t_k,x_{1n},x_{2m})\approx u_{kmn},\ k=0,...,N_t,\ \ n=0,...,N_x,m=0,...,N_y,$$

$$t_k=kh_t,\ x_{1n}=nh_{x_1},\ x_{2m}=mh_{x_2},$$

step sizes $h_{x_1}=h_{x_2}=0.1,h_t=1/15$ and $N_x=N_y=10,N_t=45$. This solution has generated the boundary data (2.8). Next, we have introduced noise in these data as

$$f_n\left(x^i,t_j\right)=f\left(x^i,t_j\right)\left(1+\gamma N\left(t_j\right)\right),g_n\left(x^i,t_j\right)=g\left(x^i,t_j\right)\left(1+\gamma N\left(t_j\right)\right), \tag{2.57}$$

where (x^i, t_j) is the grid point at the boundary. Here $N \in (-1, 1)$ is a pseudo random variable, which is given by function $Math.random()$ in Java and $\gamma \in [0.05, 0.5]$ is the noise level. We have chosen the grid points the same as ones in the finite difference scheme we have solved the problem (2.53), (2.54). The presence of the random noise in the date prevents us from committing "inverse crime". In (2.57) points $x^i \in \Gamma_{1T} \cup \Gamma_{2T}$. As to $\Gamma_{3T} \cup \Gamma_{4T}$, we simply set $f = g = 0$ on this part of the boundary, because of (2.7).

To find the minimizer of the functional J_ε, we have also used finite differences. We have used in (2.30) the finite difference approximations for $Mu = u_{tt} - \Delta u$ and $u_\nu \mid_{S_T}$ and have minimized the resulting functional $\widetilde{J}_\varepsilon$ with respect to the vector $\{u_{kmn}\}$, which approximates values of the function u at grid points. Here $\widetilde{J}_\varepsilon$ means the functional J_ε, which is expressed via the finite differences. The norms $\|u_{x_1}(x,0)\|_{L_2(\Omega)}$, $\|u_{x_2}(x,0)\|_{L_2(\Omega)}$ in $\|u(x,0)\|_{H^1(\Omega)}$ in the $\psi-$problem were calculated via finite differences. As to the term $\left\|D^\beta u \mid_{S_T} - D^\beta f\right\|^2_{L_2(S_T)}$ in (2.30), we have used only $\beta = 0$, thus ending up with $\|u \mid_{S_T} - f\|^2_{L_2(S_T)}$ (in the discrete sense). Note that since $\beta = 0$, our numerical results seem to be stronger than Theorem 2.1 predicts. The integrals were calculated as

$$\int\limits_{\Omega_T} (u_{tt} - \Delta u)^2 dv \approx \frac{h_t h_{x_2} h_{x_1}}{h_t^4} \sum_{k=1}^{N_t - 1} \sum_{m=1}^{N_y - 1} \sum_{n=1}^{N_x - 1} M_{kmn}^2,$$

where

$$\begin{aligned} M_{kmn} &= (u_{k+1,mn} - 2u_{kmn} + u_{k-1,mn}) - \lambda_y (u_{k,m+1,n} - 2u_{kmn} + u_{k,m-1,n}) \\ &\qquad - \lambda_x (u_{km,n+1} - 2u_{kmn} + u_{km,n-1}) \\ &= (u_{k+1,mn} + u_{k-1,mn}) - \lambda_y (u_{k,m+1,n} + u_{k,m-1,n}) - \lambda_x (u_{km,n+1} + u_{km,n-1}) - \lambda_t u_{kmn}, \end{aligned}$$

where

$$\lambda_x = \frac{h_t^2}{h_{x_1}^2}, \quad \lambda_y = \frac{h_t^2}{h_{x_2}^2}, \quad \lambda_t = 2(1 - \lambda_x - \lambda_y).$$

Also,

$$\int_0^T \int_0^{a+T} (u(t, x_2, x_1^*) - f(t, x_2))^2 dx_2 dt \approx h_t h_{x_2} \sum_{k=0}^{N_t} \sum_{m=0}^{N_{x_2}} H_{km}^2,$$

where

$$H_{km} = u_{kmn_*} - h_{km},$$

where n_* in the layer number (value of x_1^*) at which the grid function f_{km} is given.

To minimize the functional $\widetilde{J}_\varepsilon$, we have used the conjugate gradient method. Derivatives with respect to variables u_{kmn} where calculated in closed forms, using the following formula

$$\frac{\partial u_{kmn}}{\partial u_{\overline{k}\overline{m}\overline{n}}} = \delta_{k\overline{k}} \delta_{m\overline{m}} \delta_{n\overline{n}},$$

where $\delta_{k\overline{k}}$ is the Kronecker symbol. This formula can be conveniently used to obtain closed form expressions for derivatives

$$\frac{\partial \widetilde{J}_\varepsilon(u)}{\partial u_{kmn}}.$$

Let a be the vector of unknowns of the functional $\widetilde{J}_\varepsilon$. We start our iterative process from $a := a_0 = 0$. It is well known in the field of ill-posed problems that the number of iterations can often be taken as a regularization parameter, and it depends, of course on the range of parameters of a problem one considers. We have found that the optimal number of iterations for our range of parameters is 300. Thus, in all numerical examples below 300 iterations of the conjugate gradient method were used, thus ending up with a_{300}. Figure 2.2 displays typical dependencies of the functional $\widetilde{J}_\varepsilon(a_k)$ and the norm of its gradient on the iteration number k.

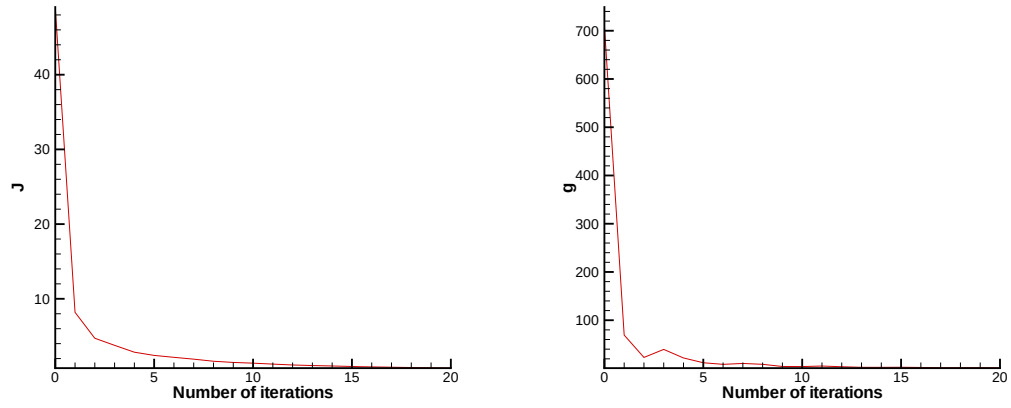

(a) $J = J_\varepsilon$ (b) $g = \|\nabla J_\varepsilon\|^2$

Figure 2.2: Typical dependence of the functional J and g on number of iterations.

2.7 Numerical Results

In this section we present results of some numerical experiments. We have always used $\varepsilon = 10^{-6}$. Larger values of ε such as 10^{-5} brought lower quality results. In our numerical experiments we have imaged both smooth slowly varying functions and the finite difference analogue of the $\delta-$ function. Let $(x_{1k}, x_{2r}) \in \Omega$ be a fixed grid point. To obtain the finite difference analogue of $\delta(x_1 - x_{1k}, x_2 - x_{2r})$, we consider the following grid points (x_{1n}, x_{2m}) and we model the function $\delta(x_{1n} - x_{1k}, x_{2m} - x_{2r})$ as

$$\delta(x_{1n} - x_{1k}, x_{2m} - x_{2r}) = \frac{3}{4h_{x_2}h_{x_1}}\delta_{nk}\delta_{mr},$$

where the multiplier at $\delta_{nk}\delta_{mr}$ is chosen such that the volume of the pyramid based on (x_{1k-1}, x_{2r-1}), (x_{1k-1}, x_{2r+1}), (x_{1k+1}, x_{2r+1}), (x_{1k+1}, x_{2r-1}) equals to 1. Hence, the support of the function $\delta(x_{1n} - x_{1k}, x_{2m} - x_{2r})$ is limited only to the point (x_{1n}, x_{2m}).

We have observed that having equal coefficient at all terms of the functional $\widetilde{J}_\varepsilon$ in (2.30) does not lead to good reconstruction results. This is because not all the terms of (2.30) provide an equal impact in this functional. For example, for the $\varphi-$problem

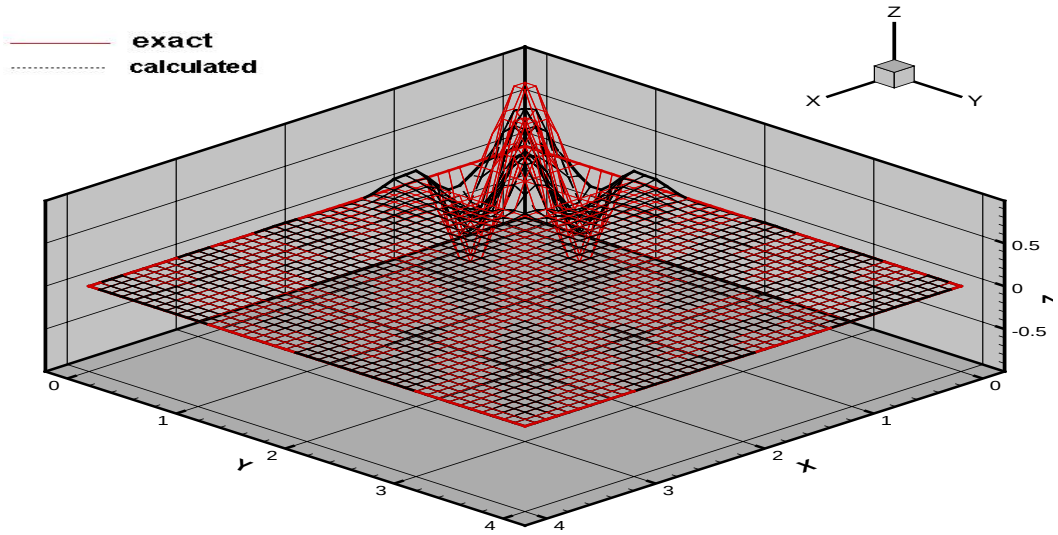

Figure 2.3: Exact (red) and calculated (black) functions φ in (2.58) without balancing coefficients with 5% noise in boundary data.

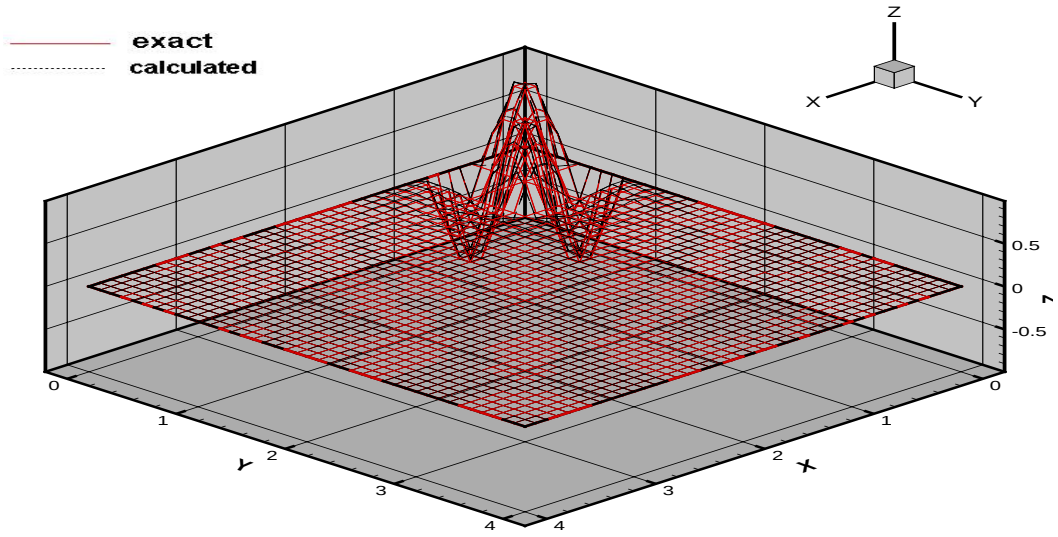

Figure 2.4: Exact (red) and calculated (black) functions φ in (2.58) with balancing coefficients with 5% noise in boundary data.

with no noise in the data for the function

$$\varphi(x) = \left\{ \begin{array}{c} \sin(2\pi x_1)\sin(2\pi x_2), x \in SQ(1) \\ 0 \text{ otherwise} \end{array} \right\} \tag{2.58}$$

we first got the result displayed in Figure 2.3. One can observe that the error at the boundary is significant. And indeed, the values of two terms in (2.30) after 300 iterations were for this case

$$\int\limits_{\Omega_T} (u_{tt} - \Delta u)^2 dxdt \approx 10^{-3}, \quad \|u - f\|_{L_2(S_T)} \approx 10^{-2}.$$

Hence, the impact of the boundary term in (2.30) is 10 greater than the impact of the $\|Mu\|^2_{L_2(Q_T)}$. To minimize the error at the boundary, we took the balancing coefficient 1000 at $1000 \cdot \|u-f\|_{L_2(S_T)}$ instead of $1 \cdot \|u-f\|_{L_2(S_T)}$. The other balancing coefficients equal to 1. The quality of the resulting image was improved, see Figure 2.4. Thus, in all our tests with the $\varphi-$problem we have taken the same balancing coefficients. In the case of the $\psi-$problem we have taken $100 \cdot \chi_\psi \|u(x,0) - \varphi\|^2_{H^1(\Omega)}$ and the other balancing coefficients equal to 1.

Note that Theorems 2.1 and 2.2 remain the same, including their proofs, if balancing coefficients are introduced.

Test 2.1 *The $\varphi-$problem.* Here $\psi(x) \equiv 0$ and the function $\varphi(x)$ to be reconstructed is one in (2.58). In Figures 2.5 and 2.6 represent resulting images with 25% and 50% noise respectively. Next, we test our method for the case when the term with χ_φ is absent in the functional $J_\varepsilon(u)$ in (2.30). Regardless on the small amount of noise in the data, both maximal (1) and minimal (-1) values of the imaged function were missed by about 22% in this case, whereas they were not missed in the previous cases with 25% and 50% noise when the term with χ_φ was not absent in (2.30). To see this, we display on Figure 2.7 the 1-dimensional cross-sections by the straight

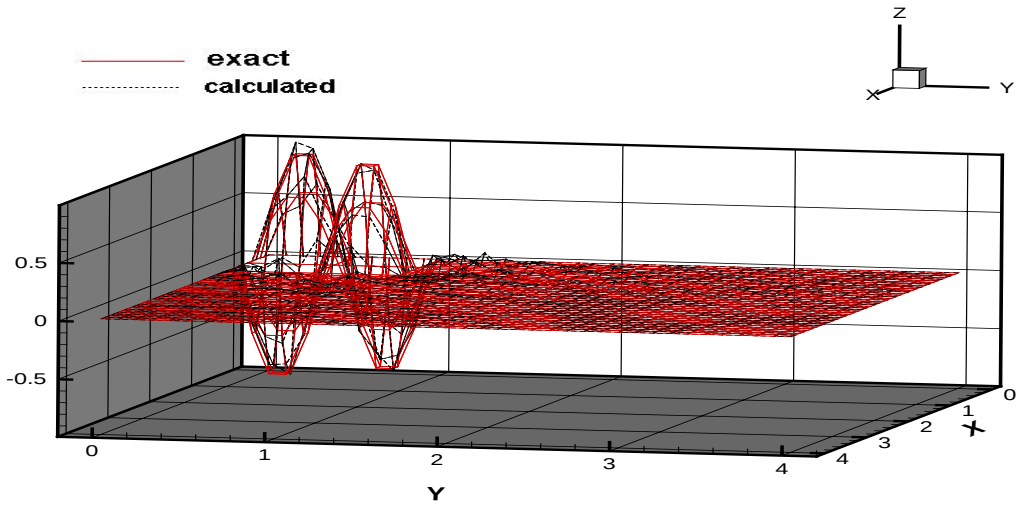

Figure 2.5: Test 2.1. Exact (red) and calculated (black) functions φ in (2.58) with 25% noise in the boundary data.

line $\{x_1 = 0.5\}$ of the correct function (2.58), the imaged function with 50% noise of Figure 2.6 and the imaged function with the absent term with χ_φ and 5% noise. One can observe that the maximal value of the calculated function is 0.7, while the maximal absolute value of the correct function is 0.9, so as the one of Figure 2.6. Here we have 0.9 instead of 1 only because the points with the absolute value of 1 are not the grid points. This emphasizes the importance of the incorporation of the term with χ_φ. We have observed the same for the $\psi-$ problem (images not shown).

Test 2.2. *The $\psi-$problem.* In this case $\varphi(x) \equiv 0$ and the function $\psi(x)$ to be reconstructed is

$$\psi(x) = \left\{ \begin{array}{c} \sin(\frac{\pi}{2}(x_1 - 0.5)\sin(\frac{\pi}{2}(x_2 - 0.5)), x \in SQ(1) \\ 0 \text{ otherwise.} \end{array} \right\}. \tag{2.59}$$

Figures 2.8, 2.9 and 2.10display resulting images of the function (7.2) with 5%, 25% and 50% of the noise level in the data respectively.

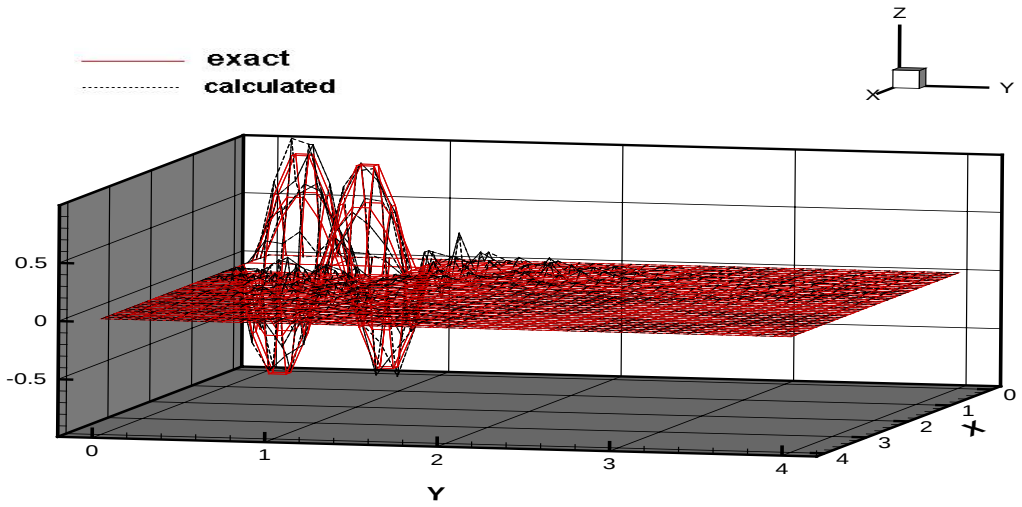

Figure 2.6: Test 2.1. Exact (red) and calculated (black) functions φ in (2.58) with 50% noise in the boundary data.

Test 2.3. *The $\varphi-$problem in $SQ(1)$ for $T \in (0.5 diam\, SQ(1), diam\, SQ(1))$, where $diam\, SQ(1) = \sqrt{2}$ is the diameter of the square $SQ(1)$.* We have decided to see what kind of results can be obtained if the boundary Cauchy data are given on the entire boundary of the square $SQ(1)$ in the case when $T \in (0.5 diam\, SQ(1), diam\, SQ(1))$. We are especially interested in the question about the influence of terms with χ_φ and χ_ψ. We have used

$$T = 0.75 < diam\, SQ(1) = \sqrt{2}, N_x = N_y = 20,\ N_t = 3.$$

and have reconstructed the function (2.58). Figure 2.11 displays the resulting image with 25% noise in the case when the term χ_φ is present in (2.30). This quality of the reconstruction is good for such a high noise level. Figure 2.12 displays the 1-dimensional cross-section of the image by the straight line $\{x_1 = 0.5\}$, as well as the 1-dimensional cross-section of the image for the case when the term with χ_φ is not present in (2.30) and 25% noise in the data is in. One can observe that the minimal

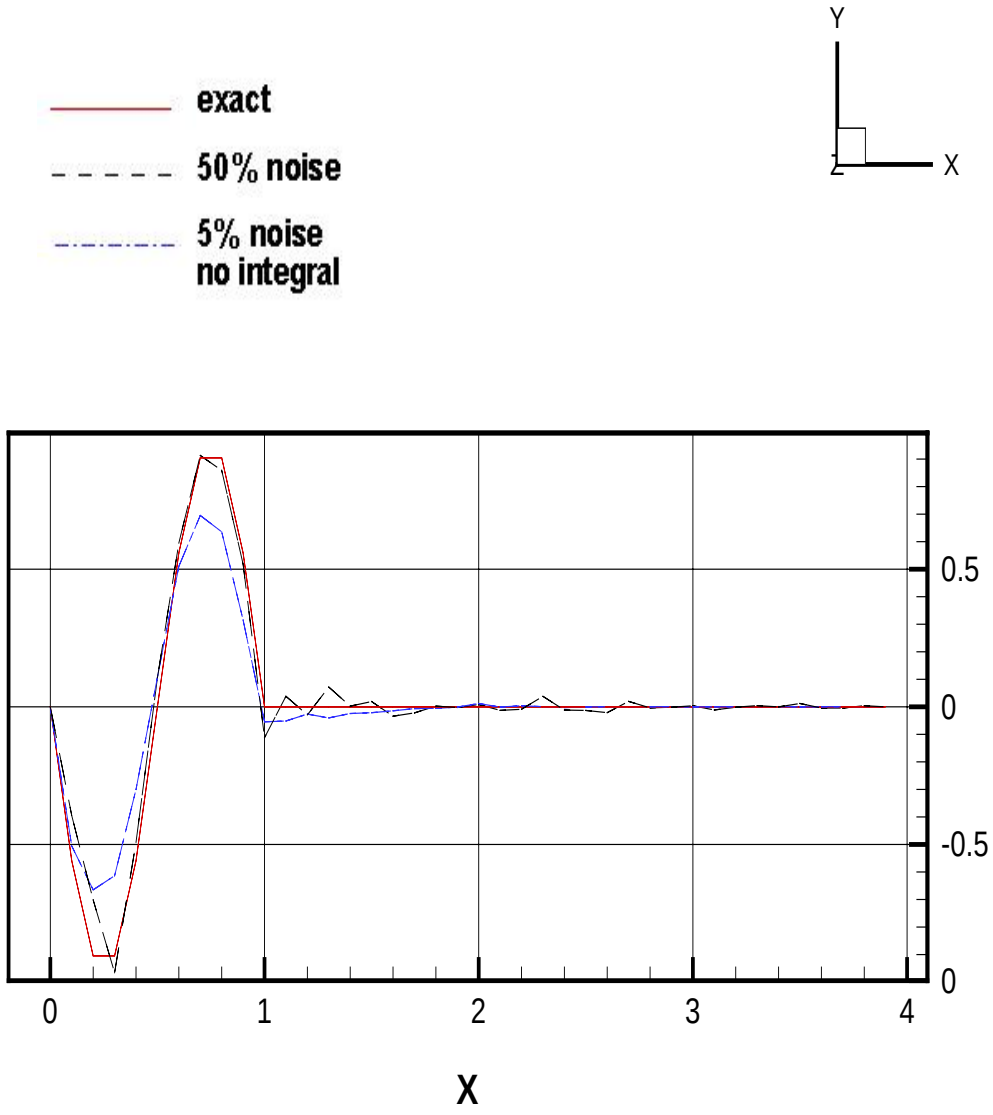

Figure 2.7: Test 2.1. Cross sections of exact (red) and calculated (black, blue) functions φ with 5%, 50% noise, "no integral" means $\chi_{\varphi=0}$. One can see that the maximal value of the case $\chi_{\varphi=0}$ is $0.7/(-0.7)$. The maximal value of the exact function is $0.9 < 1$ only because of the grid step size.

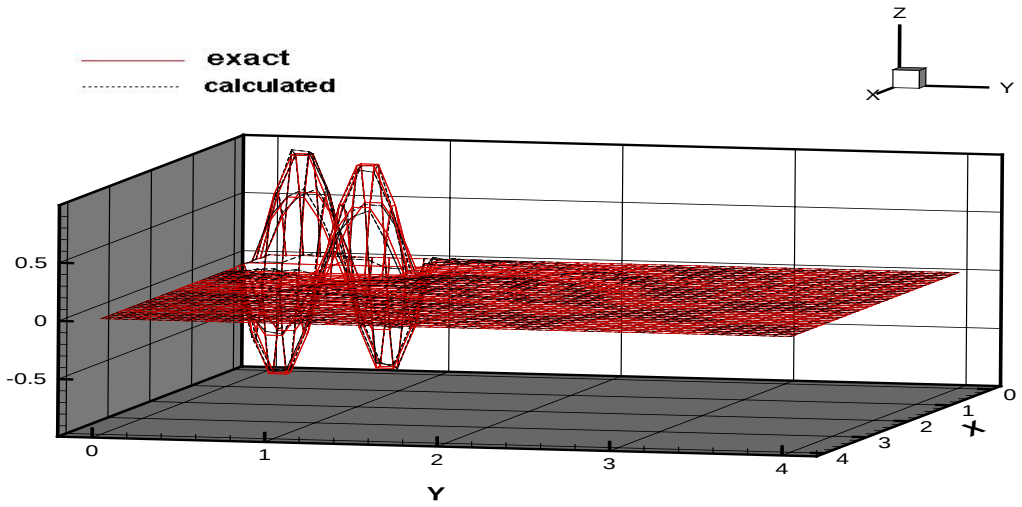

Figure 2.8: Test 2.2. Exact (red) and calculated (black) functions ψ in (2.59) with 5% noise in the boundary data.

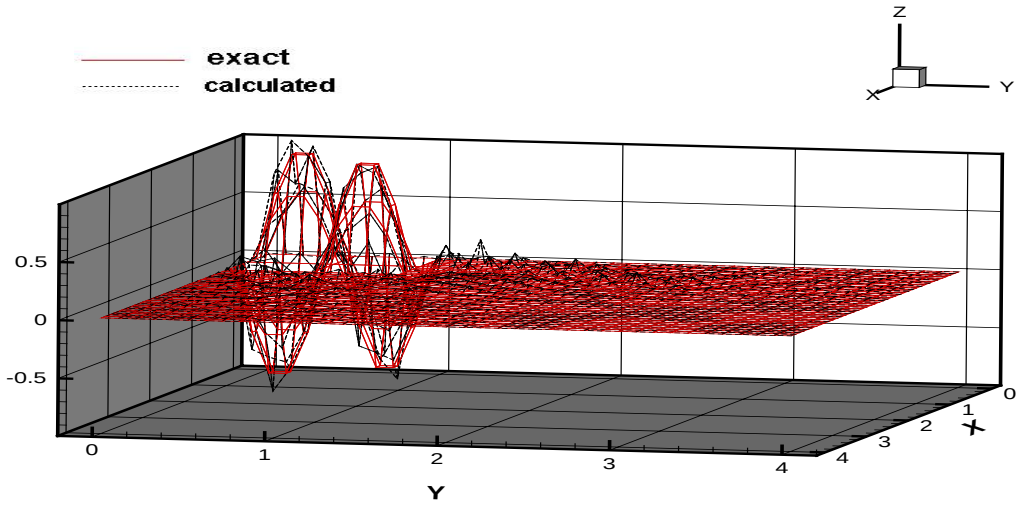

Figure 2.9: Test 2.2. Exact (red) and calculated (black) functions ψ in (2.59) with 25% noise in the boundary data.

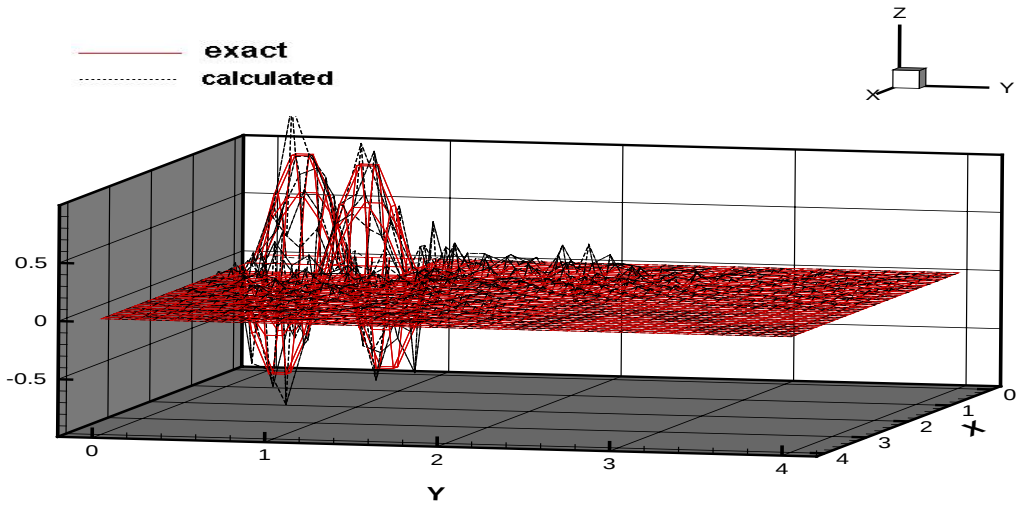

Figure 2.10: Test 2.2. Exact (red) and calculated (black) functions ψ in (2.59) with 50% noise in the boundary data.

value of (-0.9) is not achieved in the case when the term with χ_φ is not present. The calculated minimal value is (-0.7) in this case.

Test 2.4. *The $\varphi-$problem in $SQ(1)$ for $T > diam\, SQ\,(1)$.* We now test our method for the case when the boundary Cauchy data are given at the entire boundary of the rectangle $SQ\,(1)$ and $T > diam\, SQ\,(1)$. We take

$$T = 2,\ N_x = N_y = 20,\ N_t = 60.$$

The function (2.58) was reconstructed. Figure 2.13 displays the resulting image with 25% noise and Figure 2.14 displays the 1-dimensional cross-section of the image by the straight line $\{x_1 = 0.5\}$, as well as the 1-dimensional cross-section of the image for the case when the term with χ_φ is not present in (2.30) (with 25% noise). One can observe that both images are very close to the correct one. This points towards the fact, which follows from the theory of above cited publications and also from Theorem 2.1: the presence of terms with χ_φ and χ_ψ is important only when $T \in (R, 2R)$ and

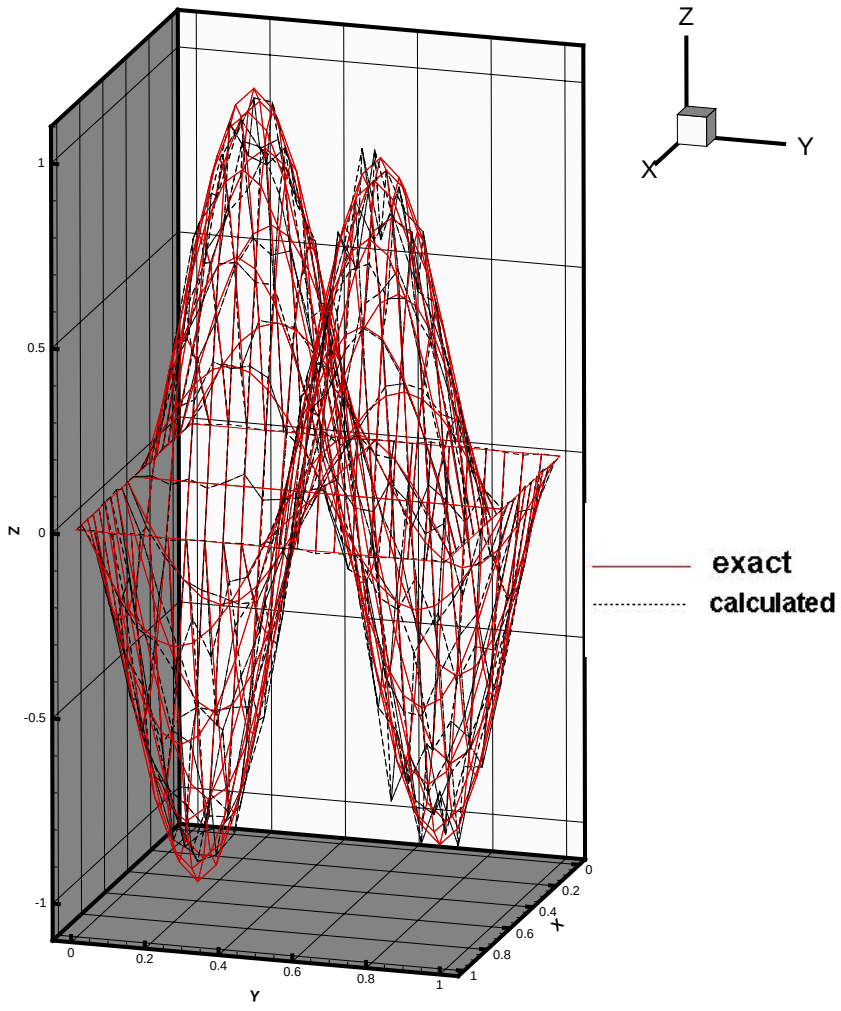

Figure 2.11: Test 2.3. Exact (red) and calculated (black) solutions of the problem $\varphi-$ in SQ(1) with 25% noise in the boundary data for $T = 0.75$.

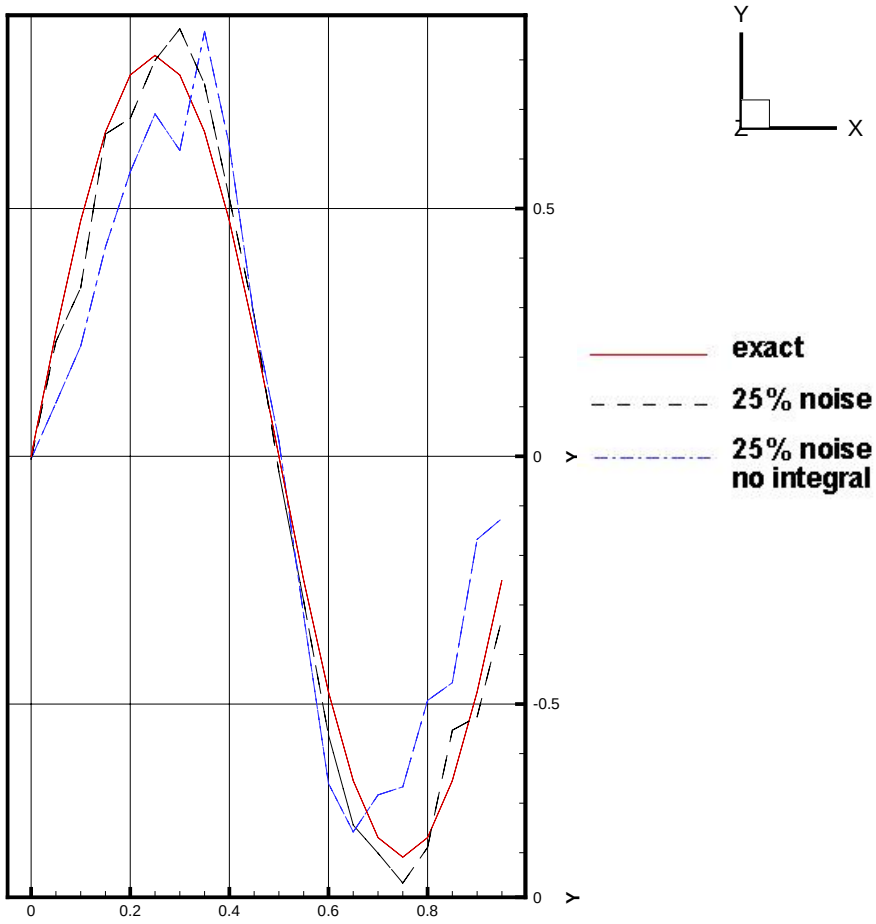

Figure 2.12: Test 2.3. Cross sections of exact (red) and calculated (black, blue) functions φ with 25% noise in the boundary data for $T = 0.75$, "no integral" means $\chi_\varphi = 0$. The maximal value of the exact function is $0.9 < 1$ only because of the grid step size.

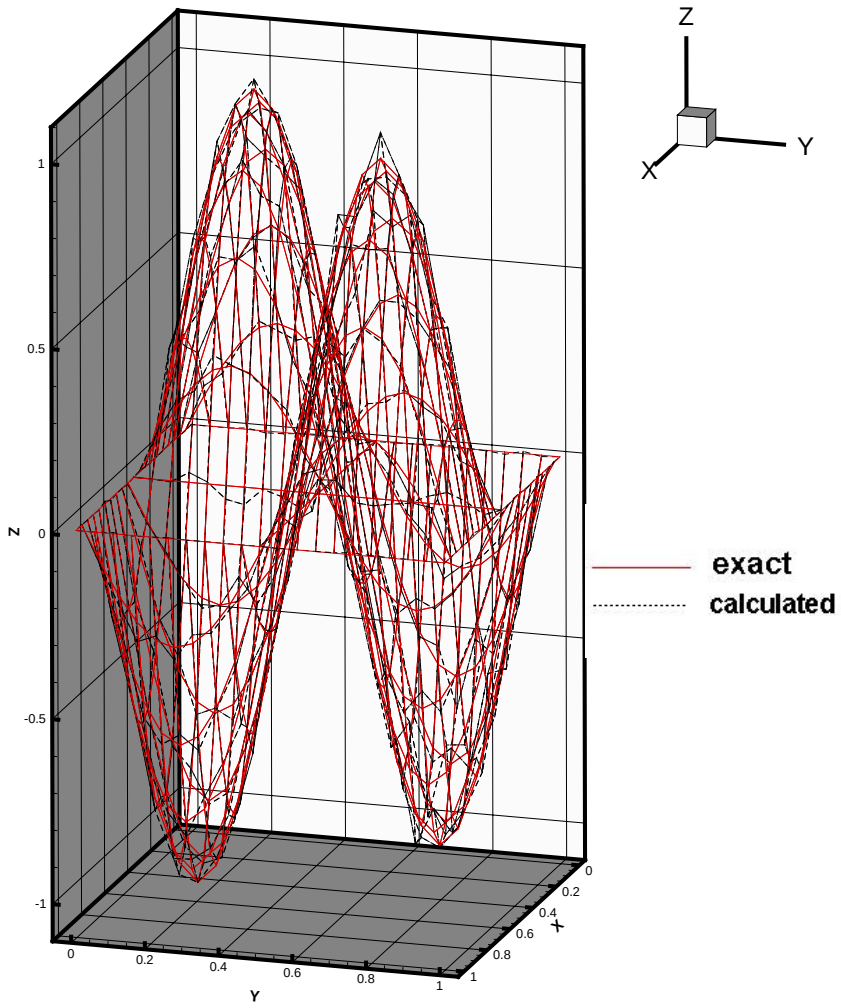

Figure 2.13: Test 2.4. Exact (red) and calculated (black) solutions of the $\varphi-$ problem in SQ(1) with 25% noise in the boundary data for $T = 2$.

it is unimportant for $T > 2R$.

Test 2.5. *The $\varphi-$problem with two $\delta-$functions.* We now again consider the Inverse Problem 2 with the domain Ω as in (2.55) and with $\psi(x) \equiv 0$. The data for the forward problem were simulated for the case

$$\varphi(x_1, x_2) = \delta(x_1 - 0.4, x_2 - 0.4) + \delta(x_1 - 0.7, x_2 - 0.7) \tag{2.60}$$

with the above described finite difference analogue of the $\delta-$ function. Figure 2.15

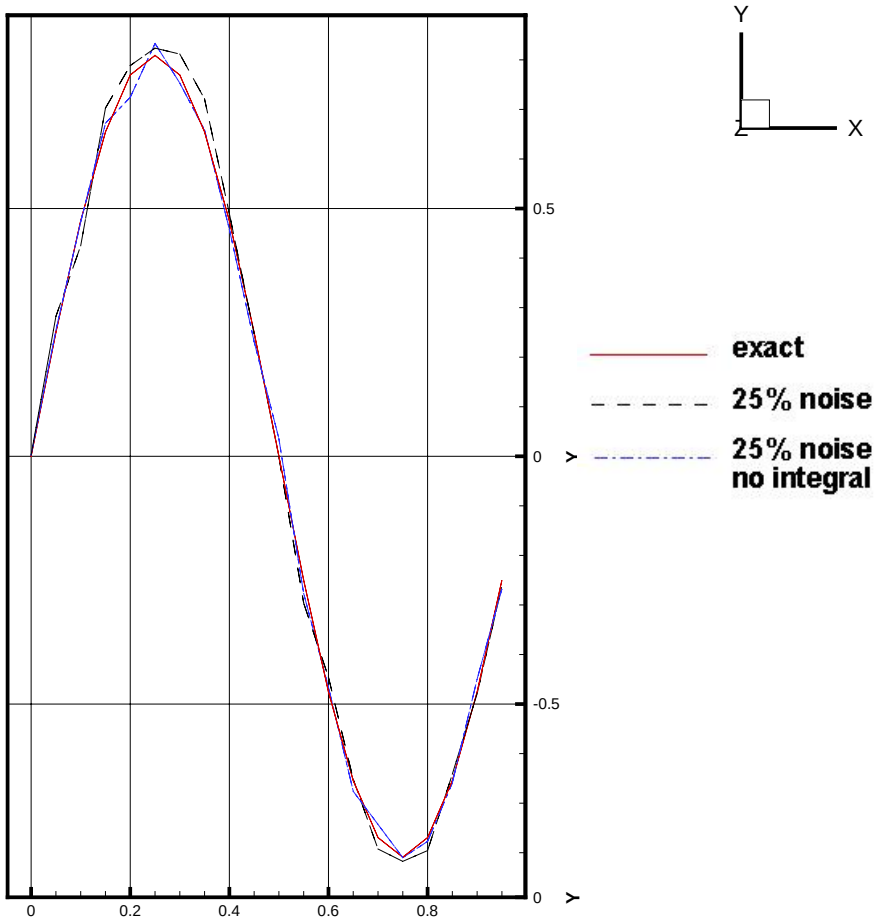

Figure 2.14: Test 2.4. Cross sections of exact (red) and calculated (black, blue) functions φ with 25% noise in the boundary data for $T = 2$, "no integral" means $\chi_\varphi = 0$. The maximal value of the exact function is $0.9 < 1$ only because of the grid step size.

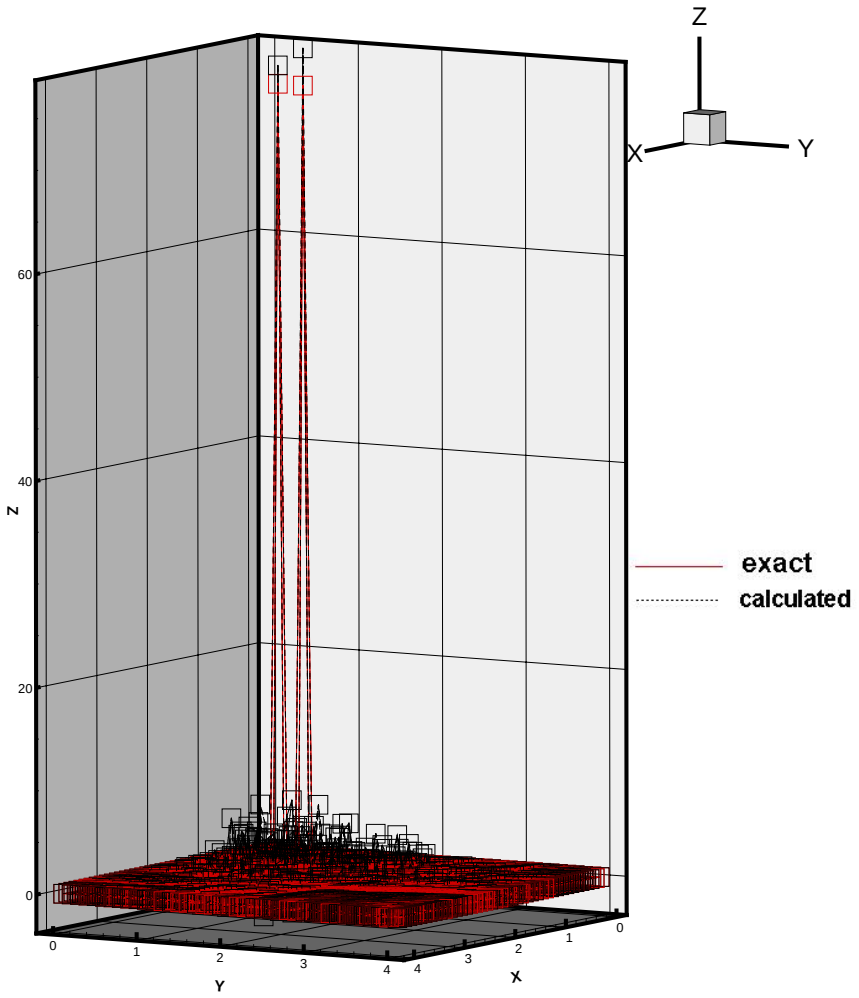

Figure 2.15: Test 2.5. Exact (red) and calculated (black) function φ with 50% noise in the boundary data. The function χ_φ in (2.30) is present. Scatter plot mode. Squares show heights. Correct heights are achieved.

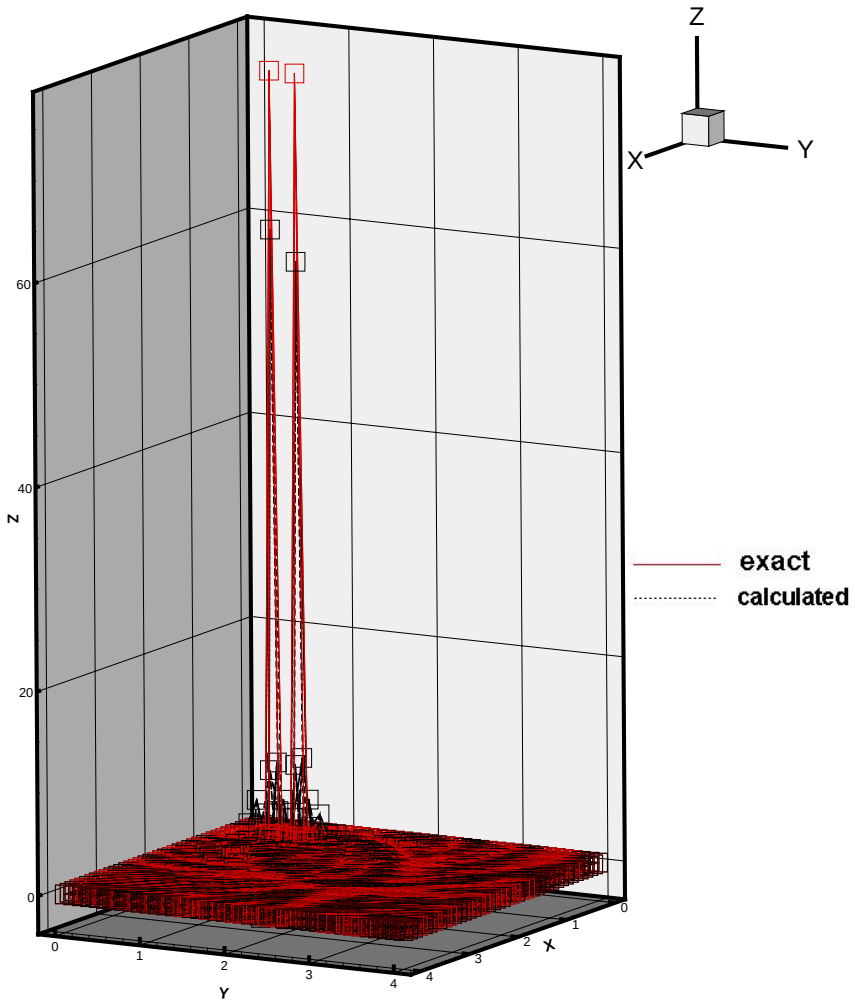

Figure 2.16: Test 2.5. Exact (red) and calculated (black) function φ with 5% noise in the boundary data and $\chi_\varphi = 0$. Scatter plot mode. Squares show heights. Correct heights are not achieved.

displays the resulting image of the function (2.60) for the case of 50% of the noise in the boundary data, scatter plot mode was used, squares show exact height. Figure 2.16, on the other hand, shows the image when the term with χ_φ is absent in (2.30) and only 5% noise in the data is present. One can see that the correct height is not reached on Figure 2.16, unlike Figure 2.15. This again shows the importance of the introduction of terms in the third line of (2.30).

Very similar results (not shown) were obtained for the $\psi-$problem with exactly the same $\delta-$ functions as ones in (2.60).

2.8 Conclusions

We have considered the inverse problems of the determination of one of initial condition in a hyperbolic equation using the lateral Cauchy data. We have presented applications of these problems to the thermoacoustic tomography, as well as to linearized inverse acoustic and inverse electromagnetic problems. The problems we consider are very close ones with the Cauchy problems for hyperbolic equations with the lateral data, and we have actually solved the latter numerically in Tests 2.3 and 2.4. We have focused on the inverse problem in an infinite domain (octant), whereas only finite domains were considered in previous numerical studies. Nevertheless, we are able to reduce our inverse problem to one in a finite domain due to the finite speed of propagation of waves. Since one initial condition is known, we were able to decrease the observation time T by twofold. We have shown numerically that it is important to know one of initial conditions if $T < diameter\,(\Omega)$, as it is required by stability and uniqueness results. However, if $T > diameter\,(\Omega)$, then both the theory and our numerical result of Test 2.4 show that one does not need to know the initial condition.

We have proposed a new version of the Quasi-Reversibility method. The main new element of this version is the inclusion of the terms characterizing *a priori* knowledge of one of initial conditions. Two other new elements are incorporation

of boundary terms in the Tikhonov functional instead of subtracting off boundary conditions and the use of finite differences instead of finite elements in the inverse solver. To prove convergence of this new version, we have modified the technique of previous works, which is based on Carleman estimates. A comprehensive numerical study of the proposed numerical method was conducted. This study has demonstrated robustness of our technique with respect up to 50% random noise in the data, similarly with previous publications [4, 13, 16]. This study has also demonstrated that this method is capable to image sharp peaks, which is important for the application to thermoacoustic tomography, for example.

CHAPTER 3: GLOBALLY CONVERGENT NUMERICAL METHOD FOR A HYPERBOLIC COEFFICIENT INVERSE PROBLEM IN THE 1D CASE

3.1 Statements of Forward and Inverse Problems

As the forward problem, we consider the Cauchy problem for a hyperbolic PDE

$$c(x)\,u_{tt} = u_{xx} \text{ in } \mathbb{R}\times(0,\infty), \tag{3.1}$$

$$u(x,0) = 0, u_t(x,0) = \delta\left(x-x^0\right), \tag{3.2}$$

where $x^0 < 0$. Equation (3.1) governs, e.g., propagation of acoustic and electromagnetic waves. In the acoustical case $1/\sqrt{c(x)}$ is the sound speed. In the 2-D case of EM waves propagation in a non-magnetic medium the coefficient $c(x)$ is $c(x) = (\mu\epsilon)(x)$, where μ and ϵ are respectively the magnetic permeability and the electric permittivity of the medium, see [32] for the derivation of (3.1) from Maxwell's equations in the 2-D case. We assume that the function $c(x)$ satisfies the following conditions

$$c(x) \geq 1, c(x) = 1 \text{ for } x \in \mathbb{R}\diagdown[0,1], \tag{3.3}$$

$$c(x) \in C^1(\mathbb{R}). \tag{3.4}$$

Consider the Laplace transform of the functions u,

$$w(x,s) = \int_0^\infty u(x,t)e^{-st}dt, \text{ for } s \geq \underline{s} = const. > 0, \tag{3.5}$$

where $\underline{s}$ is a certain number. In principle, it is sufficient to choose $\underline{s}$ such that the integral (3.3) would converge, although we choose $\underline{s}$ experimentally in our numerical

studies. We call the parameter s *pseudo frequency*. Equation for the function w is

$$w_{xx} - s^2 c(x) w = -\delta\left(x - x^0\right), \forall s \geq \underline{s}, \tag{3.6}$$

$$\lim_{|x|\to\infty} w(x,s) = 0, \forall s \geq \underline{s}. \tag{3.7}$$

Lemma 3.1. Assume that conditions (3.3) and (3.4) hold and let $x^0 < 0$. Let the function $w(x,s) \in C^2\left(\mathbb{R}^3 \diagdown \{|x - x^0| < \varepsilon\}\right), \forall \varepsilon > 0$ be the solution of the problem (3.6), (3.7). Then the following asymptotic behavior of the function w is valid for $x \neq x^0$, $k = 0, 1; j = 0, 1, 2$

$$D_x^j D_s^k w(x,s) = D_x^j D_s^k \left\{ (2s)^{-1} \exp\left[-s \left| \int_{x^0}^{x} \sqrt{c(\xi)} d\xi \right| \right] \left[1 + O\left(\frac{1}{s}\right) \right] \right\}, s \to \infty. \tag{3.8}$$

Proof. Introduce a new variable $y = y(x)$ and new functions P, a,

$$\begin{aligned} y &= y(x) = \int_{x^0}^{x} \sqrt{c(\xi)} d\xi + x^0, \\ P(y,t) &= u(x(y),t) c^{-1/4}(y), \\ a(y) &= c^{1/4}(y)((c^{-1/4}(y))'' - 2(c^{-1/4}(y)))'. \end{aligned}$$

Then $P(y,t)$ is the solution of the following Cauchy problem

$$\begin{aligned} P_{tt}(y,t) - P_{yy}(y,t) &= -a(y) P(y,t), \\ P(y,0) &= 0, P_t(y,0) = \delta\left(y - x^0\right). \end{aligned}$$

Note that the coefficient $a(y)$ has a finite support. Using D'Alembert formula for the 1-D non-homogeneous wave equation and using the fundamental solution of this equation, one can represent the function P as the solution of a Volterra-like integral

equation, thus coming up with the following properties

$$P(y,t)|_{0<t<|y-y_0|} \equiv 0, P(y,t) = \frac{1}{2} + P_1(y,t),$$

where the function P_1 is such that $P_1 \in C^2\left(t \geq |y-x^0|\right), P_1(y,|y-x^0|) = 0$. Consider the Laplace transform of the functions P,

$$A(y,s) = \int\limits_0^\infty P(y,t)e^{-st}dt, \text{ for } s \geq \underline{s} = const. > 0.$$

Then

$$A(y,s) = \int\limits_0^\infty P(y,t)e^{-st}dt = \int\limits_{|y-x^0|}^\infty (\frac{1}{2} + P_1(y,t))e^{-st}dt =$$

$$\frac{1}{2s}\exp\left(-s\left|y-x^0\right|\right) + \frac{1}{s^2}\exp\left(-s\left|y-x^0\right|\right)P_{1t}(y,|y-x^0|) - \frac{1}{s^2}\int\limits_{|y-x^0|}^\infty e^{-st}P_{1tt}(y,t)dt$$

$$= \frac{\exp\left(-s\left|y-x^0\right|\right)}{2s}\left[1 + O\left(\frac{1}{s}\right)\right], s \to \infty.$$

Since $w(x,s) = A(y(x),s)$, then we obtain (3.8). $\square$

Inverse Problem. Suppose that the coefficient $c(x)$ in equation (3.6) satisfies conditions (3.3), (3.4) and is unknown in the interval $(0,1)$. Determine the function $c(x)$ for $x \in (0,1)$, assuming that the following functions $\varphi_0(s), \varphi_1(s)$ are known for a single source position $x^0 < 0$

$$w(0,s) = \varphi_0(s), \quad w_x(0,s) = \varphi_1(s), \forall s \in [\underline{s}, \overline{s}], \tag{3.9}$$

where $\overline{s} > \underline{s}$ is a number, which should be chosen experimentally in numerical studies.

We note that in experiments usually only the function $\varphi_0(s)$ can be made available as the Laplace transform (3.5) of $u(0,t)$. However, since the coefficient $c(x) = 1$ is

known for $x < 0$, then solving the forward problem (3.6), (3.7) for $x \in (-\infty, 0)$ with the boundary condition $w(0,s) = \varphi_0(s)$, one can uniquely determine the function $w(x,s)$ for $x < 0$, thus coming up with the function $w_x(0,s) = \varphi_1(s)$.

3.2 Layer Stripping with Respect to the Pseudo Frequency

By the maximum principle $w(x,s) > 0$. Hence, we can consider the function $\widetilde{v} = \ln w / s^2$. Then (3.6) leads to

$$\widetilde{v}_{xx} + s^2 \widetilde{v}_x^2 = c(x), \quad x \in (0,1), \tag{3.10}$$

$$\widetilde{v}(0,s) = \varphi_2(s), \quad \widetilde{v}_x(0,s) = \varphi_3(s), \ \forall s \in [\underline{s}, \overline{s}], \tag{3.11}$$

where $\varphi_2 = \ln \varphi_0 / s^2, \varphi_3 = \varphi_1 / (s^2 \varphi_0)$. The term $\delta(x - x^0)$ is not present in (3.10) because $x^0 \notin (0,1)$. We now eliminate $c(x)$ from equation (3.10) via the differentiation with respect to s, since $\partial_s c(x) = 0$. Introduce a new function $q(x,s) = \partial_s \widetilde{v}(x,s)$. Lemma 3.1 implies that

$$D_x^j(\widetilde{v}) = O\left(\frac{1}{s}\right), D_x^j(q) = O\left(\frac{1}{s^2}\right), s \to \infty; j = 0,1,2, \tag{3.12}$$

$$\widetilde{v}(x,s) = -\int_s^\infty q(x,\tau)\, d\tau. \tag{3.13}$$

We truncate the integral in (3.13) as

$$\widetilde{v}(x,s) = -\int_s^{\overline{s}} q(x,\tau)\, d\tau + V(x), \tag{3.14}$$

where $\overline{s} > s_0$ is a large parameter which should be chosen in numerical experiments and $V(x) = \widetilde{v}(x, \overline{s})$. We call the function $V(x)$ in (3.14) the "tail". It is important that the tail function is unknown. On the other hand, by (3.12) the tail is small for the large values of $\overline{s}$. However, the numerical experience of [27–29, 31] shows that

it would be better to somehow approximate the tail function via updating it in an iterative procedure. Since the tail function $V(x)$ is unknown, the follow up equation (3.15) contains two unknowns: q and V. Nevertheless, we can approximate both these functions, because we treat them differently. Indeed, while we approximate the function q via inner iterations, we approximate the function V via outer iterations, see section 3.3 and also [27–29, 31] for this issue.

Thus, we obtain from (3.14)-(3.16) the following (approximate) nonlinear integral differential equation

$$q_{xx} - 2s^2 q_x \int_s^{\overline{s}} q_x(x,\tau)\, d\tau + 2s \left[\int_s^{\overline{s}} q_x(x,\tau)\, d\tau \right]^2 \tag{3.15}$$

$$+2s^2 q_x V' - 4sV' \int_s^{\overline{s}} q_x(x,\tau)\, d\tau + 2s\left(V'\right)^2 = 0.$$

In addition, (3.11), (3.12) and (3.15) imply that the following Dirichlet and Neumann boundary conditions ψ_0, ψ_1 are given for the function q

$$q(0,s) = \psi_0(s), q_x(0,s) = \psi_1(s), \ \forall s \in [\underline{s}, \overline{s}], \tag{3.16}$$

where $\psi_0(s) = \varphi_2'(s), \psi_1(s) = \varphi_3'(s)$. We now find the Neumann boundary condition for the function q at $x = 1$. By (3.3), (3.6) and (3.7) $w(x,s) = C(s)\, e^{-sx}$ for $x \geq 1$. Hence,

$$q_x(1,s) = s^{-2}. \tag{3.17}$$

If integrals would be absent in (3.15) and also the tail function would be known, then the problem (3.17), (3.16) would be trivial Cauchy problem for the linear ODE. However, the presence of integrals implies the nonlinearity, which is the main difficulty here. Furthermore, solving the problem (3.15), (3.16) as the Cauchy problem would lead to the instability with respect to x because of the nonlinearity. Indeed, the

classic existence theorem for the Cauchy problem for a nonlinear ODE guarantees existence only in a small x-interval. In addition, this approach would not give us a lot of information for our target 2-D and 3-D problems. Thus, below we focus on the following question: *How to solve numerically the problem (3.17), (3.18), (3.19)?*

We approximate the function $q(x,s)$ as a piecewise constant function with respect to the pseudo frequency s. That is, we assume that there exists a partition $\underline{s} = s_N < s_{N-1} < ... < s_1 < s_0 = \overline{s}$ of the interval $[\underline{s}, \overline{s}]$ with the sufficiently small grid step size $h = s_{i-1} - s_i$ such that $q(x,s) = q_n(x)$ for $s \in (s_n, s_{n-1}]$. We approximate the boundary condition (3.16), (3.17) as a piecewise constant function,

$$q_n(0) = \overline{\psi}_{0,n},\ q_n'(0) = \overline{\psi}_{1,n},\ q_n'(1) = s_n^{-2}, \tag{3.18}$$

where $\overline{\psi}_{0,n}$ and $\overline{\psi}_{1,n}$ are averages of functions ψ_0 and ψ_1 over the interval (s_n, s_{n-1}). Rewrite (3.15) for $s \in (s_n, s_{n-1}]$ using this piecewise constant approximation. Then multiply the resulting approximate equation by the s-dependent Carleman Weight Function (CWF) of the form

$$\mathcal{C}_{n,\lambda}(s) = \exp\left[-\lambda\left|s - s_{n-1}\right|\right], s \in (s_n, s_{n-1}] \tag{3.19}$$

and integrate with respect to $s \in (s_n, s_{n-1}]$. We obtain the following approximate equation for the function $q_n(x)$

$$\begin{aligned} q_n'' - A_{1,n}\left(h\sum_{j=1}^{n-1} q_j' - V'\right)q_n' &= B_n\left(q_n'\right)^2 - A_{2,n}h^2\left(\sum_{j=1}^{n-1} q_j'(x)\right)^2 \\ +2A_{2,n}V'\left(h\sum_{j=1}^{n-1} q_j'\right) - A_{2,n}\left(V'\right)^2, n &= 1, ..., N, \end{aligned} \tag{3.20}$$

where $A_{1,n} = A_{1,n}(\lambda, h), A_{2,n} = A_{2,n}(\lambda, h), B_n = B_n(\lambda, h)$ are certain parameters

depending on λ and h, see details in [27]. An important point is that

$$|B_n(\lambda, h)| \leq 8\overline{s}^2\lambda^{-1}, \text{ for } \lambda h, \overline{s} \geq 1. \tag{3.21}$$

Therefore by taking $\lambda >> 1$, we mitigate the influence of the nonlinear term with $(q_n')^2$ in (3.19) and this is why the CWF was introduced.

The idea is to approximately solve the sequence of boundary value problems (3.18), (3.20) sequentially starting from q_1. Since boundary conditions (3.18) are over-determined ones, it seems natural to somehow apply a version of the QRM here, because it is designed to solve boundary value problems with over-determined boundary conditions. In fact, we will iterate with respect to the nonlinear term in (3.20) because of (3.21). Hence, on each iterative step we will solve a linear problem derived from (3.18), (3.20) and the QRM will find the "least squares" solution of the latter. The reason why, in addition to functions q_n, we can also approximate the tail function V is that V is approximated from outer iterations, which means that we treat functions q_n and V differently.

Remark 3.1. *Our attempts to use in (3.18) only one boundary condition at $x = 0$ and the second one at $x = 1$ did not produce good quality images, unlike the 2-D and 3-D cases of complete data collection [27–29, 31]. Both types of the boundary condition at $x = 1$ were tried, Dirichlet and Neumann, and neither produced good results. We conjecture that this is because the 1-D case is less informative than multidimensional cases, basically because the wave cannot get around an abnormality. Thus, we use in our computations over-determined boundary data (3.18) and also add one more piece of data sometimes, namely, $q_n(1)$. In computations the above integrals with the CWF, which generate parameters $A_{1,n}, A_{2,n}, B_n$, should be calculated in closed forms. This is because the function $\mathcal{C}_{n,\lambda}(s)$ changes rapidly for large λ, which means that the integration step size should be taken too small. In principle, one can decrease the step*

size h in the s-direction instead of using the CWF. However, the introduction of the CWF provides more flexibility for the choice of parameters for computations, since parameters h and λ are independent, as long as $\lambda h \geq 1$. In addition, taking h too small would increase the computational time, because one would need to compute too many functions q_n then.

3.3 The Algorithm

Our algorithm reconstructs iterative approximations $c_{n,k}(x) \in C[0,1]$ of the function $c(x)$. On the other hand, to iterate with respect to tails, we need to solve the forward problem (3.6), (3.7) in $\mathbb{R}$ on each iterative step. To do this, we need to extend each function $c_{n,k}(x)$ outside of the interval $(0,1)$. A numerical procedure of this extension is described on (3.84). Thus we assume below that $c_{n,k}(x) \in C(\mathbb{R})$ and $c_{n,k}(x) = 1$ for $x \in \mathbb{R} \setminus (0,1)$. In addition, in the course of our algorithm we use cut-offs to ensure that $c_{n,k}(x) \geq 1$ in $(0,1)$.

3.3.1 Iterative Process

We now describe the algorithm step-by-step. Each step requires an approximate solution of an analog of the boundary value problem (3.18), (3.20). This is done via the QRM, which is described in subsection 3.3.2.

Step 1^1. Choose an initial tail function $V_{1,1}(x) \in C^2[0,1]$. Choose a large parameter $\lambda >> 1$. To compute the first approximation $q_{1,1}$ for the function q_1 with this tail, use the QRM of subsection 3.3.2 to find an approximate solution of the following over-determined boundary value problem in $(0,1)$

$$\begin{aligned} q''_{1,1} + A_{1,1}V'_{1,1}q'_{1,1} &= -A_{2,1}\left(V'_{1,1}\right)^2, \\ q_{1,1}(0) &= \overline{\psi}_{0,1}, q'_{1,1}(0) = \overline{\psi}_{1,1}, q'_{1,1}(1) = s_1^{-2}. \end{aligned} \tag{3.22}$$

We obtain the function $q_{1,1} \in C^2[0,1]$. Reconstruct an approximation $\widetilde{c}_{1,1}(x) \in C[0,1]$ for the unknown coefficient $c(x)$ using the function $q_{1,1}(x)$ and formulas (3.10),

(3.14), where in (3.14) $V(x) := V_{1,1}(x, \overline{s})$ and in (3.10) $s := s_1$. Next, construct the function $c_{1,1}(x) \in C[0,1]$ via applying the cut-off as

$$c_{1,1}(x) = \max\left(\widetilde{c}_{1,1}(x), 1\right), x \in [0,1]. \tag{3.23}$$

Next, we extend the function $c_{1,1}(x) = 1$ for $x \in \mathbb{R} \setminus (0,1)$.

Step 1^k, $k \geq 2$. Iterate with respect to the tail. Suppose that the function $c_{1,k-1} \in C(\mathbb{R})$ is reconstructed. Solve the forward problem (3.6), (3.7), with $c(x) := c_{1,k-1}(x)$, $s = \overline{s}$. Let $w_{1,k}(x, \overline{s})$ be the solution of this forward problem. Update the tail function as

$$V_{1,k}(x) = \overline{s}^{-2} \ln w_{1,k}(x, \overline{s}) \in C^2[0,1].$$

Next, solve the boundary value problem for the equation

$$q''_{1,k} + A_{1,1} V'_{1,k} q'_{1,k} = B_n \left(q'_{1,k-1}\right)^2 - A_{2,1} \left(V'_{1,k}\right)^2$$

with the boundary conditions (3.22). We obtain the function $q_{1,k} \in C^2[0,1]$. Compute a new approximation $c_{1,k} \in C(\mathbb{R})$ for the unknown coefficient similarly with the Step 1^1. Make several steps $1^1, 1^2, .., 1^{m_1}$ (the number of steps is specified in our numerical experiments). Thus, we have m_1 iterations with respect to the tail. As a result, we obtain functions $q_{1,m_1} \in C^2[0,1], c_{1,m_1} \in C(\mathbb{R}), V_{1,m_1} \in C^2[0,1]$. Next, set

$$q_1 := q_{1,m_1} \in C^2[0,1], c_1 := c_{1,m_1} \in C(\mathbb{R}).$$

Step n^1. Having functions $q_1, ..., q_{n-1} \in C^2[0,1]$ and the tail function $V_{n-1,m_{n-1}} \in C^2[0,1]$, set $q_{n,0}(x) := q_{n-1}(x), V_{n,1}(x) := V_{n-1,m_{n-1}}(x)$ in $[0,1]$. Next, using the QRM, find an approximate solution of solve the following boundary value problem

(3.24) in $(0,1)$ for the function $q_{n,1}$

$$q''_{n,k} - A_{1,n}\left(h\sum_{j=1}^{n-1} q'_j - V'_{n,k}\right) q'_{n,k} = B_n\left(q'_{n,k-1}\right)^2 - A_{2,n}h^2\left(\sum_{j=1}^{n-1} q'_j(x)\right)^2 + \quad (3.24)$$
$$+2A_{2,n}V'_{n,k}\left(h\sum_{j=1}^{n-1} q'_j(x)\right) - A_{2,n}\left(V'_{n,k}\right)^2,$$
$$q_{n,k}(0) = \overline{\psi}_{0,n}, q'_{n,k}(0) = \overline{\psi}_{1,n}, q'_{n,k}(1) = s_n^{-2}.$$

where in (3.24) the vector function $(q_{n,k}, q_{n,k-1}, V_{n,k})$ is replaced with $(q_{n,1}, q_{n,0}, V_{n,1})$. Hence, we obtain the function $q_{n,1} \in C^2[0,1]$. Similarly with Step 1^1 compute a new approximation $c_{n,1} \in C(\mathbb{R})$ for the unknown coefficient $c(x)$ using the function $q_{n,1}(x)$, functions $q_1, ..., q_{n-1}$ and formulas (3.10), (3.14), where in (3.14) $V(x) := V_{n,1}(x)$ and in (3.10) $s := s_n$.

Step n^k, $k \geq 2$. Iterate with respect to the tail. Suppose that the function $c_{n,k-1} \in C(\mathbb{R})$ is constructed. Solve the forward problem (3.6), (3.7), in which $c(x) := c_{n,k-1}(x)$, $s = \overline{s}$. Let $w_{n,k}(x, \overline{s})$ be the solution of this forward problem. Update the tail function as $V_{n,k}(x) = \overline{s}^{-2} \ln w_{n,k}(x, \overline{s}) \in C^2[0,1]$. Next, find an approximate solution of the boundary value problem (3.24) via QRM. Reconstruct a new approximation $c_{n,k} \in C(\mathbb{R})$ for the unknown coefficient similarly with the Step 1^1. Make several steps $n^1, n^2, .., n^{m_n}$. Thus, we have iterated m_n times with respect to the tail. As a result, we obtain the functions q_n, c_n, V_{n,m_n}, where

$$q_n := q_{n,m_n} \in C^2[0,1], c_n := c_{n,m_n} \in C(\mathbb{R}), V_{n,m_n}(x) \in C^2[0,1].$$

If functions $c_n(x)$ did not yet converge, then proceed with Step $(n+1)^1$, provided that $n < N$. However, if either functions $c_n(x)$ converged, or $n = N$, then stop. The convergence criterion for functions $c_n(x)$, which we have established in our computational experiments, is described in section 3.6. In principle, however, there might be several convergence criteria, which indicates that a better one might be

found. Thus, we do not specify such a criterion in this section.

3.3.2 The quasi-reversibility method

Let

$$a_{n,k}(x) = A_{1,n}\left(h\sum_{j=1}^{n-1} q'_j - V'_{n,k}\right)$$

and let $H_{n,k}$ be the right hand side of equation (3.23). Then the boundary value problem (3.24) can be rewritten as

$$q''_{n,k} - a_{n,k}q'_{n,k} = H_{n,k}, \tag{3.25}$$

$$q_{n,k}(0) = \overline{\psi}_{0,n}, q'_{n,k}(0) = \overline{\psi}_{1,n}, q'_{n,k}(1) = s_n^{-2}. \tag{3.26}$$

Because of the over-determination of boundary conditions in (3.26), we find a "least squares" solution of this problem, for which the QRM is a very suitable one. In other words we minimize the following Tikhonov functional

$$J^{\varepsilon}_{n,k}(q) = \|q''(x) - a_{n,k}q'(x) - H_{n,k}\|^2_{L_2(0,1)} + \varepsilon\|q\|^2_{H^3(0,1)}, \tag{3.27}$$

subject to boundary condition (3.26), where the small regularization parameter $\varepsilon \in (0,1)$. Let $\widehat{q}$ be the minimizer of this functional. Then we set $q_{n,k}(x) := \widehat{q}(x)$. We note that the problem of local minima does not occur here because (3.27) is the sum of square norms of two expressions, which are linear with respect to q, also see Lemma 3.3 in section 3.4. The second term in the right hand side of (3.27) is the Tikhonov regularization term. We use the $H^3(0,1)$ norm here in order to ensure that the minimizer $\widehat{q} \in C^2[0,1]$. Indeed, by the embedding theorem $H^3(0,1) \subset C^2[0,1]$. The latter smoothness is used in turn to ensure that functions $c_{n,k} \in C[0,1]$, see the previous subsection.

3.4 Global Convergence Theorem

By the concept of Tikhonov for ill-posed problems [38], which we follow, one should assume first that there exists an "ideal" exact solution of an ill-posed problem with the "ideal" exact data. Next, one should assume the presence of an error of the level ζ in the data, where $\zeta > 0$ is a small parameter. Suppose that an approximate solution is constructed for each sufficiently small ζ. This solution is called a "regularized solution", if it tends to the exact solution as $\zeta \to 0$. Denote:

$$\|\cdot\|_2 := \|\cdot\|_{L^2(0,1)}, \|\cdot\|_{2,2} := \|\cdot\|_{H^2(0,1)}, \|\cdot\|_1 := \|\cdot\|_{C^1[0,1]}.$$

3.4.1 Exact solution

First, we briefly introduce the definition of the exact solution, see details in [27]. We assume that there exists a coefficient $c^*(x) \geq 1$ satisfying conditions (3.3), (3.4), and this function is an exact solution of our Inverse Problem with the exact data $\varphi_0^*(s), \varphi_1^*(s)$ in (3.9),

$$\varphi_0^*(s) = w^*(0,s), \ \varphi_1^*(s) = w_x^*(0,s), \ \forall s \in [\underline{s}, \overline{s}].$$

Here the function $w^*(x,s) \in C^2(\mathbb{R} \setminus \{|x - x^0| < \gamma\}), \forall \gamma > 0, \forall s \geq \underline{s}$ is the solution of the forward problem (3.6), (3.7) with $c(x) := c^*(x)$. Let

$$\widetilde{v}^*(x,s) = s^{-2} \ln[w^*(x,s)], \ q^*(x,s) = \partial_s \widetilde{v}^*(x,s), \ V^*(x) = \widetilde{v}^*(x,\overline{s}).$$

By (3.10)

$$c^*(x) = \widetilde{v}_{xx}^*(x,s) + s^2 (\widetilde{v}_x^*(x,s))^2. \tag{3.28}$$

The function q^* satisfies equation (3.15), in which the tail $V(x)$ is replaced with $V^*(x)$. Boundary conditions for q^* are the same as ones in (3.16) and (3.17) where

functions $\psi_0(s), \psi_1(s)$ are replaced with $\psi_0^*(s), \psi_1^*(s)$, where

$$\psi_0^*(s) = \left(\varphi_0^* s^2\right)^{-1} \partial_s \varphi_0^* - 2s^{-3} \ln \varphi_0^*, \ \psi_1^*(s) = \left(\varphi_1^* s^2\right)^{-1} \partial_s \varphi_1^* - 2s^{-3} \ln \varphi_1^*.$$

Definition. We call the function $q^*(x,s)$ *the exact solution* of the problem (3.15)-(3.17) with the exact boundary conditions $\psi_0^*(s), \psi_1^*(s)$.

Therefore, $q^*(x,s) \in H^3(0,1) \times C^\infty[\underline{s}, \overline{s}]$. We approximate functions $q^*(x,s)$ and $\psi^*(x,s)$ via piecewise constant functions with respect to $s \in [\underline{s}, \overline{s}]$. Let

$$q_n^*(x) = \frac{1}{h} \int\limits_{s_n}^{s_{n-1}} q^*(x,s)\, ds, \ \overline{\psi}_{0,n}^* = \frac{1}{h} \int\limits_{s_n}^{s_{n-1}} \psi^*(s)\, ds, \overline{\psi}_{1,n}^* = \frac{1}{h} \int\limits_{s_n}^{s_{n-1}} \psi_x^*(s)\, ds.$$

Hence, it is natural to assume that

$$\max_{1 \le n \le N} \|q_n^*\|_{H^3(0,1)} \ \le \ C^*, C^* \ge 1, \tag{3.29}$$

$$\left|\overline{\psi}_{0,n}^* - \overline{\psi}_{0,n}\right| + \left|\overline{\psi}_{1,n}^* - \overline{\psi}_{1,n}\right| \ \le \ C^*(\sigma + h), \tag{3.30}$$

where the constant $C^* = C^*\left(\|q^*\|_{H^3(0,1) \times C^1[\underline{s}, \overline{s}]}\right) > 0$ depends only on $H^3(0,1) \times C^1[\underline{s}, \overline{s}]$ norm of the function $q^*(x,s)$ and $\sigma > 0$ is a small parameter characterizing the level of the error in the data $\psi_0(s), \psi_1(s)$. We use $H^3(0,1)$ norm rather than $C^2[0,1]$ because of the quasi-reversibility, see (3.34). The parameter h can also be considered as a part of the error in the data, since we have replaced a smooth s-dependent function with a piecewise constant one. In addition

$$q_n^*(0) = \overline{\psi}_{0,n}^*, q_n^{*\prime}(0) = \overline{\psi}_{1,n}^*, q_n^{*\prime}(1) = s_n^{-2}. \tag{3.31}$$

The function q_n^* satisfies the following analogue of equation (3.23)

$$\begin{aligned} & q_n^{*''} - A_{1,n}\left[h\sum_{j=1}^{n-1} q_j^{*'}(x) - V^{*'}\right] q_n^{*'} \\ = \; & B_n\left(q_n^{*'}\right)^2 - A_{2,n}h^2\left(\sum_{j=1}^{n-1} q_j^{*'}(x)\right)^2 \\ & +2A_{2,n}V^{*'}\left(h\sum_{j=1}^{n-1} q_j^{*'}(x)\right) - A_{2,n}\left(V^{*'}\right)^2 + F_n(x,h,\lambda), \end{aligned} \tag{3.32}$$

where the function $F_n(x,h,\lambda) \in C[0,1]$ and

$$\max_{\lambda h \geq 1} \|F_n(x,h,\lambda)\|_2 \leq C^* h. \tag{3.33}$$

3.4.2 Estimates, existence and uniqueness for the quasi-reversibility

Lemma 3.2. *([14], page 188).* For any function $u(x) \in H^2(0,1)$, $u(0) = u'(0) = 0$, and for any $\mu \geq 1$ the following Carleman estimate holds

$$\int_0^1 (u'')^2 e^{-2\mu x} dx \geq \frac{1}{16}\int_0^1 [\mu(u')^2 + \mu^3 u^2 + 8(u'')^2] e^{-2\mu x} dx.$$

Lemma 3.3. Let functions $H \in L_2(0,1), a \in C[0,1], \|a\|_{C[0,1]} \leq a_0 = const.$. Consider the problem of the minimization of the functional $J^\varepsilon(u)$,

$$J^\varepsilon(u) = \|u'' + a(x)u' - H(x)\|_2^2 + \varepsilon\|u\|_{H^3(0,1)}^2, \tag{3.34}$$

subject to initial conditions

$$u(0) = u'(0) = 0, \tag{3.35}$$

where $\varepsilon \in (0,1)$ is a small parameter. Then there exists unique minimizer $u_0 \in H^3(0,1)$ of the functional (3.34) with conditions (3.35) and the following estimates

hold

$$\|u_\varepsilon\|_{H^3(0,1)} \leq \frac{C}{\sqrt{\varepsilon}} \|H\|_2 , \tag{3.36}$$

$$\|u_\varepsilon\|_{2,2} \leq K \|H\|_2 , \tag{3.37}$$

where the positive constant C depends only on the interval $(0,1)$ and

$$K = 8e^{\mu_0}, \mu_0 = \max\left(1, 64a_0^2\right). \tag{3.38}$$

In particular, if $\varepsilon = 0$, then the unique minimizer $u_0 \in H^2(0,1)$ also exists and (3.37) holds.

Proof. Let $(,)$ be the inner product in $L_2(0,1)$ and $[,]$ be the inner product in $H^3(0,1)$. Denote $Lu = u'' + au'$. Then (3.34) implies that the function u_ε must satisfy

$$(Lu_\varepsilon, Lv) + \varepsilon^2 [u_\varepsilon, v] = (H, Lv), \forall v \in H^3(0,1), v(0) = v'(0) = 0. \tag{3.39}$$

The Riesz theorem immediately implies existence and uniqueness of the function u_ε as well as the estimate (3.36). To prove (3.37), set $v := u_\varepsilon$. Then the Cauchy-Schwarz inequality and Lemma 3.2 imply that for any $\mu > 0$

$$\begin{aligned} \|H\|_2^2 &\geq (Lu, Lu) \geq \int_0^1 (Lu)^2 e^{-2\mu x} dx \geq \int_0^1 (\frac{1}{2}(u'')^2 - a_0^2 (u')^2) e^{-2\mu x} dx \\ &\geq \frac{1}{32} \int_0^1 [\mu (u')^2 + \mu^3 u^2 + 8(u'')^2] e^{-2\mu x} dx - \int_0^1 a_0^2 (u')^2 e^{-2\mu x} dx. \end{aligned}$$

Taking in this inequality $\mu = \mu_0$, we obtain (3.37). By (3.37) the scalar product $\{u, v\} := (Lu_\varepsilon, Lv)$ is defined and generates the norm, which is equivalent with the norm $\|\bullet\|_{2,2}$. Hence, the existence of the minimizer u_0 for the case $\varepsilon = 0$ follows from Riesz theorem. Next, estimate (3.37) for the case $\varepsilon = 0$ follows from the above. $\square$

Remark 3.2. *Since boundary terms at $x = 1$ are not involved in the Carleman estimate of Lemma 3.2, we do not use a boundary condition at $x = 1$ in our convergence analysis. Still, we use both Dirichlet and Neumann boundary conditions at $x = 1$ in numerical experiments, see section 3.6. While the Neumann boundary condition is natural to use for a better stability, see (3.18) and (3.26), the Dirichlet boundary condition is not desirable to employ. Nevertheless, the latter condition provides better results, see more discussion in subsections 3.6.6, 3.6.7. Naturally, Lemma 3.3 remains the same for the case of extra boundary conditions at $x = 1$, so as Theorem 3.1. Thus, (3.37) and (3.38) provide us with a specific constant K is used in the global convergence Theorem 3.1 instead of an unspecified constant K in the Schauder theorem, which was used in [27–29, 31]. We stress that although an estimate for K can be obtained via simply estimating the solution of the Cauchy problem $u'' + a(x)u' - H(x) = 0, u(0) = u'(0) = 0$, we use a different proof via the quasi-reversibility. The reason is twofold. First, we use the QRM in our numerical tests due to the over-determination in boundary conditions (Remark 3.1). Second, we wish to work out the methodology for 2D and 3D cases.*

3.4.3 Global convergence theorem

Assume that

$$\overline{s} > 1, \ \lambda h \geq 1. \tag{3.40}$$

Then [27] $\max_{1 \leq n \leq N} \{|A_{1,n}| + |A_{2,n}|\} \leq 8\overline{s}^2$. Introduce the constant

$$M^* = M^* \left(\|q^*\|_{C^2[0;L] \times C^1[\underline{s},\overline{s}]}, \overline{s} \right) = 16 C^* \overline{s}^2 \geq 2C^* \max_{1 \leq n \leq N} \{|A_{1,n}| + |A_{2,n}|\} \tag{3.41}$$

In the formulation of Theorem 3.1 we provide estimates via M^* and also use (3.41) to obtain estimates via $\overline{s}$. Recall that by the embedding theorem $H^2(0, L) \subset C^1[0, L]$. In the course of the proof of Theorem 3.1 we will estimate norms of differences $\|q_{n,k} - q_n^*\|_{2,2}$ between our approximate and exact solutions. Naturally, we will use Lemma

3.3 then. However, there is one inconvenience in this lemma linked with the zero Cauchy data (3.35). Thus, we assume that

$$\overline{\psi}_{0,n}^{*} = \overline{\psi}_{0,n}, \overline{\psi}_{1,n}^{*} = \overline{\psi}_{1,n}. \tag{3.42}$$

In principle, this assumption is not necessary. Indeed, one can consider the following functions instead $q_{n,k}, q_n^*$

$$\overline{q}_{n,k} = q_{n,k} - \overline{\psi}_{0,n} - x\overline{\psi}_{1,n}, \overline{q}_n^* = q_n^* - \overline{\psi}_{0,n}^* - x\overline{\psi}_{1,n}^*.$$

These functions satisfy (3.35). Equations for these functions can be obtained from the above equations for $q_{n,k}, q_n^*$ in an obvious fashion. Next, using estimates (3.30), one can modify both the formulation and the proof of Theorem 3.1 in a straightforward manner. We have chosen not to do so for the sake of brevity only. By the embedding theorem $H^2(0,1) \subset C^1[0,1]$ and with a positive constant $C_1 \geq 1$ the following inequality holds $\|f\|_1 \leq C_1 \|f\|_{2,2}, \forall f \in H^2(0,1)$.

Theorem 3.1. Suppose that (3.29), (3.40) and (3.42) hold. Let the exact coefficient $c^*(x)$ satisfies conditions (3.3), (3.4). For any function $c \in C(R)$ such that $c(x) \geq 1$, $c(x) = 1$ in $\mathbb{R} \setminus (0,1)$ consider the solution $w_c(x,\overline{s}) \in C^2(\mathbb{R} \setminus \{|x - x^0| < \gamma\}), \forall \gamma > 0$ of the problem (3.6), (3.7). Let $V_c(x) = \overline{s}^{-2} \ln w_c(x,\overline{s}) \in C^2(\mathbb{R} \setminus \{|x - x^0| < \gamma\}), \forall \gamma > 0$ be the corresponding tail function. Suppose that the cut-off pseudo frequency $\overline{s}$ is so large that for any such function $c(x)$ the following estimate holds

$$\|V_c\|_{C^2[0,1]} \leq \xi, \tag{3.43}$$

where $\xi \in (0,1)$ is a sufficiently small number. Let $V_{1,1}(x,\overline{s}) \in C^2[0,1]$ be the initial tail function and let

$$\|V_{1,1}\|_{C^2[0,1]} \leq \xi. \tag{3.44}$$

Denote $\eta = 2(h+\sigma+\varepsilon+\xi)$. Let in Lemma 3.3 $a_0 < 1$ and thus $K = 8e$. Let $\overline{N} \leq N$ be the total number of functions q_n calculated by the above algorithm. Suppose that the number $\overline{N} = \overline{N}(h)$ is connected with the step size h via $\overline{N}(h)\, h = \beta$, where the constant $\beta > 0$ is independent on h. Let β be so small that

$$\beta \leq \frac{1}{KM^* C_1} = \frac{1}{16KC^* \overline{s}^2 C_1} \leq \frac{1}{16KC^* \overline{s}^2}. \tag{3.45}$$

In addition, let the number η and the parameter λ of the CWF satisfy the following estimates

$$\eta \leq \eta_0(K, M^*) = \eta_0\left(\|q^*\|_{H^3(0,1)\times C^1[\underline{s},\overline{s}]}, \overline{s}\right) = \frac{1}{64K\overline{s}^2}, \tag{3.46}$$

$$\lambda \geq \lambda_0(K, M^*, \eta) = \max\left(\frac{(M^*C^*)^2}{4}, 3KM^*, \frac{1}{\eta^2}\right). \tag{3.47}$$

Then for every integer $n \in \left[1, \overline{N}\right]$ the following estimates hold

$$\|q_{n,k} - q_n^*\|_{2,2} \leq 2KM^*\left(\frac{1}{\sqrt{\lambda}} + \eta\right) \leq 64C^* K\overline{s}^2\eta, \tag{3.48}$$

$$\|q_{n,k}\|_{2,2} \leq 2C^*, \tag{3.49}$$

$$\|c_{n,k} - c^*\|_2 \leq KM^*\left(\frac{1}{\sqrt{\lambda}} + \eta\right) \leq 32C^*\overline{s}^2\eta. \tag{3.50}$$

Remark 3.3. *1. Although by (3.45) and (3.46) parameters β and η seem to be too small, it often happens in the computational practice of inverse problems that theoretical estimates in convergence theorems are more pessimistic than ones obtained in numerical studies. And our computational experience shows that one can choose reasonable values of these parameters. Still, Theorem 3.1 ensures the global convergence, which is important for computations.*

2. The convergence estimate (3.50) depends on a parameter $\eta = 2(h+\sigma+\varepsilon+\xi)$, in which parameters h, ε, ξ, although sufficiently small of course, cannot be made too

small in any particular computation. So, Theorem 3.1 basically tells one that one can indeed get a good first approximation for the solution. But as soon as (3.50) holds, one cannot guarantee that all follow up iterations would lead to a solution, which would be closer to the exact than one on a few first ones. A logical conclusion from this is that one should consider a two stage numerical procedure. On the first stage one would obtain a good first guess for the solution using the above globally convergent method. And on the second stage one would use a locally convergent numerical method, which, however, would take the solution obtained on the first stage as the first approximation. The point is that locally convergent numerical methods do not depend on parameters h, ε, ξ. *Still, the* main input *which any locally convergent numerical methods needs is a good first guess for the solution, and this is exactly what the globally convergent part provides. Such a two stage procedure was recently implemented in [29, 31] in 2-D and 3-D cases of the data collection at the entire boundary. However, when working on this 1-D case, we were not prepared to use the second stage here. Hence, we have appropriately modified the algorithm of section 3.3. The main point is that Theorem 3.1 is basically valid for this modification, see subsection 3.6.2.*

3. Truncating integrals at a high pseudo frequency $\overline{s}$ *is a natural thing to do, because one routinely truncates high frequencies in physics and engineering. By truncating integrals, we actually come up with a different, although a quite reasonable mathematical model. One of the back bones of the theory of ill-posed problems is that the number of iterations can be chosen as a regularization parameter, see, e.g., page 157 of [34]. Therefore, we have a vector* $\left(\overline{s}, \overline{N}, m_1, ..., m_{\overline{N}}\right)$ *of regularization parameters. Setting* $\overline{N}(h)\, h = \beta = const. > 0$ *is in an agreement with, e.g., Lemma 6.2 on page 156 of [34], since this lemma shows a connection between the error in the data and the number of iterations (that lemma is proven for a different algorithm).*

We assume below in this section that conditions of Theorem 3.1 hold. We obtain

from (3.40), (3.41), (3.46) and (3.47) that

$$\frac{M^*C^*}{2\sqrt{\lambda}} \leq 1, \frac{3KM^*}{\lambda} < 1, \frac{1}{\sqrt{\lambda}} \leq \eta. \tag{3.51}$$

Denote

$$\widetilde{q}_{n,k} = q_{n,k} - q_n^*, \widetilde{V}_{n,k} = V_{n,k} - V^*,\ \widetilde{c}_{n,k} = c_{n,k} - c^*.$$

We first prove

Lemma 3.4. Suppose that estimates (3.48), (3.49) are true for functions $q_1, ..., q_{n-1}$ as well as for functions $q_{n,1}, ..., q_{n,k}$ $(1 \leq k \leq m_n)$. Then the estimate (3.50) holds.

Proof. Introduce functions $\widetilde{v}_{n,k}(x), \widetilde{v}_n^*(x)$ as

$$\widetilde{v}_{n,k}(x) = -h\left(\sum_{j=1}^{n-1} q_j(x) + q_{n,k}(x)\right) + V_{n,k}(x), \tag{3.52}$$

$$\widetilde{v}_n^*(x) = -h\left(\sum_{j=1}^{n-1} q_j^*(x) + q_n^*(x)\right) + V^*(x). \tag{3.53}$$

It follows from the definition of functions $q_n^*(x)$ that $\widetilde{v}_n^*(x) = \widetilde{v}^*(x, s_n)$. By our algorithm $c_{n,k}(x) = \widetilde{v}_{n,k}''(x) + s_n^2\left(\widetilde{v}_{n,k}'(x)\right)^2$. Subtracting (3.28) (at $\underline{s} := s_n$) from this formula, we obtain

$$\widetilde{c}_{n,k} = \left(\widetilde{v}_{n,k}'' - \widetilde{v}_n^{*\prime\prime}\right) + s_n^2\left(\widetilde{v}_{n,k}' - \widetilde{v}_n^{*\prime}\right)\left(\widetilde{v}_{n,k}' + \widetilde{v}_n^{*\prime}\right). \tag{3.54}$$

By (3.43), (3.45), (3.48), (3.52) and (3.53)

$$\|\widetilde{v}_{n,k} - \widetilde{v}_n^*\|_{2,2} \leq 2KM^*\beta\left(\frac{1}{\sqrt{\lambda}} + \eta\right) + \eta \leq \frac{1}{8}\left(\frac{1}{\sqrt{\lambda}} + \eta\right) + \eta \leq \left(\frac{1}{\sqrt{\lambda}} + \eta\right). \tag{3.55}$$

(3.40), (3.41), (3.43), (3.45), (3.46), (3.49), (3.52) and (3.53) imply that $\|\widetilde{v}_{n,k} + \widetilde{v}_n^*\|_1 \leq 4C^*C_1\beta + \eta \leq 4C^*$. Combining this with (3.46), the third inequality (3.51), (3.54)

and (3.55), we obtain

$$\left\|\widetilde{c}_{n,k}\right\|_2 \leq M^* \left(\frac{1}{\sqrt{\lambda}} + \eta\right) \leq 32 C^* \overline{s}^2 \eta,$$

which is (3.50). $\square$

Lemma 3.5. Assume that (3.49) holds. Then the following estimate is true

$$\left\| A_{1,n} \left(h \sum_{j=1}^{n-1} q_j' - V_{n,k}' \right) \right\|_{C[0,1]} \leq \frac{1}{8}.$$

Proof follows immediately from (3.41), (3.45) and (3.46). $\square$

Corollary 1. *In conditions of Theorem 3.1* $K = 8e$.

This Corollary follows immediately from Lemmata 3.3 and 3.5.

Proof of Theorem 3.1 This proof basically consists in estimating norms $\left\|\widetilde{q}_{n,k}\right\|_{2,2}$ for $k = 1, ..., m_n$ from the above. Compared with proofs in [27,31], the main difficulty here is that we have to analyze integral identities which come out of (3.39), instead of pointwise equations. We start from$\left\|\widetilde{q}_{1,k}\right\|_1$. By (3.43) and (3.44)

$$\left\|\widetilde{V}_{1,1}\right\|_1 \leq 2\xi \leq \eta. \tag{3.56}$$

Let $L_{1,1} q_{1,1} = q_{1,1}'' + A_{1,1} V_{1,1}' q_{1,1}$. Then (3.32),(3.39) imply that for all $v \in H^3(0,1), v(0) = v'(0) = 0$

$$\left(L_{1,1} q_{1,1}, L_{1,1} v\right) + \varepsilon \left[q_{1,1}, v\right] = \left(-A_{2,1} \left(V_{11}'\right)^2, L_{1,1} v\right), \tag{3.57}$$

$$\left(L_{1,1} q_1^*, L_{1,1} v\right) + \varepsilon \left[q_1^*, v\right] = \left(B_1 \left(q_1^{*\prime}\right)^2 + A_{1,1} \widetilde{V}_{1,1}' q_1^* - A_{2,1} \left(V^{*\prime}\right)^2 + F_1, L_{1,1} v\right) - \varepsilon \left[q_1^*, v\right]. \tag{3.58}$$

Subtracting (3.58) from (3.57), we obtain

$$(L_{1,1}\widetilde{q}_{1,1}, L_{1,1}v) + \varepsilon^2 [\widetilde{q}_{1,1}, v] = \tag{3.59}$$
$$\left(-B_1 (q_1^{*\prime})^2 - A_{1,1}\widetilde{V}'_{1,1}q_1^{*'} - A_{2,1}\widetilde{V}'_{1,1}(V'_{11} + V^{*\prime}) - F_1, L_{1,1}v\right) + \varepsilon^2 [q_1^*, v].$$

Estimate terms in the right hand side of (3.59). By (3.21), (3.29), (3.41) and the first inequality (3.51)

$$B_1 (q_1^*)^2 \leq \frac{8\overline{s}^2}{\lambda} (C^*)^2 \leq \frac{1}{\sqrt{\lambda}}. \tag{3.60}$$

Next, by (3.29) and (3.56)

$$\left|A_{1,1}\widetilde{V}'_{1,1}q_1^{*'}\right| \leq \frac{M^*}{2}\eta. \tag{3.61}$$

Also by (3.41), (3.43), (3.44), (3.46) and (3.56)

$$\left|A_{2,1}\widetilde{V}'_{1,1}(V'_{11} + V^{*\prime})\right| \leq \frac{M^*}{2C^*}\eta^2 \leq \frac{\eta}{8}. \tag{3.62}$$

Next, by (3.33) $\|F_1\|_2 \leq C^*\eta/2$. Combining this with (3.60)-(3.62), we obtain

$$\left\|-B_1 (q_1^{*\prime})^2 - A_{1,1}\widetilde{V}'_{1,1}q_1^{*'} - A_{2,1}\widetilde{V}'_{1,1}(V'_{11} + V^{*\prime}) - F_1\right\|_2 \leq \frac{1}{\sqrt{\lambda}} + \left(\frac{M^*}{2} + \frac{C^*}{2} + \frac{1}{8}\right)\eta. \tag{3.63}$$

By (3.42) $\widetilde{q}_{1,1}(0) = \widetilde{q}'_{1,1}(0) = 0$. Setting in (3.59) $v := \widetilde{q}_{1,1}$, using the Cauchy-Schwarz inequality, Lemmata 3.3, 3.5, Corollary 1, (3.29) and (3.63), we obtain

$$\|\widetilde{q}_{1,1}\|_{2,2} \leq K\left[\frac{1}{\sqrt{\lambda}} + \left(\frac{M^*}{2} + \frac{3C^*}{2} + \frac{1}{8}\right)\eta\right] \leq 2KM^*\left(\frac{1}{\sqrt{\lambda}} + \eta\right). \tag{3.64}$$

Since $\|q_{1,1}\|_{2,2} \leq \|\widetilde{q}_{1,1}\|_{2,2} + \|q_1^*\|_{2,2} \leq \|\widetilde{q}_{1,1}\|_{2,2} + C^*$, then (3.64), the third inequality (3.51) and (3.46) imply that (3.49) is true for $q_{1,1}$, i.e. $\|q_{1,1}\|_{2,2} \leq 2C^*$. Next, Lemma 3.4 implies that (3.50) holds for $\|c_{1,1} - c^*\|_2$.

Assume now that estimates (3.48)-(3.50) are valid for functions $\widetilde{q}_{1,k-1}, q_{1,k-1}, k \geq$

2 and prove them for $\widetilde{q}_{1,k}, q_{1,k}$. By (3.50) and (3.43)

$$\|V_{1,k}\|_{C^2[0,1]} \leq \xi, \left\|\widetilde{V}_{1,k}\right\|_{C^2[0,1]} \leq \eta. \tag{3.65}$$

We obtain similarly with (3.59)

$$(L_{1,1}\widetilde{q}_{1,k}, L_{1,1}v) + \varepsilon^2 [\widetilde{q}_{1,k}, v] = \tag{3.66}$$
$$\left(B_1\widetilde{q}'_{1,k-1}\left(q'_{1,k-1} + q_1^{*\prime}\right) - A_{1,1}\widetilde{V}'_{1,1}q_1^{*'} - A_{2,1}\widetilde{V}'_{1,1}\left(V'_{11} + V^{*\prime}\right) - F_1, L_{1,1}v\right) + \varepsilon^2 [q_1^*, v].$$

By (3.21), (3.41) and the second inequality (3.51)

$$\begin{aligned} \left\|B_1\widetilde{q}'_{1,k-1}\left(q'_{1,k-1} + q_1^{*\prime}\right)\right\|_2 &\leq \frac{24C^*\overline{s}^2}{\lambda}KM^*\left(\frac{1}{\sqrt{\lambda}} + \eta\right) \\ &= \frac{3}{\lambda}K\left(M^*\right)^2\left(\frac{1}{\sqrt{\lambda}} + \eta\right) \leq M^*\left(\frac{1}{\sqrt{\lambda}} + \eta\right). \end{aligned} \tag{3.67}$$

Hence, using (3.65), similarly with (3.63), (3.64), we obtain from (3.66)

$$\|\widetilde{q}_{1,k}\|_{2,2} \leq KM^*\left(\frac{1}{\sqrt{\lambda}} + \eta\right) + K\left(\frac{M^*}{2} + \frac{3C^*}{2} + \frac{1}{8}\right)\eta \leq 2KM^*\left(\frac{1}{\sqrt{\lambda}} + \eta\right).$$

Hence, the estimate for $\|\widetilde{q}_{1,k}\|_{2,2}$ is the same as one in (3.64), which means that estimates (3.48)-(3.50) are valid for functions $q_{1,k}, c_{1,k}$.

Assume now that estimates (3.48)-(3.50) are valid for functions $q_{j,k}, c_{j,k}$, where $j = 1, ..., n-1; k = 1, ..., m_j$. We will prove now that they are also valid for functions $q_{n,1}, c_{n,1}$. First, we obtain similarly with (3.65)

$$\|V_{n,1}\|_{C^2[0,1]} \leq \xi, \left\|\widetilde{V}_{n,1}\right\|_{C^2[0,1]} \leq \eta. \tag{3.68}$$

Denote

$$L_{n,1}q_{n,1} = q''_{n,1} - A_{1,n}\left(h\sum_{j=1}^{n-1} q'_j(x) - V'_{n,1}\right)\widetilde{q}'_{n,1}$$

Using (3.23) and (3.32), we obtain similarly with (3.59) and (3.66)

$$\left(L_{n,1}\widetilde{q}_{n,1}, L_{n,1}v\right) + \varepsilon^2\left[\widetilde{q}_{n,1}, v\right] = \left(B_n\widetilde{q}'_{n-1}\left(q'_{n-1} + q_n^{*'}\right) - F_n, L_{n,1}v\right)$$

$$+ \left(\left(A_{1,n}q_n^{*'} - A_{2,n}h\sum_{j=1}^{n-1}\left(q'_j + q_j^{*'}\right) + 2A_{2,n}V'_{n,1}\right)\left(h\sum_{j=1}^{n-1}\widetilde{q}'_j\right), L_{n,1}v\right) \tag{3.69}$$

$$\left(\left(2A_{2,n}h\sum_{j=1}^{n-1}q_j^{*'} - A_{1,n}q_n^{*'} - A_{2,n}\left(V'_{n,1} + V^{*'}\right)\right)\widetilde{V}'_{n,1}, L_{n,1}v\right) + \varepsilon^2\left[q_1^*, v\right].$$

We now estimate each term in the right hand side of (3.69). Using (3.33), we obtain similarly with (3.67)

$$\left\|B_n\widetilde{q}'_{n-1}\left(q'_{n-1} + q_n^{*'}\right) - F_n\right\|_2 \leq M^*\left(\frac{1}{\sqrt{\lambda}} + \eta\right) + \frac{C^*}{2}\eta. \tag{3.70}$$

By (3.29), (3.41), (3.45), (3.46) and (3.49)

$$\left\|A_{1,n}q_n^{*'} - A_{2,n}h\sum_{j=1}^{n-1}\left(q'_j + q_j^{*'}\right) + 2A_{2,n}V'_{n,1}\right\|_{C[0,1]} \leq M^*\left(1 + \frac{3}{2}\beta\right) \leq \frac{3}{2}M^*. \tag{3.71}$$

Next, by (3.48)

$$\left\|h\sum_{j=1}^{n-1}\widetilde{q}'_j\right\|_2 \leq 2KM^*\beta\left(\frac{1}{\sqrt{\lambda}} + \eta\right).$$

Combining this with (3.71), we obtain

$$\left\|\left(A_{1,n}q_n^{*'} - A_{2,n}h\sum_{j=1}^{n-1}\left(q'_j + q_j^{*'}\right) + 2A_{2,n}V'_{n,1}\right)\left(h\sum_{j=1}^{n-1}\widetilde{q}'_j\right)\right\|_2 \leq \tag{3.72}$$

$$\leq 3K\left(M^*\right)^2\beta\left(\frac{1}{\sqrt{\lambda}} + \eta\right).$$

Next, since by (3.45) and (3.46) $\beta + \eta/2 < 1/4$, then

$$\left\| \left(2A_{2,n} h \sum_{j=1}^{n-1} q_j^{*'} - A_{1,n} q_n^{*'} - A_{2,n} \left(V'_{n,1} + V^{*'} \right) \right) \widetilde{V}'_{n,1} \right\|_2 \leq \tag{3.73}$$
$$\leq \left(M^* \beta + \frac{M^*}{2} + \frac{M^*}{2} \right) \eta \leq \frac{3}{4} M^* \eta.$$

Using (3.69)-(3.73), we obtain

$$\begin{aligned} \| L_{n,1} \widetilde{q}_{n,1} \| &\leq M^* \left(\frac{1}{\sqrt{\lambda}} + \eta \right) + \frac{3C^*}{2} \eta + 3K \left(M^* \right)^2 \beta \left(\frac{1}{\sqrt{\lambda}} + \eta \right) + \frac{3}{4} M^* \eta \\ &\leq M^* \left(1 + \frac{3C^*}{2M^*} + 3KM^* \beta \right) \left(\frac{1}{\sqrt{\lambda}} + \eta \right) \leq 2M^* \left(\frac{1}{\sqrt{\lambda}} + \eta \right). \end{aligned}$$

Hence, Lemmata 3.3 and 3.5 imply that (3.48) is true for $\| q_{n,1} - q_n^* \|_{2,2}$. Similarly with the above we obtain that (3.49) and (3.50) are true for norms $\| q_{n,1} \|_{2,2}, \| c_{n,1} - c^* \|_2$. The proof for the pair $(n,k), k \geq 2$ is similar. $\square$

3.5 A Simplified 1-D Mathematical Model of Imaging of Plastic Antipersonnel Land Mines

First, we describe a mathematical model for the Coefficient Inverse Problem of detection and imaging of antipersonnel land mines that are buried under the ground. This model is similar with one used in [39] in the 2-D case. Some assumptions and simplifications have been made with our model. At the same time, we use realistic ranges of parameters. First, we work with a one-dimensional model, which is a simplification of course. As we have stated in Introduction section 1.2, we intend to work with 2-D and 3-D CIPs in the future using the methodology of this chapter. So, in these future cases our mathematical models will not use the latter simplification. The irregularity of the ground surface has been neglected to avoid the complication of gathering the data for the direct problem. Also, we assume that the dielectric permittivity ε of the medium does not have a discontinuity at the ground surface

where measurements of the back reflected electric signal are performs. Further, we neglect the electric conductivity of the medium, which can be justified in the case when the background is a dry sand, for example, and we work exactly with this case.

Let the ground be $\{x > 0\}$. Suppose that a polarized electric field is generated by a pulse at the point $x^0 < 0$ at the initial time $t = 0$. In other words, the electric source $\{x^0\}$ is located above the ground. The following hyperbolic equation can be derived from the Maxwell equations [32]

$$\begin{aligned} \mu\varepsilon(x)u_{tt} &= u_{xx},\ (x,t) \in \mathbb{R} \times (0,\infty), \\ u(x,0) &= 0,\ u_t(x,0) = \delta\left(x - x^0\right), \end{aligned} \tag{3.74}$$

where the function $u(x,t)$ is one component of the electric field and the parameter $\mu = 4\pi \times 10^{-7}\,(Henry/m)$ is the magnetic permeability in the free space and $\varepsilon = \varepsilon_0\varepsilon_r(x)$ is the dielectric permittivity, where $\varepsilon_0 \approx 8.854 \times 10^{-12}\,(Farad/m)$ is the dielectric permittivity of the free space and $\varepsilon_r(x)$ is the dimensionless relative dielectric permittivity of the medium. The Laplace transform (3.5) applied to (3.74) leads to the following analog of the problem (3.6), (3.7)

$$w_{xx} - s^2\mu\varepsilon_0\varepsilon_r(x)w = -\delta\left(x - x^0\right), \forall s \geq \underline{s}, \tag{3.75}$$

$$\lim_{|x|\to\infty} w(x,s) = 0, \forall s \geq \underline{s}. \tag{3.76}$$

It is well known that the maximal depth of an antipersonnel land mine is about 10cm. So, we model these mines as small smooth symmetric "bumps" of the diameter 4cm and their centers should be at the maximal depth of 10cm. But the total length of the interval on which we consider the inverse problem is 20cm=0.2m in our calculations. To transform this interval into $(0,1)$ (see above), we make change of variables in (3.75) $x' = x/0.2, x'_0 = x^0/0.2$. Note that $\delta(x - x^0) = \delta(x' - x'_0)/0.2$. We now use the data about the value of the dielectric constant from http://www.clippercontrols.com/info

1. By these data $\varepsilon_r = 5$ in dry sand and $\varepsilon_r = 22$ in trinitrotoluene (TNT). Hence, to have the background value of the unknown coefficient equals 1, we denote in (3.75)

$$c(x) = \frac{\varepsilon_r(x)}{5}, s' = \left(0.2\sqrt{5\mu}\right) s, \widehat{w} = \frac{w}{0.2}. \tag{3.77}$$

Finally, for convenience, we keep the same notations for $(x', x_0', s', \widehat{w}) := (x, x^0, s, w)$ as before. Then equations (3.75), (3.76) become identical with equations (3.6), (3.7), which we now reproduce for reader's convenience

$$w_{xx} - s^2 c(x) w = -\delta\left(x - x^0\right), \forall s \geq \underline{s}, \tag{3.78}$$

$$\lim_{|x|\to\infty} w(x,s) = 0, \forall s \geq \underline{s}. \tag{3.79}$$

Note that since the interval (0,20) cm is transformed now into $(0,1)$ and centers of our mine-like inclusions of the thickness of 4cm are between 2 cm and 10 cm, then we are interested to image such mine-like targets whose centers are between 0.2 and 0.5,

$$\text{centers of interest in our specific application} \in [0.2, 0.5]. \tag{3.80}$$

We are interested in the identification of antipersonnel plastic mines, which is difficult in a practical scenario since the metal component in them is not large. Hence, we need one parameter inside the mine which can give us sufficient contrast against the surrounding dry sand. We use the parameter c from (3.77), which is proportional to the dielectric constant. Since

$$\frac{\varepsilon_r(\text{TNT})}{\varepsilon_r(\text{dry sand})} = \frac{22}{5} \approx 4,$$

then in our computations the height of inclusions is about 4, i.e., inclusion/background contrast in $c(x)$ is about 4:1. Thus, if one can quantify the coefficient $c(x)$, then points whose values are close to 4, will be those inside or close to the mine. Thus,

finding an approximation for this coefficient with solution of the Coefficient Inverse Problem would provide us a useful information about a target which we would 'suspect' is a land mine.

3.6 Numerical Study

3.6.1 The Forward Problem

In this chapter, we work with the computationally simulated data. That is, the data are generated by computing the forward problem (3.78), (3.79) with the given function $c(x)$. Then this forward problem is "forgotten" and only so generated boundary data are used. To solve the forward problem (3.78), (3.79), we use FDM and the sweep method. To eliminate the $\delta(x - x^0)$ function from (3.78), consider first the fundamental solution of equation (3.78) with $c(x) \equiv 1$, which is the value this function attains outside of the interval of interest $(0, 1)$, see (3.3). This solution is

$$w_0(x, s) = \frac{\exp(-s|x - x^0|)}{2s}.$$

Because of (3.79), we can solve the problem (3.78), (3.79) on a finite truncated interval with zero Dirichlet boundary conditions at its edges. We took $x^0 = -1$ and next we have chosen the interval $x \in (-6, 4)$. Let $\widetilde{w} = w - w_0$. We have solved by the sweep method the following problem

$$\widetilde{w}_{xx} - s^2 c(x)\widetilde{w} = s^2(c(x) - 1)w_0, \tag{3.81}$$

$$\widetilde{w}(-6, s) = \widetilde{w}(4, s) = 0. \tag{3.82}$$

The singularity is absent in the right hand side of (3.81) because $c(x) - 1 = 0$ for $x < 0$ and $x^0 < 0$. We have chosen the step size in x to be $h_x = 0.01$. Now, we have solved the problem (3.81), (3.82) for $s \in [0.5, 1.22]$ with the grid step size in

s direction being $h = 0.01$. The reason why we have chosen this s-interval as one preferable to others is that we have found in our reconstructions that this is the optimal frequency interval for depths of inclusions we are interested in, see Figure 3.3(c), 3.4(c). Furthermore, the sensitivity of the back reflected data at $x = 0$ drops for larger s, for locations of inclusions of our applied interest, see Figure 3.3(c). Thus, because of the poor sensitivity for larger s, $s = 1.22$ can be counted as that truncated large value $\overline{s}$ introduced above.

3.6.2 The two stage algorithm

Following the second part of Remark 3.3 after Theorem 3.1, we modify in this subsection the general algorithm described in section 3.3. We point out that because of the application of our interest, we are mostly interested in imaging of small mine-like inclusions rather than in imaging of slowly changing functions. The main point is that Theorem 3.1 is still applicable even to our amended algorithm, except of the smoothness requirement, which still can be fixed, see the next paragraph. In this subsection we describe our numerical algorithm, which consists of two main steps. In our numerical experiments we have taken $\overline{N} = N = 72$, meaning that the step size in the s-direction is $h = 0.01$ and the length of the s-interval on which we compute functions q_n is $\beta = 0.72$, see Theorem 3.1. In addition, the number of iterations with respect to the tail was in our computations is $m_1 = m_2 = ... = m_N := m = 10$. To implement the QRM numerically, we partition the interval $[0, 1]$ in 100 equals subintervals $0 = x_0 < x_1 < ... < x_{100} = 1, x_i - x_{i-1} = h_q = 0.01$, see details about the numerical implementation of the QRM in subsection 3.6.3.

In actual computations we relax the $H^3(0, 1)$ smoothness requirements of the QRM imposed in subsection 4.2. Namely, in (3.27) use $\varepsilon = 0$ on the first stage of computing and we use $\varepsilon \in (0, 1)$ and the $H^2(0, 1)$ norm in (3.27) on the second stage, also see Lemma 3.3 for $\varepsilon = 0$. The true reason why we can relax that requirement is that we work in a finite dimensional space when computing, and all norms are

equivalent in such a space. The global convergence theorem 3.1 is not directly applicable in this case for a *single* reason: because we can guarantee only that functions $c_{n,k}(x) \in L_2(0,1)$ rather than being continuous. Nevertheless, a discrete analog of this theorem can be proven. To do this, one can apply almost straightforwardly the idea of [10] of the proof of convergence of the discrete analog of the QRM for the Laplace equation and, in particular the discrete Carleman estimate of this reference. The same problem with smoothness occurs in 2-D and 3-D cases. as our preliminary studies indicate, and it can also be handled this way. Because of space considerations, we leave this development outside of the current publication and plan to work it out in the future.

Remark 3.4. *In our computations we have used 100 mesh points in* $[0,1]$. *However, when we have tried to increase this number to 200, results of the QRM worsened. Most likely this was because the dimension of our above mentioned finite dimensional space was becoming too large, thus making it "almost" infinitely dimensional. Note that above mentioned discrete estimates of [10] naturally worsen when the grid step size decreases. Hence, one would need to introduce the* $H^3(0,1)$ *smoothness requirements of subsection 3.3.2 if decreasing the step size* h_q. *In other words, there exists a natural trade-off between* h_q *and the smoothness.*

Step 1. Finding the geometry. Proceed with the algorithm of section 3.3 with the truncation (3.23) and $\varepsilon = 0$ in (3.34). In addition to boundary conditions (3.26) in the QRM we have also added the Dirichlet boundary condition at $x = 1$,

$$q_{n,k}(1) = d_n, \tag{3.83}$$

where the number d_n is known from the forward problem solution, see Remark 3.2. On this stage we average discrete approximations $c_{n,k}$ for the coefficient $c(x)$. Suppose a discrete function $c_{n,k}(x_i)$ is found, where $x_i \in (0,1)$ are grid points. Then we compute

another function $b_{n,k}(x_i)$ and re-define the value $c_{n,k}(x_i)$ as

$$b_{n,k}(x_i) = \frac{1}{5}\sum_{j=i-2}^{i+2} c_{n,k}(x_j), \tag{3.84}$$
$$b_{n,k}(x_0) = b_{n,k}(x_1) = b_{n,k}(x_{99}) = b_{n,k}(x_{100}) = 1, c_{n,k}(x_i) := b_{n,k}(x_i).$$

Next, we compute the discrete function $c_{n,k}(x)$ as in section 3.3. We repeat the run along the interval $s \in [0.5, 1.22]$ several times as follows. Suppose that on the first s-sweep we have computed the function $c_N(x) := c_N^{(1)}(x)$, which corresponds to the last s-subinterval $[s_N, s_{N-1}] = [0.5, 0.49]$. Hence, we have also computed the corresponding tail function $V_N(x)$. Then we return to the first $s-$interval $[s_1, \overline{s}] = [1.21, 1.22]$, set $V_{1,1}^{(2)}(x) := V_N(x)$ and repeat the algorithm of section 4 via finding a new function $c_1(x) := c_1^{(2)}(x)$, next a new function $c_2(x) := c_2^{(2)}(x)$, etc., until new functions $c_N^{(2)}(x), V_N^{(2)}(x)$ are found. We repeat this sweep over the interval $s \in [0, 5, 1.22]$ r times until the stabilization occurs, i.e. until the following inequality takes place

$$\|c_N^{(r)}(x) - c_N^{(r-1)}(x)\|_{L^2(0,1)} \leq \tau, \tag{3.85}$$

where τ is a sufficiently small number of our choice. We have taken $\tau = 10^{-5}$

As soon as (3.85) takes place, we set $c_N^{(r)}(x) := c_1^{(1)}(x)$ and go to the Stage 2. The reason why we use Stage 2 is that Stage 1 gives us only accurate locations of our mine-like inclusions. However, the computed value of the coefficient $c(x) := c^{(1)}(x)$ in them is significantly lower than the correct value, see Figure 3.1.

Step 2. Finding the contrast. Having the first approximation for the solution from Step 1, we now proceed with Step 2. This step provides us with good values for contrasts in our inclusions.

Step 2.1. We take the last tail function $V_N^{(r)}(x)$ computed on the first step as the starting value for the algorithm of Section 3.3. In other words, in Step 1^1 of section 3.3 we set $V_{1,1}(x) := V_N^{(r)}(x)$. Next, we proceed with a modified algorithm of section

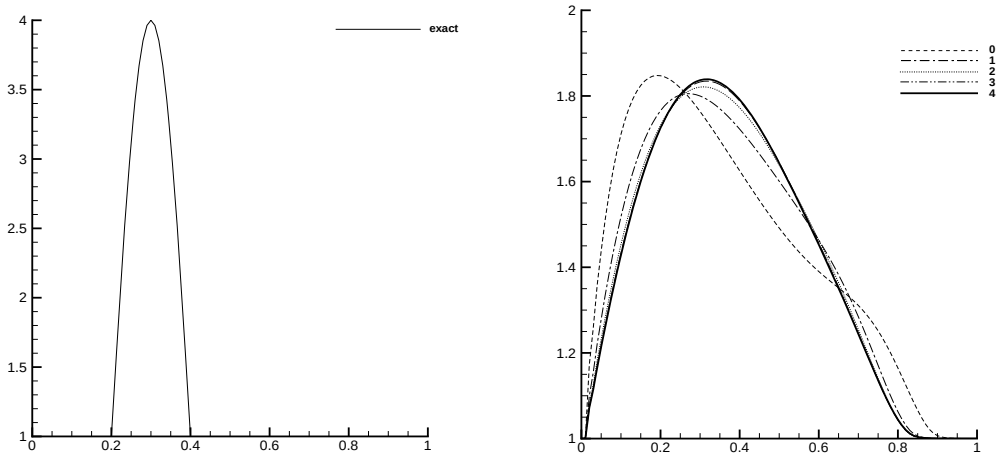

(a) (b) Computed $c_N^{(r)}(x)$ where (3.84) holds.

Figure 3.1: A typical example of images we obtain on Step 1. (a) displays the correct coefficient. (b) shows the computed $c_N^{(r)}(x)$ where (3.84) holds. In all our experiments $r = 5$, i.e. stabilization on Step 1 took place after 5 s-sweeps. The location of the mine-like target is imaged with a good accuracy. However, only 45% (1.8/4) of the contrast is imaged. Thus, it is necessary to proceed with Step 2.

3.3. Namely, let functions $q_{n,k}^{(r)}(x) \in H^2(0,1)$ be functions $q_{n,k}^{(r)}(x)$ computed on the last s-sweep in step 1. Then we minimize the following functionals in the QRM, see (3.24)-(3.27) and (3.83)

$$J_{n,k}^{\varepsilon}(q_{n,k}) = \|q_{n,k}''(x) - a_{n,k}q_{n,k}'(x) - H_{n,k}\|_{L_2(0,1)}^2 + \varepsilon \left\| q_{n,k} - q_{n,k}^{(r)} \right\|_{H^2(0,1)}^2, \quad (3.86)$$

$$q_{n,k}(0) = \overline{\psi}_{0,n}, q_{n,k}'(0) = \overline{\psi}_{1,n}, q_{n,k}'(1) = d_n, q_{n,k}'(1) = s_n^{-2}. \quad (3.87)$$

This way we obtain functions $\overline{q}_{n,k}^{(1)}, \overline{V}_N^{(1)}, \overline{c}_{n,k}^{(1)}$ as described in section 3.3. However, unlike Step 1, we do not average functions $\overline{c}_{n,k}^{(1)}$, i.e. we do not apply the procedure (3.83).

Step 2.n. Having functions $\overline{q}_{n,k}^{(n-1)}, \overline{V}_N^{(n-1)}, \overline{c}_{n,k}^{(n-1)}$, repeat the sweep over the $s-$interval via setting $\overline{V}_{1,1}^{(n)}(x) := \overline{V}_N^{(n-1)}$ and finding $\overline{q}_{n,k}^{(n)}$ via the minimization of the functional (3.85) in which $q_{n,k}^{(r)}$ is replaced with $\overline{q}_{n,k}^{(n-1)}$. Again, unlike Step 1, we do not apply the procedure (3.83) to functions $\overline{c}_{n,k}^{(n)}$.

Stopping criterion for Step 2. We make steps $2.1, ...2.n_2$, where the final sweep number n_2 is chosen in numerical experiments. So, we obtain the function $\overline{c}_N^{n_2}(x)$.

Since we do not average functions $\overline{c}_{n,k}^{(n)}$, then typically the function $\overline{c}_N^{n_2}(x)$ looks like one on Figure 3.2(a), i.e. it is non-smooth. Next, to smooth out the image, we apply a post processing to the function $\overline{c}_N^{n_2}(x)$. This post processing consists in averaging over 5 points as in (3.83) and linear interpolation near the edge $x = 1$. This way we obtain the final reconstruction result $c_{rec}(x)$. The linear interpolation "by values at $x = 0.78$ and $x = 1$" is necessary due to the occurrence of some artifacts for $x \in [0.78; 1]$, which is shown on Figures 3.2(a), 3.2(b).

$$c(x) = \frac{c(1) - c(0.78)}{0.22}(x - 0.78) + c(0.78), x \in (0.78; 1).$$

3.6.3 Parameters used in computations

To summarize our parameters used in computations, we first remind that: λ is the parameter of the CWF in (3.19), h_x is the mesh size in the forward problem solution, h_q is the mesh size in the QRM discretization, h is the mesh size in the s-direction, m is the number of iterations with respect to the tail for each q_n and parameters τ and ε are defined in (3.84) and (3.85) respectively. It is *important* that parameters, once chosen, were used in all our numerical experiments. In other words, once chosen for one configuration, parameters were not conveniently "adjusted" to other configurations.

Table 3.1: Parameters used in computations

x^0	λ	h_x	h_q	h	m	τ	ε	n_2	s-interval
-1	10	0.01	0.01	0.01	10	10^{-5}	0.05	15	$[0.5, 1.22]$

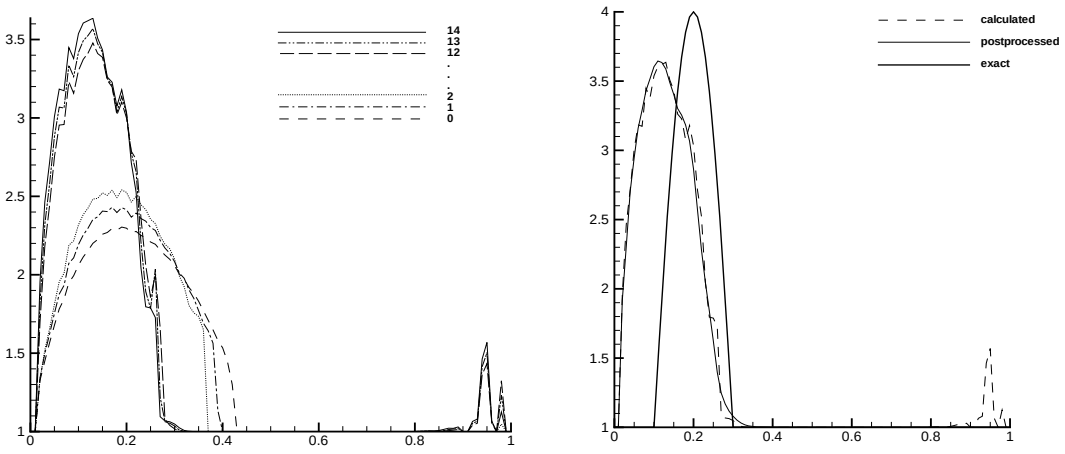

(a) (b)

Figure 3.2: (a) shows coefficients $\widetilde{c}_j(x)$ calculated on n_2 steps for Stage 2. (b) shows postprocessing procedure.

3.6.4 Numerical Implementation of the Quasi Reversibility Method

We have minimized functionals (3.85) with respect to values of the discrete function $q_{n,k}(x_i)$ at mesh points. To do this, we have used the conjugate gradient method. In this subsection we explain how we have calculated derivatives with respect to $q_{n,k}(x_i)$ analytically. For brevity we provide this explanation only for Step 1, since Step 2 is similar. In (3.85) denote for brevity

$$\begin{aligned} q &: = q_{n,k}, a := a_{n,k}, H := H_{n,k}, \\ q_i &= q(x_i), a_i = a(x_i), H_i = H(x_i), 0 < x_i < 1. \end{aligned}$$

By the QRM we will minimize on Step 1

$$J(q) = h_q \sum_{i=1}^{M_x-1} \left(\frac{q_{i+1} - 2q_i + q_{i-1}}{h_x^2} - a_i q_i - H_i \right)^2 = h_q \sum_{i=1}^{M_x-1} J_i^2,$$

subject to boundary conditions

$$q(0) = \overline{q}_0, q'(0) = \overline{q}_1, q'(1) = \overline{q}_2, q(1) = \overline{q}_3,$$

where numbers $\overline{q}_0, \overline{q}_1, \overline{q}_2, \overline{q}_3$ are given. Here M_x is the number of mesh points in $[0,1]$, and in our case $M_x = 100$. Hence,

$$\frac{\partial J}{\partial q_j} = 2h_q \sum_{i=1}^{M_x - 1} \frac{\partial J_i}{\partial q_j} J_i. \tag{3.88}$$

An important observation simplifying the calculation of the gradient is that

$$\frac{\partial J_i}{\partial q_j} = \frac{\delta_{i+1,j} - 2\delta_{i,j} + \delta_{i-1,j}}{h_x^2} - a_i \delta_{i,j}, j = 2, ..., M_x - 2, \tag{3.89}$$

Formulas (3.88), (3.89) explain the calculation of the gradient of the QRM functional J. In addition, formulas (3.10), (3.23) and (3.52) become in the discrete case

$$\begin{aligned} \widetilde{v}_{n,k}(x_i) &= -h_q \left(\sum_{j=1}^{n-1} q_j(x_i) + q_{n,k}(x_i) \right) + V_{n,k}(x_i), \\ c_{n,k}(x_i) &= \max \left[\frac{\widetilde{v}_{n,k}(x_{i-1}) - 2\widetilde{v}_{n,k}(x_i) + \widetilde{v}_{n,k}(x_{i+1})}{h_q^2} + s_n^2 \left(\frac{\widetilde{v}_{n,k}(x_{i+1}) - \widetilde{v}_{n,k}(x_i)}{2h_q} \right)^2, 1 \right] \end{aligned}$$

3.6.5 Results of the reconstruction

In this subsection we present results of our reconstructions. We have performed numerical experiments to reconstruct $c(x)$ as inclusions. In all our tests we have introduced the multiplicative random noise in the boundary data, w_σ, by adding relative error to computed data w_{obs} using the following expression

$$w_\sigma(x_i, s_j) = w_{obs}(x_i, s_j)[1 + \alpha\sigma], \ i = 0, 1, M_x - 1, M_x; \ , j = 1, .., N.$$

Here, α is a random number in the interval $[-1; 1]$, and σ is the noise level. We use $\sigma = 0.05$ of the multiplicative random noise in the observed boundary data w_{obs}. The starting value for the tail was chosen $V_{1,1}(x, \overline{s}) = 0$, which reflects the fact that no advanced knowledge about tails is available. Because of the application of our

interest, we model our mine-like targets as a inclusions of the width 0.2, the height $a > 1$ and with different centers $x^* \in [0.2, 0.5]$, see section 3.5 and, in particular, (3.80). To avoid dealing with discontinuities, we model our inclusions as continuous functions which look as the cos function.

Test 3.1. We test our numerical method for the case $a = 3$ and with two centers at $x^* = 0.2$ and at $x^* = 0.4$. That is, we calculate the data via the solution of the forward problem for the function $c(x)$ defined as

$$c(x) = \begin{cases} 1 + 3\cos(0.5\pi(x - x^*)/0.1), & |x - x^*| < 0.1 \\ 1, \quad \text{otherwise} \end{cases}. \tag{3.90}$$

As we can see, in both cases the location of the center of the imaged inclusion is shifted to the left by about the radius of this inclusion 0.1. The error in the 4:1 inclusion/background contrast is 10% (1-3.6/4) for $x^* = 0.2$ and 33% $(1 - 2.7/4)$ for $x^* = 0.4$. The 10% error can be explained by the fact that the function $c(x)$ does not exactly equal 4 within inclusion. As to a much larger error of 33% for $x^* = 0.4$, we refer to Figure 3.3(c) for a possible explanation. Indeed, this figure shows that at larger distances from the left edge $x = 0$ the sensitivity function $f(s) = w(0, s)\left[w_0(0, s)\right]^{-1}$ becomes closer to 1, i.e. the data loose their sensitivity when the target moves away from the back reflected edge $x = 0$. One can see on Figure 3.3(c) that the sensitivity of the data is much better for $x^* = 0.2$ than for $x^* = 0.4$ and $x^* = 0.5$. This explains a better accuracy of Figure 3.3(a).

Test 3.2. Consider now a more realistic case when the medium is a slowly changing background with a mine-like targets embedded in it. Consider functions $h_1(x), h_2(x)$ defined by

$$\begin{aligned} h_1(x) &= \cos^2(0.5\pi(x - 0.5)/0.45), \\ h_2(x) &= 3\cos(0.5\pi(x - x^*)/0.1). \end{aligned}$$

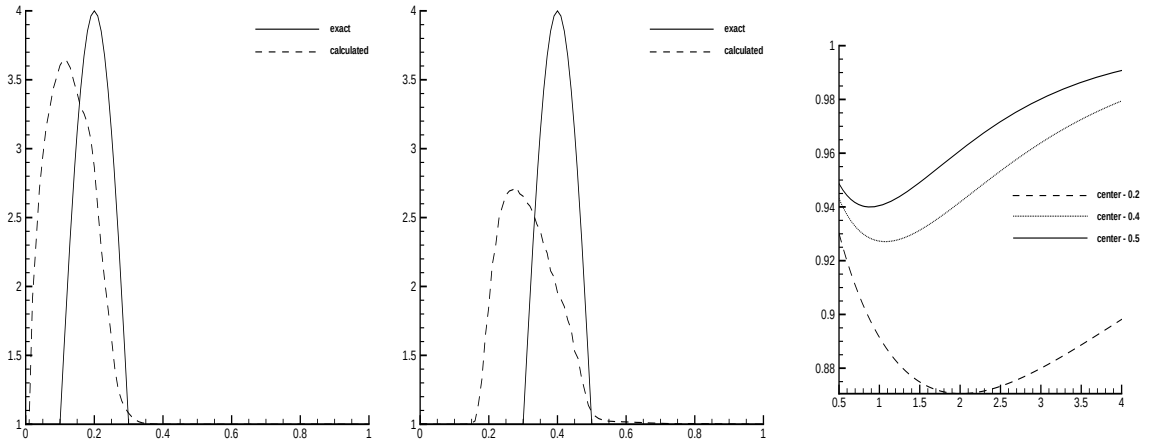

(a) (b) (c)

Figure 3.3: Test 3.1:(a) displays exact and calculated functions (3.90) for $x^* = 0.2$. (b) displays exact and calculated functions for $x^* = 0.4$. (c) displays the "sensitivity" function $f(s) = w(0,s)\left[w_0(0,s)\right]^{-1}$ for $s \in [0.5, 4]$ for different centers $x^* = 0.2, 0.4, 0.5$ of mine-like targets.

And calculate the data for the function $c(x)$ defined by

$$c(x) = \begin{cases} 1 + h_1(x), x \in (0.05; 0.095), & |x - x^*| \geq 0.1, \\ 1 + h_2(x), & |x - x^*| < 0.1, \\ 1 + h_1(x), & |x - x^*| < 0.1, \\ 1, & \text{otherwise} \end{cases} \tag{3.91}$$

As one can see from Figure 3.4, the quality of the reconstruction of the mine-like target is better than one in the case of the uniform background (Test 3.1), especially for $x^* = 0.4$. As to the slowly changing background, it is not reconstructed accurately. The latter is insignificant for our specific application, since we only want to image mine-like inclusion. An explanation of a poor quality of the reconstruction of the slowly changing background follows from our next test (Figure 3.5(c)). One can see on Figure 3.4(c) that the sensitivity of the data for $x^* = 0.2$ and $x^* = 0.4$ is better than on Figure 3.3(c). This partially explains a better accuracy in this case.

Test 3.3. We test our numerical method for two sets of *blind* data. These

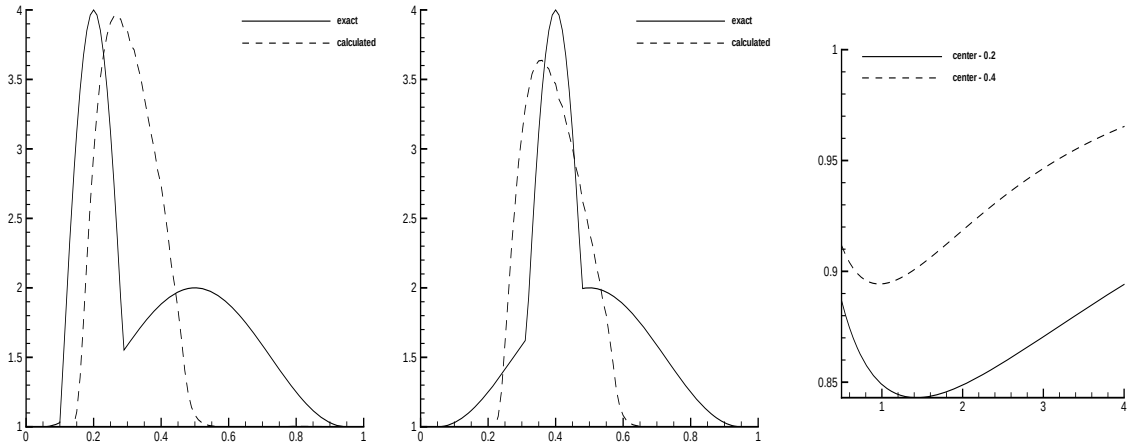

(a) (b) (c)

Figure 3.4: Test 3.2: (a) and (b) display exact and calculated functions (3.91) for $x^* = 0.2$ and $x^* = 0.4$ respectively. (c) displays the "sensitivity" function $f(s) = w(0,s)\left[w_0(0,s)\right]^{-1}$ for $s \in [0.5,4]$ for different centers $x^* = 0.2, 0.4$.

data were kindly produced for us, by our request, by Professor Paul Sacks from Iowa State University (he has kindly allowed us to reproduce results of our tests here). He has calculated the solution of the above forward problem by a method, which is different from ours. No noise was introduced. Next, he has given us resulting values of $q_n(0), q_n'(0), q_n(1)$. However, when applying our code to these data, we did not know the answer. This answer became known to us only after we got our solution. Our results are displayed on Figure 3.5. As one can see, in the case of a slowly changing background, the accuracy of the reconstruction from the blind data is about the same as in Test 3.3. However, in the case of a constant background (Figure 3.5(a)) the accuracy is even better than one of Figure 3.3(b).

Figure 3.5(c) displays two superimposed curves of the function $w(0,s)$ for the case of Figure 3.5(b): one for the exact coefficient $c(x)$ and the second one for the calculated coefficient $c(x)$. One can see that these two curves are practically indistinguishable. The fundamental reason of this is the ill-posed nature of our CIP: we see an example when a small fluctuation of the data correspond to a large deviation of the solution.

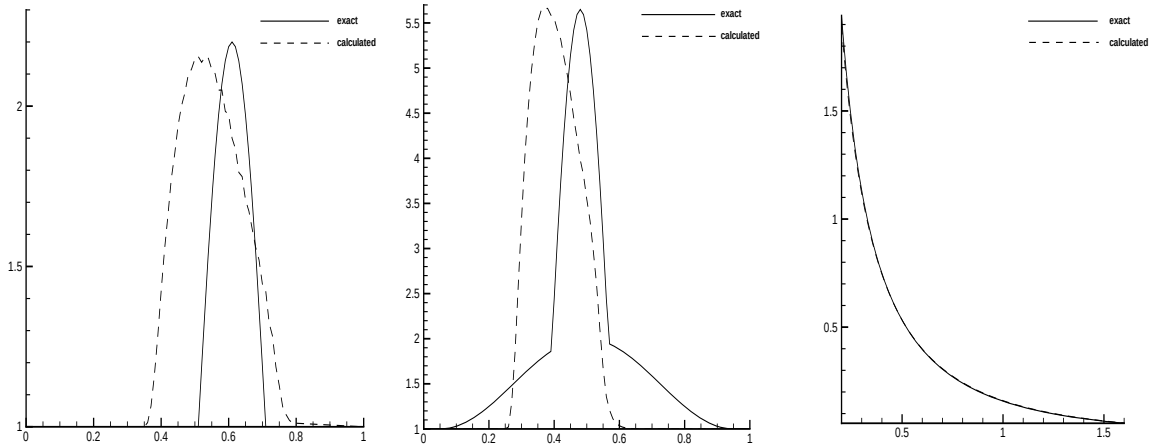

(a) (b) (c)

Figure 3.5: Test 3.3: Two sets of blind data kindly produced for us by Professor Paul Sacks. (a) shows the case a mine-like target embedded in the uniform background. (b) displays the case of a mine-like target embedded in a slowly changing background. To understand why we cannot image the slowly changing background along with mine-like targets, we have superimposed on (c) two functions $w(0,s)$ for (b): one for the exact coefficient c(x) and the second one for the calculated coefficient c(x). There is a very little difference between these two curves.

So, Figure 3.5(c) provides an explanation of our inability to image the slowly changing background in the case when a mine-like inclusion is embedded in it, also see Test 3.2 for a similar observation.

3.6.6 The case of the back reflected data only

In above tests 3.1-3.3 we have assumed that both functions $q(1,s), q_x(1,s)$ are known. While by (3.17) the function $q_x(1,s) = s^{-2}$ is known automatically, the Dirichlet boundary condition $q(1,s)$ is unknown when one works with the back reflected data. So, we now test the case when the function $q(1,s)$ is unknown. We have tried to figure out an approximation for this function using Step 1 for the function $c(x)$ given in (3.90). Suppose that on the s-sweep number k of Step 1 we have found the function $\widehat{c}_N^{(k)}(x)$. Using this function, we have calculated the solution of the forward problem (3.81), (3.82) with $c := \widehat{c}_N^{(k)}(x)$. Next, we have calculated the

function $q(1,s)$ and compared it with the exact function $q^*(1,s)$ via

$$\varepsilon_{rel} = \frac{\|q_{calc}(1,s) - q^*(1,s)\|_{L^2(0.5,1.22)}}{\|q^*(1,s)\|_{L^2(0.5,1.22)}}.$$

Table 3.2: Finding the optimal number of s-sweeps in Step 1 for the case of the backreflected data only

x^*	Number of s-sweeps	ε_{rel}
0.2	1	0.06
0.4	1	0.02
0.2	2	0.05
0.4	2	0.01
0.2	3	0.03
0.4	3	0.007

Table 3.6.6 provides summary of results. We have used the function $q_{calc}(1,s)$ obtained after 3 sweeps as an approximation for the correct function $q^*(1,s)$. Next, we performed calculations with $q_{calc}(1,s)$ as described in subsections 3.6.2, 3.6.3. Figure 3.6 displays results for two values $x^* = 0.2$ and $x^* = 0.4$. Similar results (not shown) were obtained for the case when the function (3.91) was reconstructed.

3.6.7 Why the function $q(1,s)$ is likely not informative?

We now show that the function $q(1,s)$ is likely not informative in fact. Consider the case when $c(x) = 1 + \widetilde{c}(x)$, where $\widetilde{c}(x) = 0$ for $x \notin (0,1)$ and

$$|\widetilde{c}(x)| << 1. \tag{3.92}$$

The solution of the forward problem (3.6), (3.7) can be represented via the following integral equation

$$w(x,s) = \frac{1}{2s} e^{-s|x-x_0|} - \frac{1}{2s} \int_0^1 e^{-s|x-\xi|} \widetilde{c}(\xi)\, w(\xi,s)\, d\xi.$$

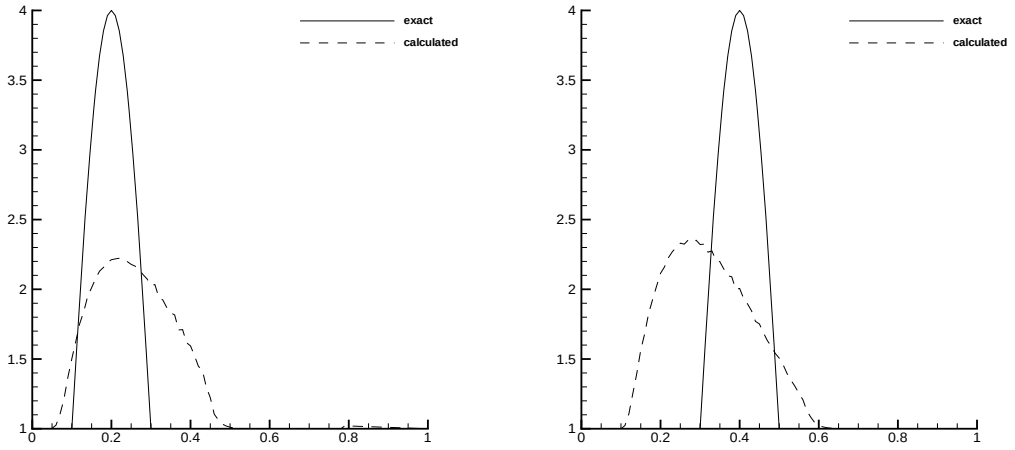

(a) (b)

Figure 3.6: (a) and (b) display results of the reconstruction of the function (3.90) for the case when the function $q(1,s)$was found approximately via the procedure of this subsection after 3 s-sweeps. Locations of mine-like targets are reconstructed with a good accuracy. However, the inclusion/background contrast is reconstructed poorly, see a discussion in next section.

Since in our case $s \in [0.5, 1.22]$, then by (3.92) solution of this equation can be represented via convergent resolvent series

$$w(x,s) = \frac{1}{2s} e^{-s|x-x_0|} + \sum_{n=1}^{\infty} w_n(x,s) \approx \frac{1}{2s} e^{-s|x-x_0|} + w_1(x,s),$$

where

$$w_1(x,s) = \frac{1}{4s^2} \int_0^1 \exp\left[-s\left(|x-\xi-x_0| + |\xi-x_0|\right)\right] \widetilde{c}(\xi) d\xi,$$

which corresponds to the linearization with respect to $\widetilde{c}$, i.e., the well known Born approximation (note that we have not used the linearization before this subsection). Since $x_0 < 0$, we obtain

$$w_1(1,s) = \frac{\exp\left[-s(1-2x_0)\right]}{4s^2} \int_0^1 \widetilde{c}(\xi) d\xi.$$

In other words, in the case (3.92) the function $q(1,s)$ contains only the information about the integral of the function $\widetilde{c}(x)$ over $(0,1)$. Clearly, there is not much information about $\widetilde{c}(x)$ in this integral.

3.7 Discussion

We have presented a globally convergent numerical method for a 1-D CIP. This method is a modification of the technique described in [27–29,31]. The key point of the modification is the use of over determined boundary conditions, which weren't used in [27–29, 31]. The latter logically led to the application of the Quasi-Reversibility Method [14, 20]. We consider this chapter as a prelude to our use of the QRM for 2-D and 3-D cases. The reason of using over-determined boundary conditions is our intention to work with the back reflected data only, since the latter is the case of many applications. In particular, in our numerical experiments here we have considered an application to imaging of the dielectric permittivity in inclusions modeling antipersonnel land mines [39].

We have proven a global convergence theorem for our method. Since its proof is based on the Carleman estimate for the operator d^2/dx^2 and Carleman estimates allow to obtain specific estimates for all constants involved, then this theorem includes a specific upper estimate for the constant $K = 8e$. This is an advantage over the global convergence Theorem 6.1 of [27], since in that result an explicit estimate for a constant involved in the classic Schauder theorem was not obtained.

The resulting convergence estimate (3.50) depends on a small parameter η. Although (3.50) guarantees that the resulting solution is sufficiently close to the correct one, still η cannot be made infinitely small in any practical computation. Therefore, a logical conclusion is that in order to enhance the solution obtained by the globally convergent part, one should subsequently use a locally convergent method which would take the solution obtained on by the globally convergent method as a good first guess. Indeed, a good first guess is the main ingredient which any locally convergent algorithm needs,

and this is exactly what our technique provides. On the other hand, locally convergent numerical methods for CIPs are independent on all components of the parameter η except of the level of error in the data σ. This two stage scheme was carried out in [28, 29] in 2-D and in [31] in 3-D, and results were quite good (for the case of non-over determined data). Our preliminary results for the QRM in the 2-D case indicate that such a two stage procedure should be implemented for the QRM. However, when working on this chapter, we were not prepared to use a locally convergent method on the second stage. Thus, we have modified our globally convergent algorithm. Still, the main point is that Theorem 3.1 almost works for this modified version. The part which does not work is the lower smoothness conditions we have actually used in our computations. The latter can be justified by the fact that we actually work in a finite dimensional space of discrete functions, in which all norms are equivalent. In addition, the technique of [10] of the convergence proof for the discrete version of the QRM can be modified for our case and discrete analogs of lemmata 3.2, 3.3 can be obtained. On the other hand, when we have tried to increase the number of mesh points in QRM, computational results worsened. The latter can be explained by the fact that the case of "too many" mesh points is sort of close to the continuous case, when one indeed needs a higher smoothness prescribed by Lemma 3.3 and, subsequently, Theorem 3.1.

First, we have tried in our computations to use non-over determined boundary conditions and thus, to solve a regular boundary value problem for the ODE for each function q_n. However, this attempt has failed to produce good quality solutions for reasons which we cannot explain at this moment (Remark 3.1). Thus, we have used the QRM. We have obtained rather accurate solutions of our CIP in our numerical tests, in the case when both Dirichlet and Neumann boundary conditions for functions q_n are known at both edges of the interval $(0, 1)$: recall that the Neumann condition at $x = 1$ is given automatically, whereas the Dirichlet boundary condition is not given. Furthermore, we have established analytically that the latter condition likely

does not carry a lot of information. We have tested two cases of the medium: (1) when a mine-like target is embedded in the uniform background and (2) when this target is embedded in a slowly changing background. Our sensitivity curves of Figures 3.3(c) and 3.4(c) at least partially explain the quality of results. Results of imaging of these targets in the second case were more accurate. However, the slowly changing background was imaged poorly, which is still acceptable for our application. An explanation of the poor image of that background is linked with the ill-posed nature of our CIP. Indeed, we have shown that the boundary data for the forward problem solution with our computed coefficient, which actually represented the image of the mine-like target only, are very close to the original boundary data, which included both that target and the slowly changing background. In particular, we presented two tests for the case of blind data.

The case when the Dirichlet boundary condition at $x = 1$ was unknown, was computed with a lesser accuracy. Specifically, while locations of mine-like targets were imaged accurately, the inclusion/background contrast was imaged poorly. Still, we believe that an application of the above mentioned two-stage procedure should provide a better accuracy in the contrast. In addition, the 2-D and 3-D data are more informative, because waves can get around targets in these cases, unlike the 1-D case considered here. So, we believe that our future images with 2-D and 3-D CIPs with the backscattering data only will have a good quality, and our preliminary computations provide a good indication of this.

CHAPTER 4: GLOBALLY CONVERGENT NUMERICAL METHOD FOR A HYPERBOLIC COEFFICIENT INVERSE PROBLEM IN THE 2D CASE

4.1 Statements of Forward and Inverse Problems

We work with the 2-d case only. Some properties of the solution of the forward problem were established in the 3-d case in [40]. Their extensions to the 2-d case can be done along the same lines, although it is space consuming. Hence, for brevity we use these properties here, assuming that they hold for 2-d.

Denote $\mathbf{x} = (x, z) \in \mathbb{R}^2$. As the forward problem, we consider the Cauchy problem for a hyperbolic PDE

$$c(\mathbf{x}) u_{tt} = \Delta u \text{ in } \mathbb{R}^2 \times (0, \infty), \tag{4.1}$$

$$u(\mathbf{x}, 0) = 0, u_t(\mathbf{x}, 0) = \delta(\mathbf{x} - \mathbf{x}_0). \tag{4.2}$$

Equation (4.1) governs, e.g. propagation of acoustic and electromagnetic waves. In the acoustical case $1/\sqrt{c(\mathbf{x})}$ is the sound speed. In the 2-d case of EM waves propagation in a non-magnetic medium the coefficient $c(\mathbf{x})$ is $c(\mathbf{x}) := \varepsilon_r(\mathbf{x})$, where $\varepsilon_r(\mathbf{x})$ is the spatially distributed dielectric constant, i.e. $\varepsilon_r(\mathbf{x}) = \varepsilon(\mathbf{x})/\varepsilon_0$, where $\varepsilon(\mathbf{x})$ is the spatially distributed electric permittivity of the medium and ε_0 is the dielectric permittivity of the vacuum, see [32] for the derivation of (4.1) from Maxwell's equations in the 2-d case. Let $\Omega \subset \mathbb{R}^2$ be a convex bounded domain with the piecewise smooth boundary $\partial\Omega$. As it is always the case of the QRM, we need to assume a certain over-smoothness of the solution. So, we assume that the function $c(\mathbf{x})$ satisfies the

following conditions

$$c(\mathbf{x}) \geq 1, c(\mathbf{x}) = 1 \text{ for } \mathbf{x} \in \mathbb{R}^2 \setminus \Omega, \tag{4.3}$$

$$c(\mathbf{x}) \in C^4\left(\mathbb{R}^2\right). \tag{4.4}$$

We will work with the Laplace transform of the functions u,

$$w(\mathbf{x}, s) = \int_0^\infty u(\mathbf{x}, t) e^{-st} dt, \text{ for } s \geq \underline{s} = const. > 0, \tag{4.5}$$

where $\underline{s}$ is a certain number. In our numerical studies we choose $\underline{s}$ experimentally. We call the parameter s *pseudo frequency*. Equation for the function w is

$$\Delta w - s^2 c(\mathbf{x}) w = -\delta(\mathbf{x} - \mathbf{x}_0), \forall s \geq \underline{s}, \tag{4.6}$$

$$\lim_{|\mathbf{x}| \to \infty} w(\mathbf{x}, s) = 0, \forall s \geq \underline{s}. \tag{4.7}$$

The condition (4.7) was established in [40] for sufficiently large values of $\underline{s}$. In addition, for these values of $\underline{s}$ [40]

$$w(\mathbf{x}, s) > 0. \tag{4.8}$$

In the course of the proof of the convergence theorem (section 4.5) we will work with functions $c \in C^1(\mathbb{R}^2) \subset C^\gamma(\mathbb{R}^2), \forall \gamma \in (0,1)$. Below $C^{k+\gamma}$ are Hölder spaces, where $k \geq 0$ is an integer. It follows from the classic theory of elliptic PDEs [43] that if $c \in C^{k+\gamma}(\mathbb{R}^2)$, then $w \in C^{k+2+\gamma}(\mathbb{R}^2 \setminus \{|x - x_0| < \theta\}), \forall \theta > 0$.

In our derivations we need an asymptotic behavior of the function $w(\mathbf{x}, s)$ at $s \to \infty$, which is formulated in Lemma 4.1. Although this lemma is now formulated only for the 3-d case, we assume that it is valid in the 2-d case as well, see the beginning of this section.

Lemma 4.1. *[27].* Assume that conditions (4.3) and (4.4) are satisfied and that we

work in $\mathbb{R}^3$. Let the function $w(\mathbf{x},s) \in C^{5+\gamma}\left(\mathbb{R}^3 \diagdown \{|\mathbf{x}-\mathbf{x}_0|<\theta\}\right)$, $\forall \theta > 0$ be the solution of the problem (4.6), (4.7). Assume that geodesic lines, generated by the eikonal equation corresponding to the function $c(\mathbf{x})$ are regular, i.e. any two points in $\mathbb{R}^3$ can be connected by a single geodesic line. Let $l(\mathbf{x},\mathbf{x}_0)$ be the length of the geodesic line connecting points $\mathbf{x}$ and $\mathbf{x}_0$. Then the following asymptotic behavior of the function w and its derivatives takes place for $|\alpha| \leq 2, k = 0,1, \mathbf{x} \neq \mathbf{x}_0$

$$D_{\mathbf{x}}^{\alpha} D_s^k w(\mathbf{x},s) = D_{\mathbf{x}}^{\alpha} D_s^k \left\{ \frac{\exp\left[-sl(\mathbf{x},\mathbf{x}_0)\right]}{f(\mathbf{x},\mathbf{x}_0)} \left[1 + O\left(\frac{1}{s}\right)\right]\right\}, s \to \infty, \tag{4.9}$$

where $f(\mathbf{x},\mathbf{x}_0)$ is a certain function and $f(\mathbf{x},\mathbf{x}_0) \neq 0$ for $\mathbf{x} \neq \mathbf{x}_0$.

An interesting question here is about an easily verifiable sufficient condition of the regularity of geodesic lines. In general, such a condition is unknown, except of the trivial case when the function $c(\mathbf{x})$ is close to a constant. To our best knowledge, the only case of such a condition in 2-d is

$$\Delta \ln c(\mathbf{x}) \geq 0, \forall \mathbf{x} \in \mathbb{R}^2,$$

see [45] as well as Theorem 2 in Chapter 2 of [42]. However, this condition is not satisfied in our computational examples. So, we verify (4.9) numerically in our computations (subsection 7.2 of [27]): this is a typical case when the computational experience is less pessimistic than the theory. Thus, everywhere below we assume that the asymptotic behavior (4.9) is valid.

To simplify the presentation and also because of our target application to imaging of plastic land mines, we now specify the domain $\Omega \subset \mathbb{R}^2$. Let $B > 0$ be a constant.

Below

$$\Omega = (-B, B) \times (0, 2B), \partial\Omega = \cup_{i=1}^{4} \Gamma_i, \tag{4.10}$$

$$\Gamma_1 = \partial\Omega \cap \{z = 0\}, \Gamma_2 = \partial\Omega \cap \{x = B\}, \tag{4.11}$$

$$\Gamma_3 = \partial\Omega \cap \{x = -B\}, \Gamma_4 = \partial\Omega \cap \{z = 2B\}. \tag{4.12}$$

Inverse Problem. *Suppose that the coefficient $c(\mathbf{x})$ in equation (4.6) satisfies conditions (4.3), (4.4) and is unknown in the domain Ω. Determine the function $c(\mathbf{x})$ for $\mathbf{x} \in \Omega$, assuming that the following functions $\varphi_0(x, s)$ and $\varphi_1(x, s)$ are known for a single source position $\mathbf{x}_0 \notin \overline{\Omega}$*

$$w(\mathbf{x}, s)|_{\Gamma_1} = \varphi_0(x, s), w_z(\mathbf{x}, s)|_{\Gamma_1} = \varphi_1(x, s), \forall s \in [\underline{s}, \overline{s}], \tag{4.13}$$

where $\overline{s} > \underline{s}$ is a number, which should be chosen experimentally in numerical studies.

Note that in experiments usually only the function $u(x, 0, t)$ is measured. One can approximately assume that the function $u(x, 0, t)$ is known for all $x \in \mathbb{R}$ implying that the function $\varphi_0(x, s)$ is known for all $x \in \mathbb{R}$ and for all $s \in [\underline{s}, \overline{s}]$ via the Laplace transform (4.5) of $u(x, 0, t)$. Next, since the coefficient $c(\mathbf{x}) = 1$ is known for $z < 0$, then solving the forward problem (4.6), (4.7) in the half plane $\{z < 0\}$ with the boundary condition $w(x, 0, s) = \varphi_0(x, s)$, one can uniquely determine the function $w(\mathbf{x}, s)$ for $z < 0$, thus coming up with the function $w_z(x, 0, s) = \varphi_1(x, s)$.

The question of uniqueness of this CIP is a well known long standing problem. Currently it can be addressed positively via the method of Carleman estimates only in the case when the $\delta(\mathbf{x} - \mathbf{x}_0)$ in (4.2) is replaced with such a function $f(\mathbf{x})$ that $f(\mathbf{x}) \neq 0$ in $\overline{\Omega}$ [14]. Nevertheless, the authors believe that, because of the applied aspect, it makes sense to develop a globally convergent method for this CIP, assuming that uniqueness holds.

4.2 Layer Stripping With Respect to s

By (4.8) we can consider the function $v = \ln w/s^2$. Hence, (4.6) and (4.13) lead to

$$\Delta v + s^2 |\nabla v|^2 = c(\mathbf{x}), \quad \mathbf{x} \in \Omega, \tag{4.14}$$

$$v|_{\Gamma_1} = \varphi_2(x,s), \quad v_z|_{\Gamma_1} = \varphi_3(x,s), \ \forall s \in [\underline{s}, \overline{s}], \tag{4.15}$$

where $\varphi_2 = \ln \varphi_0/s^2, \varphi_3 = \varphi_1/(s^2\varphi_0)$. The term $\delta(\mathbf{x} - \mathbf{x}_0)$ is not present in (4.14) because $\mathbf{x}_0 \notin \overline{\Omega}$. We now eliminate the function $c(\mathbf{x})$ from equation (4.14) via the differentiation with respect to s, since $\partial_s c(\mathbf{x}) = 0$. Introduce a new function $q(\mathbf{x}, s) = \partial_s v(\mathbf{x}, s)$. Lemma 4.1 implies that

$$D^\alpha_{\mathbf{x}}(v) = O\left(\frac{1}{s}\right), D^\alpha_{\mathbf{x}}(q) = O\left(\frac{1}{s^2}\right), s \to \infty; |\alpha| \leq 2, \tag{4.16}$$

$$v(\mathbf{x}, s) = -\int_s^\infty q(\mathbf{x}, \tau)\, d\tau. \tag{4.17}$$

We truncate the integral in (4.17) as

$$v(\mathbf{x}, s) \approx -\int_s^{\overline{s}} q(\mathbf{x}, \tau)\, d\tau, \tag{4.18}$$

where $\overline{s} > \underline{s}$ is a large parameter which should be chosen in numerical experiments. Actually, $\overline{s}$ is one of regularization parameters of our method. In fact, we have truncated here the function $V(\mathbf{x}, \overline{s})$, which we call the *tail function*,

$$V(\mathbf{x}, \overline{s}) = -\int_{\overline{s}}^\infty q(\mathbf{x}, \tau)\, d\tau.$$

By (4.16)

$$\left\| D_{\overline{s}}^{k} V\left(\mathbf{x}, \overline{s}\right) \right\|_{C^2\left(\overline{\Omega}\right)} = O\left(\frac{1}{\overline{s}^{k+1}}\right), k = 0, 1;\ \overline{s} \to \infty. \tag{4.19}$$

Although by (4.19) the tail is small for the large values of $\overline{s}$, the numerical experience of [27,31,40,41,44] shows one should that it would be better to somehow approximate the tail function updating it via an iterative procedure.

Thus, still taking into account the tail, we obtain from (4.14) and (4.18) the following nonlinear integral differential equation

$$\begin{aligned} &\Delta q - 2s^2 \nabla q \cdot \int_s^{\overline{s}} \nabla q\left(x, \tau\right) d\tau + 2s \left[\int_s^{\overline{s}} \nabla q\left(x, \tau\right) d\tau \right]^2 \\ &+ 2s^2 \nabla q \nabla V - 2s \nabla V \cdot \int_s^{\overline{s}} \nabla q\left(x, \tau\right) d\tau + 2s \left(\nabla V\right)^2 = 0. \end{aligned} \tag{4.20}$$

Let $\psi_0\left(x, s\right) = \partial_s \varphi_2\left(x, s\right), \psi_1\left(s\right) = \partial_s \varphi_3\left(x, s\right)$. Then (4.15) implies that

$$q|_{\Gamma_1} = \psi_0\left(x, s\right), q_z|_{\Gamma_1} = \psi_1\left(x, s\right),\ \forall s \in \left[\underline{s}, \overline{s}\right]. \tag{4.21}$$

A slight modification of arguments of subsection 2.2 of [40] shows that, for if $s > \underline{s}$ and $\underline{s}$ is sufficiently large, then the function $w\left(\mathbf{x}, s\right)$ tends to zero together with its appropriate $\left(\mathbf{x}, s\right)-$derivatives as $|\mathbf{x}| \to \infty$ (in both 3-d and 2-d cases), which is slightly more general than (4.7). Hence, we have the following radiation condition

$$\lim_{B \to \infty} \left(\frac{\partial w}{\partial \nu_i} + sw \right) |_{\Gamma_i} = 0, i = 2, 3, 4.$$

where ν_i is the outer normal vector on Γ_i. Since $q(\mathbf{x}, s) = \partial_s\left(s^{-2} \ln w\right)$, then we obtain from the latter the following approximate Neumann boundary condition for the function q at Γ_i

$$\partial_{\nu_i} q\ |_{\Gamma_i} = s^{-2},\ i = 2, 3, 4. \tag{4.22}$$

So, while conditions (4.21) change with the change of the unknown coefficient $c(\mathbf{x})$, the condition (4.22) is generic and it is independent on $c(\mathbf{x})$. Thus, we use conditions (4.22) only to stabilize the problem.

The presence of integrals in (4.20) implies the nonlinearity, which is the main difficulty here. If the functions q and V are approximated well from (4.20)-(4.22) together with their $\mathbf{x}-$derivatives up to the second order, then the target unknown coefficient $c(\mathbf{x})$ is also approximated well from (4.14), where the function v is computed from (4.18), where the function V is added. Thus, below we focus on the following question: *How to solve numerically the problem (4.20)-(4.22)?*

Remark 4.1. *Since the tail function V is unknown, equation (4.20) contains two unknown functions q and V. The reason why we can approximate both of them is that we treat them differently: while we approximate the function q via inner iterations, the function V is approximated via outer iterations.*

We approximate the function $q(\mathbf{x}, s)$ as a piecewise constant function with respect to the pseudo frequency s. That is, we assume that there exists a partition $\underline{s} = s_N < s_{N-1} < ... < s_1 < s_0 = \overline{s}$ of the interval $[\underline{s}, \overline{s}]$ with the sufficiently small grid step size $h = s_{i-1} - s_i$ such that $q(\mathbf{x}, s) = q_n(\mathbf{x})$ for $s \in (s_n, s_{n-1}]$. We approximate the boundary condition (4.21), (4.22) as

$$q_n|_{\Gamma_1} = \overline{\psi}_{0,n}(x),\ \partial_z q_n|_{\Gamma_1} = \overline{\psi}_{1,n}(x),\ \partial_\nu q_n|_{\Gamma_i} = (s_n s_{n-1})^{-1}, i = 2, 3, 4. \tag{4.23}$$

where $\overline{\psi}_{0,n}$, $\overline{\psi}_{1,n}$ and $(s_n s_{n-1})^{-1}$ are averages of functions ψ_0, ψ_1 and s^{-1} over the interval (s_n, s_{n-1}). Rewrite (4.20) for $s \in (s_n, s_{n-1}]$ using this piecewise constant approximation. Then multiply the resulting approximate equation by the s-dependent Carleman Weight Function (CWF) of the form

$$\mathcal{C}_{n,\mu}(s) = \exp\left[-\mu\left|s - s_{n-1}\right|\right], s \in (s_n, s_{n-1}],$$

and integrate with respect to $s \in (s_n, s_{n-1}]$. We obtain the following approximate equation in Ω for the function $q_n(\mathbf{x}), n = 1, ..., N$

$$L_n(q_n) := \Delta q_n - A_{1n}\left(h\sum_{j=1}^{n-1}\nabla q_j - \nabla V_n\right)\nabla q_n = \tag{4.24}$$

$$= B_n(\nabla q_n)^2 - A_{2,n}h^2\left(\sum_{j=1}^{n-1}\nabla q_j\right)^2 + 2A_{2,n}\nabla V_n\left(h\sum_{j=1}^{n-1}\nabla q_j\right) - A_{2,n}(\nabla V_n)^2.$$

We have intentionally inserted dependence of the tail function V_n from the iteration number n here because we will approximate these functions iteratively. In (4.24) $A_{1,n} = A_{1,n}(\mu, h), A_{2,n} = A_{2,n}(\mu, h), B_n = B_n(\mu, h)$ are certain numbers depending on μ and h, see specific formulas in [27]. It is convenient to set in (4.24)

$$q_0 \equiv 0. \tag{4.25}$$

Since boundary value problems (4.23), (4.24) are actually generated by equation (4.20), which contains Volterra-like s-integrals, then these problems can be solved sequentially starting from q_1. Since boundary conditions (4.23) are over-determined ones, it is natural to apply a version of the QRM here, because the QRM finds "least squares" solutions in the case of over-determined boundary conditions.

Remark 4.2. *As to (4.24), an important point is that* $|B_n(\mu, h)| \leq 8\bar{s}^2/\mu$ *for* $\mu h \geq 1$ *[27]. We have used* $\mu = 50$ *in our computations. Hence, assuming that* $\mu >> 1$,*we ignore the nonlinear term in (4.24) below via setting* $B_n(\nabla q_n)^2 := 0$. *This allows us to solve a linear problem for each* q_n.

4.3 The Algorithm

Our algorithm reconstructs iterative approximations $c_{n,k}(\mathbf{x}) \in C^1\left(\overline{\Omega}\right)$ of the function $c(\mathbf{x})$. On the other hand, to iterate with respect to the tails, we need to solve the forward problem (4.6), (4.7) in $\mathbb{R}^2$ on each iterative step. To do this,

we extend each function $c_{n,k}(\mathbf{x})$ outside of the Ω, so that the resulting function $\widehat{c}_{n,k}(\mathbf{x}) = 1$ outside of $\Omega, \widehat{c}_{n,k}(\mathbf{x}) = c_{n,k}(\mathbf{x})$ in a subdomain $\Omega' \subset\subset \Omega$ and $\widehat{c}_{n,k} \in C^1(\mathbb{R}^2)$. In addition, to ensure the ellipticity of the operator in (4.6), we need to have $\widehat{c}_{n,k}(\mathbf{x}) \geq const. > 0$ in $\mathbb{R}^2$. So, we now describe a rather standard procedure of such an extension. Choose a function $\chi(\mathbf{x}) \in C^\infty(\mathbb{R}^2)$ such that

$$\chi(\mathbf{x}) = \begin{cases} 1 \text{ in } \Omega', \\ \text{between 0 and 1 in } \Omega \diagdown \Omega', \\ 0 \text{ outside of } \Omega. \end{cases}$$

The existence of such functions $\chi(\mathbf{x})$ is well known from the Real Analysis course. Define the target extension of the function $c_{n,k}$ as $\widehat{c}_{n,k}(\mathbf{x}) := (1 - \chi(\mathbf{x})) + \chi(\mathbf{x}) c_{n,k}(\mathbf{x}), \forall x \in \mathbb{R}^2$. Hence, $\widehat{c}_{n,k}(\mathbf{x}) = 1$ outside of Ω and $\widehat{c}_{n,k} \in C^1(\mathbb{R}^2)$. Let $\widetilde{\Omega} \subseteq \Omega$ be a subdomain and $\Omega' \subset\subset \widetilde{\Omega}$. Suppose that $c_{n,k}(\mathbf{x}) \geq 1/2$ in $\widetilde{\Omega}$. Then $\widehat{c}_{n,k}(\mathbf{x}) \geq 1/2$ in Ω. Indeed, $\widehat{c}_{n,k}(\mathbf{x}) - 1/2 = (1 - \chi(\mathbf{x}))/2 + \chi(\mathbf{x})(c_{n,k}(\mathbf{x}) - 1/2) \geq 0$.

4.3.1 The iterative process

We now present our algorithm. On each iterative step n we approximate both the function q_n and the tail function V_n, see Remark 4.1. Each iterative step requires an approximate solution of the boundary value problem (4.23), (4.24). This is done via the QRM, which is described in subsection 4.3.2. First, we choose an initial tail function $V_{1,1}(\mathbf{x}) \in C^2(\overline{\Omega})$ and use (4.25). As to the choice of $V_{1,1}$, it was taken as $V_{1,1} \equiv 0$ in [27]. In later publications [31, 40, 41, 44] $V_{1,1}$ was taken as the one, which corresponds to the case $c(\mathbf{x}) \equiv 1$, where $c(\mathbf{x}) := 1$ is the value of the unknown coefficient outside of the domain of interest Ω, see (4.3). An observation was that while both these choices give the same result, the second choice leads to a faster convergence and both choices satisfy conditions of the global convergence theorem. For each q_n we have inner iterations with respect to tails.

Step n^k, where $n, k \geq 1$. Recall that by (4.25) $q_0 \equiv 0$. Suppose that functions

$q_i \in H^5(\Omega), i = 1, ..., n-1$ and tails $V_1, ..., V_{n-1}, V_{n,k} \in C^2\left(\overline{\Omega}\right)$ are constructed. To construct the function $q_{n,k}$, we use the QRM (subsection 4.3.2) to find an approximate solution of the following boundary value problem in Ω

$$\Delta q_{n,k} - A_{1n}\left(h\sum_{j=1}^{n-1}\nabla q_j - \nabla V_{n,k}\right)\nabla q_{n,k} =$$

$$-A_{2,n}h^2\left(\sum_{j=1}^{n-1}\nabla q_j\right)^2 + 2A_{2,n}\nabla V_{n,k}\cdot\left(h\sum_{j=1}^{n-1}\nabla q_j\right) - A_{2,n}\left(\nabla V_{n,k}\right)^2, \tag{4.26}$$

$$q_{n,k}|_{\Gamma_1} = \overline{\psi}_{0,n}(x),\ \partial_z q_{n,k}|_{\Gamma_1} = \overline{\psi}_{1,n}(x),\ \partial_{\nu_i} q_{n,k}|_{\Gamma_i} = (s_n s_{n-1})^{-1}, i = 2, 3, 4.$$

Hence, we obtain the function $q_{n,k} \in H^5(\Omega)$. By the embedding theorem $q_{n,k} \in C^3\left(\overline{\Omega}\right)$. To reconstruct an approximation $c_{n,k}(\mathbf{x})$ for the function $c(\mathbf{x})$, we first, use (4.18) to calculate an approximation for $v(\mathbf{x}, s_n)$ as

$$v_{n,k}(\mathbf{x}, s_n) = -hq_{n,k}(\mathbf{x}) - h\sum_{j=1}^{n-1} q_j(\mathbf{x}) + V_{n,k}(\mathbf{x}). \tag{4.27}$$

Next, using (4.14), we set for $n \geq 1$

$$c_{n,k}(\mathbf{x}) = \Delta v_{n,k}(\mathbf{x}, s_n) + s_n^2\left|\nabla v_{n,k}(\mathbf{x}, s_n)\right|^2, \mathbf{x} \in \Omega. \tag{4.28}$$

Assuming that the exact solution of our Inverse Problem $c^* \geq 1$ in $\mathbb{R}^2$ (see (4.3)), it follows from Theorem 4.2 that $c_{n,k}(\mathbf{x}) \geq 1/2$ in $\Omega_\varkappa \subset \Omega$, where the subdomain $\Omega_\varkappa$ is defined in section 4.4. Next, we construct the function $\widehat{c}_{n,k}(\mathbf{x})$ as in the beginning of this section. Hence, by (4.26)-(4.28) the function $\widehat{c}_{n,k} \in C^\gamma(\mathbb{R}^2)$. Next, we solve the forward problem (4.6), (4.7) with $c(\mathbf{x}) := \widehat{c}_{n,k}(\mathbf{x})$ for $s := \overline{s}$ and obtain the function $w_{n,k}(\mathbf{x}, \overline{s})$. Next, we set for the new tail

$$V_{n,k+1}(\mathbf{x}) = \frac{\ln w_{n,k}(\mathbf{x}, \overline{s})}{\overline{s}^2} \in C^2\left(\overline{\Omega}\right).$$

We continue these iterations with respect to tails until convergence occurs. We cannot prove this convergence. However, we have always observed numerically that functions $q_{n,k}, c_{n,k}$ and $V_{n,k}$ have stabilized at $k := m$ for a certain m. So, assuming that they are stabilized, we set

$$c_n(\mathbf{x}) := c_{n,m}(\mathbf{x}), q_n(\mathbf{x}) := q_{n,m}(\mathbf{x}), V_n(\mathbf{x}) := V_{n,m}(\mathbf{x}) := V_{n+1,1}(\mathbf{x}) \text{ for } \mathbf{x} \in \Omega.$$

We stop iterations with respect to n at $n := N$.

4.3.2 The quasi-reversibility method

Let $H_{n,k}(\mathbf{x})$ be the right hand side of equation (4.26) for $n \geq 1$. Denote

$$a_{n,k}(\mathbf{x}) = A_{1,n}\left(h\sum_{j=1}^{n-1}\nabla q_j - \nabla V_{n,k}\right) \tag{4.29}$$

Then the boundary value problem (4.26) can be rewritten as

$$\Delta q_{n,k} - a_{n,k}\cdot\nabla q_{n,k} = H_{n,k}, \tag{4.30}$$

$$q_{n,k}|_{\Gamma_1} = \overline{\psi}_{0,n}(x),\ \partial_z q_{n,k}|_{\Gamma_1} = \overline{\psi}_{1,n}(x),\ \partial_{\nu_i} q_{n,k}|_{\Gamma_i} = (s_n s_{n-1})^{-1}, i = 2,3,4. \tag{4.31}$$

Since we have two boundary conditions rather then one at Γ_1, we find the "least squares" solution of the problem (4.30), (4.31) via the QRM. Specifically, we minimize the following Tikhonov functional

$$J^{\alpha}_{n,k}(u) = \|\Delta u - a_{n,k}\cdot\nabla u - H_{n,k}\|^2_{L_2(\Omega)} + \alpha\|u\|^2_{H^5(\Omega)}, \tag{4.32}$$

subject to boundary condition (4.31), where the small regularization parameter $\alpha \in (0,1)$. Let $u(x)$ be the minimizer of this functional. Then we set $q_{n,k}(\mathbf{x}) := u(\mathbf{x})$. Local minima do not occur here because (4.32) is the sum of square norms of two expressions, both of which are linear with respect to u, also see Lemmata 4.3 and

4.4 in section 4.4. The second term in the right hand side of (4.32) is the Tikhonov regularization term. We use the $H^5(\Omega)-$norm here in order to ensure that the minimizer $u := q_{n,k} \in C^3\left(\overline{\Omega}\right)$, which implies in turn that functions $\widehat{c}_{n,k} \in C^1(\mathbb{R}^2)$.

Remark 4.3. *1. In our computations we relax the smoothness assumptions via considering the $H^2(\Omega)-$norm in the second term in the right hand side of (4.32). This is possible because in computations we actually work with finite dimensional spaces. Specifically, we work with finite differences and do not use "overly fine" mesh, which means that dimensions of our "computational spaces" are not exceedingly large. In this case all norms are equivalent not only theoretically but practically as well. To the contrary, if the mesh would be too fine, then the corresponding space would be "almost" infinite dimensional.*

2. One may pose a question on why we would not avoid the QRM via using just one of two boundary conditions at Γ_1 in (4.31), since we have the Neumann boundary condition at $\partial\Omega \diagdown \Gamma_1$. However, in this case we would be unable to prove the C^3- smoothness of the function $q_{n,k}$, because the boundary $\partial\Omega$ is not smooth. In the case of the Dirichlet boundary condition only $q_{n,k}|_{\Gamma_1}$ we would be unable to prove smoothness even assuming that $\partial\Omega \in C^\infty$, because of the Neumann boundary condition at the rest of the boundary. Besides, in our convergence estimate of the QRM in Theorem 4.1 we do not use the boundary condition (4.31) at Γ_4. Finally, since conditions $\partial_{\nu_i} q_{n,k}|_{\Gamma_i} = (s_n s_{n-1})^{-1}$ are independent on the target coefficient, it seems to be that two boundary conditions rather than one at Γ_1 should provide a better reconstruction.

4.4 Estimates for the QRM

For brevity we scale variables in such a way that in sections 4.4 and 4.5 it is assumed that $\Omega = (-1/4, 1/4) \times (0, 1/2)$. In sections 4.5 and 4.6 $C = C(\Omega) > 0$ denotes different positive constants depending only on the domain Ω. Let $\lambda, \nu > 2$ be

two parameters. Introduce another Carleman Weight Function (CWF) $K(z)$,

$$K(z) := K_{\lambda,\nu}(z) = \exp(\lambda\rho^{-\nu}), \text{ where } \rho(z) = z + \frac{1}{4}, z > 0.$$

Note that $\rho(z) \in (0, 3/4)$ in Ω and $\rho(z) \mid_{\Gamma_4} = 3/4$. Let the number $\varkappa \in (1/3, 1)$. Denote $\Omega_\varkappa = \{\mathbf{x} \in \Omega : \rho(z) < 3\varkappa/4\}$. Hence, if $\varkappa_1 < \varkappa_2$, then $\Omega_{\varkappa_1} \subset\subset \Omega_{\varkappa_2}$. Also, $\Omega_1 = \Omega$ and $\Omega_{1/3} = \varnothing$. Lemma 4.2 established the Carleman estimate for the Laplace operator. Although such estimates are well known [14, 19], we still need to prove this lemma, because we use a non-standard CWF and also because when integrating the pointwise Carleman estimate over Ω, we should take into account that only one, rather than conventional two, zero boundary condition (4.33) is given at both Γ_2 and Γ_3. These were not done before.

Lemma 4.2. Fix a number $\nu := \nu_0(\Omega) > 2$. Consider functions $u \in H^3(\Omega)$ such that (see (4.10)-(4.12)

$$u \mid_{\Gamma_1} = u_z \mid_{\Gamma_1} = u_x \mid_{\Gamma_2} = u_x \mid_{\Gamma_3} = 0. \tag{4.33}$$

Then there exists a constant $C = C(\Omega) > 0$ such that for any $\lambda > 2$ the following Carleman estimate is valid for all these functions

$$\begin{aligned}\int_\Omega (\Delta u)^2 K^2 dxdz \quad \geq \quad & \frac{C}{\lambda} \int_\Omega \left(u_{xx}^2 + u_{zz}^2 + u_{xz}^2\right) K^2 dxdz + C\lambda \int_\Omega \left[(\nabla u)^2 + \lambda^2 u^2\right] K^2 dxdz \\ & -C\lambda^3 \|u\|^2_{H^3(\Omega)} \exp\left[2\lambda\left(\frac{4}{3}\right)^{\nu_0}\right].\end{aligned}$$

Proof. It is convenient to assume initially that $\nu > 2$ is an arbitrary number.

We have

$$\begin{aligned}(\Delta u)^2 K^2 &= \left(u_{xx}^2 + u_{zz}^2 + 2u_{xx}u_{zz}\right) K^2 = \\ &\left(u_{xx}^2 + u_{zz}^2\right) K^2 + \partial_x \left(2u_x u_{zz} K^2\right) - 2u_x u_{zzx} K^2 + 4\lambda\nu\rho^{-\nu-1} u_x u_{zz} K^2 \\ &= \left(u_{xx}^2 + u_{zz}^2 + 2u_{xz}^2\right) K^2 + \partial_x \left(2u_x u_{zz} K^2\right) + \partial_z \left(-2u_x u_{xz} K^2\right) \\ &+4\lambda\nu\rho^{-\nu-1} \left(u_x u_{zz} - u_x u_{zx}\right) K^2.\end{aligned}$$

Since

$$4\lambda\nu\rho^{-\nu-1} \left(u_x u_{zz} - u_x u_{xz}\right) K^2 \geq -\frac{1}{2} \left(u_{zz}^2 + u_{xz}^2\right) K^2 - 8\lambda^2\nu^2\rho^{-2\nu-2} u_x^2 K^2,$$

then we obtain that

$$\begin{aligned}(\Delta u)^2 K^2 &\geq \frac{1}{2} \left(u_{xx}^2 + u_{zz}^2 + u_{xz}^2\right) K^2 - 8\lambda^2\nu^2\rho^{-2\nu-2} u_x^2 K^2 \\ &+\partial_x \left(2u_x u_{zz} K^2\right) + \partial_z \left(-2u_x u_{xz} K^2\right).\end{aligned} \tag{4.34}$$

Consider a new function $v = u \cdot K$. Substituting $u = v \cdot K^{-1}$, we obtain

$$\begin{aligned}(\Delta u)^2 \rho^{\nu+1} K^2 &= (y_1 + y_2 + y_3)^2 \rho^{\nu+1} \geq 2y_2(y_1 + y_3)\rho^{\nu+1}, \\ y_1 &= \Delta v,\ y_2 = 2\lambda\nu\rho^{-\nu-1} v_z,\ y_3 = (\lambda\nu)^2 \rho^{-2\nu-2}(1 - \frac{\nu+1}{\lambda\nu}\rho^{\nu})v.\end{aligned} \tag{4.35}$$

We have

$$2y_1 y_2 \rho^{\nu+1} = \partial_x \left(4\lambda\nu v_z v_x\right) + \partial_z \left[2\lambda\nu \left(v_z^2 - v_x^2\right)\right]. \tag{4.36}$$

Next, by (4.35)

$$\begin{aligned} 2y_2y_3\rho^{\nu+1} &= 4(\lambda\nu)^3\left(\rho^{-2\nu-2}-\frac{\nu+1}{\lambda\nu}\rho^{-\nu-2}\right)v_zv \\ &= \partial_z\left[2(\lambda\nu)^3\left(\rho^{-2\nu-2}-\frac{\nu+1}{\lambda\nu}\rho^{-\nu-2}\right)v^2\right] \\ &\quad +4(\lambda\nu)^3(\nu+1)\rho^{-2\nu-3}\left(1-\frac{\nu+2}{2\lambda\nu}\rho^{\nu}\right)v^2 \\ &\geq 2\lambda^3\nu^4\rho^{-2\nu-3}v^2+\partial_z\left[2(\lambda\nu)^3\left(\rho^{-2\nu-2}-\frac{\nu+1}{\lambda\nu}\rho^{-\nu-2}\right)v^2\right]. \end{aligned} \tag{4.37}$$

Summing up (4.36) and (4.37), using the backwards substitution $u = v \cdot K$ and using (4.35), we obtain

$$(\Delta u)^2\rho^{\nu+1}K^2 \geq 2\lambda^3\nu^4\rho^{-2\nu-3}u^2K^2+\partial_xU_1+\partial_zU_2, \tag{4.38}$$

where the following estimates are valid for functions U_1 and U_2

$$\begin{aligned} |U_1| &\leq C\lambda\nu\left|u_x\right|\left(\left|u_z\right|+\lambda\nu\rho^{-\nu-1}\left|u\right|\right)K^2, \\ |U_2| &\leq C\lambda\nu\left(\left|\nabla u\right|^2+\lambda^2\nu^2\rho^{-2\nu-2}u^2\right)K^2. \end{aligned} \tag{4.39}$$

Since we do not have the term $\lambda\left(\nabla u\right)^2K^2$ in the right hand side of (4.38),we continue as follows:

$$\begin{aligned} -\lambda\nu u\cdot\Delta uK^2 &= \partial_x\left(-\lambda\nu uu_xK^2\right)+\partial_z\left(-\lambda\nu uu_zK^2\right)+\lambda\nu\left(\nabla u\right)^2K^2- \\ -2\lambda^2\nu^2\rho^{-\nu-1}u_zuK^2 &= \lambda\nu\left(\nabla u\right)^2K^2-2\lambda^3\nu^3\rho^{-2\nu-2}u^2K^2+\partial_xU_3+\partial_zU_4, \end{aligned}$$

Hence,

$$\begin{aligned} -\lambda\nu u\Delta uK^2 &= \lambda\nu\left(\nabla u\right)^2K^2-2\lambda^3\nu^3\rho^{-2\nu-2}u^2K^2+\partial_xU_3+\partial_zU_4, \\ U_3 &= -\lambda\nu uu_xK^2, |U_4|\leq C\left(\lambda\nu u_z^2+\lambda^2\nu^2\rho^{-\nu-1}u^2\right)K^2. \end{aligned} \tag{4.40}$$

Add (4.40) to (4.38) and take into account (4.39) as well as the fact that

$$2\lambda^3\nu^4\rho^{-2\nu-3} > 4\lambda^3\nu^3\rho^{-2\nu-2}$$

for $\nu > 2$. Likewise, by the Cauchy inequality

$$-\lambda\nu u \cdot \Delta u K^2 \leq \lambda^2\nu^2\rho^{-\nu-1}u^2K^2/2 + (\Delta u)^2\rho^{\nu+1}K^2/2.$$

Fix the number $\nu := \nu_0 > 2$. Then we can incorporate ν_0 in C and also we can regard that $\rho^{\nu_0+1} < C$, since $\rho^{\nu_0+1} < 1$. Hence, we obtain

$$\begin{aligned} (\Delta u)^2K^2 &\geq C\lambda\left[(\nabla u)^2 + \lambda^2u^2\right]K^2 + \partial_x U_5 + \partial_z U_6, \qquad (4.41)\\ |U_5| &\leq C\lambda\left|u_x\right|\left(\left|u_z\right| + \lambda\left|u\right|\right)K^2,\ \ |U_6| \leq C\lambda\left[\left|\nabla u\right|^2 + \lambda^2u^2\right]K^2. \end{aligned}$$

Now we set in (4.34) $\nu := \nu_0$, divide it by λd with a positive constant $d = d(\nu_0)$ such that $4\lambda\nu_0^2\rho^{-2\nu_0-2}/d \leq C/2$ and next add it to (4.41). Then we can choose a constant obtain the following pointwise Carleman estimate for the Laplace operator in the domain Ω

$$\begin{aligned} (\Delta u)^2K^2 &\geq \frac{C}{\lambda}\left(u_{xx}^2 + u_{zz}^2 + u_{xz}^2\right)K^2 + C\lambda\left[(\nabla u)^2 + \lambda^2u^2\right]K^2 + \partial_x U_7 + \partial_z U_8, (4.42)\\ |U_7| &\leq C\lambda\left|u_x\right|\left(\left|u_{zz}\right| + \left|u_z\right| + \lambda\left|u\right|\right)K^2,\ \ |U_8| \leq C\lambda\left[\left|u_{xz}\right|^2 + \left|\nabla u\right|^2 + \lambda^2u^2\right]K^2. \end{aligned}$$

We now integrate (4.42) over the rectangle Ω using the Gauss-Ostrogradsky formula. It is important that because of (4.33) and the estimate for $|U_7|$, resulting boundary integrals over Γ_1, Γ_2 and Γ_3 will be zero. Finally, to obtain the estimate of this lemma, we note that

$$K^2\left(\frac{1}{2}\right) = K^2(z)\,|_{\Gamma_4} = \min_{\overline{\Omega}} K^2(z) = \exp\left[2\lambda\left(\frac{4}{3}\right)^{\nu_0}\right].$$

Thus,

$$\int\limits_{\Gamma_4} \lambda \left[|u_{xz}|^2 + |\nabla u|^2 + \lambda^2 u^2 \right] K^2 dx \leq C\lambda^3 \left\| u \right\|^2_{H^3(\Omega)} \exp\left[2\lambda \left(\frac{4}{3} \right)^{\nu_0} \right]. \square$$

We now establish both existence and uniqueness of the minimizer of the functional (4.32).

Lemma 4.3. Suppose that in (4.32) $H_{n,k} \in L_2(\Omega)$ and that there exists a function $\Phi \in H^5(\Omega)$ satisfying boundary conditions (4.31), except of maybe at Γ_4. Assume that in (4.29) both components $a^{(j)}_{n,k}, j = 1, 2$ of the vector function $a_{n,k}$ are such that $a^{(j)}_{n,k} \in C\left(\overline{\Omega}\right)$ and $\left\| a^{(j)}_{n,k} \right\|_{C\left(\overline{\Omega}\right)} \leq 1$. Then there exists unique minimizer $u_\varepsilon \in H^5(\Omega)$ of the functional (4.32). Furthermore,

$$\left\| u_\varepsilon \right\|_{H^5(\Omega)} \leq \frac{C}{\sqrt{\alpha}} \left(\left\| H_{n,k} \right\|_{L_2(\Omega)} + \left\| \Phi \right\|_{H^5(\Omega)} \right).$$

Proof. We assume here that $\left\| a^{(j)}_{n,k} \right\|_{C\left(\overline{\Omega}\right)} \leq 1$ for the purpose of Theorem 4.2 only, since actually we can impose any *a priori* upper estimate on these numbers. Let u be a minimizer of $J^\alpha_{n,k}(u)$ satisfying boundary conditions (4.31). Denote $U = u - \Phi$. The function U satisfies boundary conditions (4.33). By the variational principle

$$\left(G_{n,k} U, G_{n,k} v \right) + \alpha \left[U, v \right] = \left(H_{n,k} - G_{n,k} \Phi, G_{n,k} v \right),$$

for all functions $v \in H^5(\Omega)$ satisfying boundary conditions (4.33). Here

$$G_{n,k} U := \Delta U - a_{n,k} \cdot \nabla U. \tag{4.43}$$

Here and below $(\cdot, \cdot)$ denotes the scalar product in $L_2(\Omega)$ and $[\cdot, \cdot]$ denotes the scalar product in $H^5(\Omega)$. The rest of the proof follows from the Riesz theorem. $\square$

In the course of the proof of Theorem 4.2 we will need

Lemma 4.4. Consider an arbitrary function $g \in H^5(\Omega)$. Let the function $u \in H^5(\Omega)$ satisfies boundary conditions (4.33) as well as the variational equality

$$(G_{n,k}u, G_{n,k}v) + \alpha [u, v] = (H_{n,k}, G_{n,k}v) + \alpha [g, v], \tag{4.44}$$

for all functions $v \in H^5(\Omega)$ satisfying (4.33). Then

$$\|u\|_{H^5(\Omega)} \leq \frac{\|H_{n,k}\|_{L_2(\Omega)}}{\sqrt{\alpha}} + \|g\|_{H^5(\Omega)}.$$

Proof. Set in (4.44) $v := u$ and use the Cauchy-Schwarz inequality. $\square$

Theorem 4.1. Consider an arbitrary function $g \in H^5(\Omega)$. Let $u \in H^5(\Omega)$ *be the function satisfying (4.33) and (4.44). Let* $\left\|a_{n,k}^{(j)}\right\|_{C(\overline{\Omega})} \leq 1$, where $a_{n,k}^{(j)}, j = 1, 2$ are two components of the vector function $a_{n,k}$ in (4.36). Choose an arbitrary number $\overline{\varkappa}$ such that $\overline{\varkappa} \in (\varkappa, 1)$. Consider the numbers b_1, b_2,

$$b_1 = \frac{1}{2\left(1 + (1 - \overline{\varkappa}^{\nu_0})(3\overline{\varkappa})^{-\nu_0}\right)} < \frac{1}{2},\ b_2 = \frac{1}{2} - b_1 > 0,$$

where ν_0 is the parameter of Lemma 4.2. Then there exists a sufficiently small number $\alpha_0 = \alpha_0(\nu_0, \varkappa, \overline{\varkappa}) \in (0, 1)$ such that for all $\alpha \in (0, \alpha_0)$ the following estimate holds

$$\|u\|_{H^2(\Omega_\varkappa)} \leq C\frac{\|H_{n,k}\|_{L_2(\Omega)}}{\alpha^{b_1}} + \alpha^{b_2}\|g\|_{H^5(\Omega)}.$$

Proof. Setting (4.44) $v := u$ and using the Cauchy-Schwarz inequality, we obtain

$$\|G_{n,k}u\|^2_{L_2(\Omega)} \leq F^2 := \|H_{n,k}\|^2_{L_2(\Omega)} + \alpha\|g\|^2_{H^5(\Omega)}. \tag{4.45}$$

Note that $K^2(0) = \max_{\overline{\Omega}} K^2(z) = \exp(2\lambda \cdot 4^{\nu_0})$. Hence, $K^{-2}(0)\|K \cdot G_{n,k}u\|^2_{L_2(\Omega)} \leq$

F^2. Clearly $(G_{n,k}u)^2 K^2 \geq (\Delta u)^2 K^2/2 - C(\nabla u)^2 K^2$. Hence,

$$\int\limits_{\Omega} (\Delta u)^2 K^2 dxdz \leq C \int\limits_{\Omega} (\nabla u)^2 K^2 dxdz + K^2(0) F^2. \tag{4.46}$$

Applying Lemma 4.2 to (4.46), choosing $\lambda > 1$ sufficiently large and observing that the term with $(\nabla u)^2$ in (4.46) will be absorbed for such λ, we obtain

$$\begin{aligned}
& \lambda K^2(0) F^2 + C\lambda^4 \|u\|^2_{H^3(\Omega)} \exp\left[2\lambda\left(\frac{4}{3}\right)^{\nu_0}\right] \\
\geq\ & C \int\limits_{\Omega} \left(u_{xx}^2 + u_{zz}^2 + u_{xz}^2 + |\nabla u|^2 + u^2\right) K^2 dxdz \\
\geq\ & C \int\limits_{\Omega_\varkappa} \left(u_{xx}^2 + u_{zz}^2 + u_{xz}^2 + |\nabla u|^2 + u^2\right) K^2 dxdz \\
\geq\ & C \exp\left[2\lambda\left(\frac{4}{3\varkappa}\right)^{\nu_0}\right] \|u\|^2_{H^2(\Omega)}.
\end{aligned}$$

Comparing the first line with the last in this sequence of inequalities, dividing by the exponential term in the last line, taking $\lambda \geq \lambda_0(C, \varkappa, \overline{\varkappa}) > 1$ sufficiently large and noting that for such λ

$$\lambda^4 \exp\left[-2\lambda\left(\frac{4}{3\varkappa}\right)^{\nu_0}\right] < \exp\left[-2\lambda\left(\frac{4}{3\overline{\varkappa}}\right)^{\nu_0}\right],$$

we obtain a stronger estimate,

$$\|u\|^2_{H^2(\Omega_\varkappa)} \leq CK^2(0) F^2 + C\|u\|^2_{H^3(\Omega)} \exp\left[-2\lambda\left(\frac{4}{3\overline{\varkappa}}\right)^{\nu_0}(1 - \overline{\varkappa}^{\nu_0})\right] \tag{4.47}$$

Applying Lemma 4.4 to the second term in the right hand side of (4.47), we obtain

$$\|u\|^2_{H^2(\Omega_\varkappa)} \leq CF^2 \left\{\exp(2\lambda \cdot 4^{\nu_0}) + \alpha^{-1} \exp\left[-2\lambda\left(\frac{4}{3\overline{\varkappa}}\right)^{\nu_0}(1 - \overline{\varkappa}^{\nu_0})\right]\right\}. \tag{4.48}$$

Since $\alpha \in (0, \alpha_0)$ and α_0 is sufficiently small, we can choose sufficiently large $\lambda = \lambda(\alpha)$

such that

$$\exp\left(2\lambda\cdot 4^{\nu_0}\right)=\alpha^{-1}\exp\left[-2\lambda\left(\frac{4}{3\overline{\varkappa}}\right)^{\nu_0}\left(1-\overline{\varkappa}^{\nu_0}\right)\right]. \tag{4.49}$$

We obtain from (4.49) that $2\lambda\cdot 4^{\nu_0}=\ln\alpha^{-2b_1}$. Hence, (4.45) and (4.47)-(4.49) imply the validity of this theorem. $\square$

4.5 Global Convergence Theorem

We follow the concept of Tikhonov for ill-posed problems described in [46]. By this concept, one should assume that there exists an "ideal" exact solution of an ill-posed problem with the "ideal" exact data. Next, one should prove that the regularized solution is close to the exact one.

4.5.1 Exact solution

First, we need to introduce the definition of the exact solution. We assume that there exists a coefficient $c^*(\mathbf{x})$ satisfying conditions (4.3), (4.4), and this function is the unique exact solution of our Inverse Problem with the exact data $\varphi_0^*(x,s),\varphi_1^*(x,s)$ in (4.13), where $\varphi_0^*(x,s)=w^*(x,0,s)$, $\varphi_1^*(x,s)=w_z^*(x,0,s)$, $\forall s\in[\underline{s},\overline{s}]$. Here the function $w^*(\mathbf{x},s)\in C^{5+\gamma}\left(\mathbb{R}^2\diagdown\{|\mathbf{x}-\mathbf{x}_0|<\varepsilon\}\right)\times C^2([\underline{s},\overline{s}])$, $\forall\varepsilon>0$, $\forall\gamma\in(0,1)$, $\forall s\geq\underline{s}$ is the solution of the forward problem (4.6), (4.7) with $c(\mathbf{x}):=c^*(\mathbf{x})$. Let

$$v^*(\mathbf{x},s)=s^{-2}\ln\left[w^*(\mathbf{x},s)\right],\ q^*(\mathbf{x},s)=\partial_s v^*(\mathbf{x},s),\ V^*(\mathbf{x})=v^*(\mathbf{x},\overline{s}).$$

Hence, $q^*(\mathbf{x},s)\in C^{5+\gamma}(\Omega)\times C^1[\underline{s},\overline{s}]$. By (4.14)

$$c^*(\mathbf{x})=\Delta v^*(\mathbf{x},s)+s^2\left|\nabla v^*(\mathbf{x},s)\right|^2,\forall s\in[\underline{s},\overline{s}]. \tag{4.50}$$

The function q^* satisfies equation (4.20) where V is replaced with V^*. Boundary conditions for q^* are the same as ones (4.21), (4.22), where functions $\psi_0(x,s),\psi_1(x,s)$

are replaced with the exact boundary conditions $\psi_0^*(x,s), \psi_1^*(x,s)$ for $s \in [\underline{s}, \overline{s}]$,

$$q^*|_{\Gamma_1} = \psi_0^*(x,s), q_z^*|_{\Gamma_1} = \psi_1^*(x,s), \ \partial_{\nu_i} q^* \ |_{\Gamma_i} = s^{-2}, \ i = 2,3,4. \tag{4.51}$$

We call the function $q^*(\mathbf{x}, s)$ *the exact solution* of the problem (4.20)-(4.22) with the exact boundary conditions (4.51). For $n \geq 1$ let q_n^*, $\overline{\psi}_{0,n}^*$ and $\overline{\psi}_{1,n}^*$ be averages of functions q^*, ψ_0^* and ψ_1^* over the interval (s_n, s_{n-1}). Hence, it is natural to assume that

$$q_0^* \equiv 0, \max_{1 \leq n \leq N} \|q_n^*\|_{H^5(\Omega)} \leq C^*, C^* = const. > 1, \tag{4.52}$$

$$\left\| \overline{\psi}_{0,n}^* - \overline{\psi}_{0,n} \right\|_{H^2(\Gamma_1)} + \left\| \overline{\psi}_{1,n}^* - \overline{\psi}_{1,n} \right\|_{H^1(\Gamma_1)} \leq C^*(\sigma + h), \tag{4.53}$$

$$\max_{s \in [s_n, s_{n-1}]} \|q_n^* - q^*\|_{H^5(\Omega)} \leq C^* h \tag{4.54}$$

Here the constant $C^* = C^*\left(\|q^*\|_{H^5(\Omega) \times C^1[\underline{s}, \overline{s}]}\right)$ depends only on the $C^5\left(\overline{\Omega}\right) \times C^1[\underline{s}, \overline{s}]$ norm of the function $q^*(\mathbf{x}, s)$ and $\sigma > 0$ is a small parameter characterizing the level of the error in the data $\psi_0(x,s), \psi_1(x,s)$. We use the $H^5(\Omega)$ norm because of the quasi-reversibility, see (4.32). The step size $h = s_{n-1} - s_n$ can also be considered as a part of the error in the data. In addition, because of (4.51)

$$q_n^*|_{\Gamma_1} = \overline{\psi}_{0,n}^*(x), \partial_z q_n^*|_{\Gamma_1} = \overline{\psi}_{1,n}^*(x), \partial_\nu q_n^*|_{\Gamma_i} = (s_n s_{n-1})^{-1}, i = 2,3,4. \tag{4.55}$$

The function q_n^* satisfies the following analogue of equation (4.24)

$$\begin{aligned} &\Delta q_n^* - A_{1,n}\left(h\sum_{i=1}^{n-1} \nabla q_i^*(x) - \nabla V^*\right) \cdot \nabla q_n^* = -A_{2,n} h^2 \left(\sum_{i=1}^{n-1} \nabla q_i^*(x)\right)^2 \\ &+ 2A_{2,n} \nabla V^* \cdot \left(h\sum_{i=1}^{n-1} \nabla q_i^*(x)\right) - A_{2,n}(\nabla V^*)^2 + F_n(x,h,\mu). \end{aligned} \tag{4.56}$$

Since we have dropped the nonlinear term $B_n (\nabla q_n)^2$ in (4.26) (Remark 4.2), we incorporate this term in the error function $F_n (x, h, \mu) \in L_2 (\Omega)$ in (4.56). So, it is reasonably to assume that

$$\max_{\mu h \geq 1} \| F_n (\mathbf{x}, h, \xi, \mu) \|_{L_2(\Omega)} \leq C^* \left(h + \mu^{-1} \right). \tag{4.57}$$

4.5.2 Global convergence theorem

Assume that

$$\overline{s} > 1, \ \mu h \geq 1. \tag{4.58}$$

Then [27]

$$\max_{1 \leq n \leq N} \{ |A_{1,n}| + |A_{2,n}| \} \leq 8 \overline{s}^2. \tag{4.59}$$

We assume for brevity that

$$\overline{\psi}^*_{0,n} = \overline{\psi}_{0,n}, \overline{\psi}^*_{1,n} = \overline{\psi}_{1,n}. \tag{4.60}$$

The proof of Theorem 4.2 for the more general case (4.53) can easily be extended along the same lines, although it would take more space. Still, we keep the parameter σ of (4.53) as a part of the error in the data and incorporate it in the function F_n. Thus, we obtain instead of (4.57)

$$\max_{\mu h \geq 1} \| F_n (\mathbf{x}, h, \xi, \mu) \|_{L_2(\Omega)} \leq C^* \left(h + \mu^{-1} + \sigma \right). \tag{4.61}$$

We also recall that by the embedding theorem $H^5 (\Omega) \subset C^3 \left(\overline{\Omega} \right)$ and

$$\| f \|_{C^3\left(\overline{\Omega}\right)} \leq C \| f \|_{H^5(\Omega)}, \forall f \in H^5 (\Omega). \tag{4.62}$$

Theorem 4.2. Let the exact coefficient $c^* (\mathbf{x})$ satisfy conditions (4.3), (4.4). Suppose

that conditions (4.51)-(4.58), (4.60) and (4.61) are satisfied. Assume that for each $n \in [1, N]$ there exists a function $\Phi_n \in H^5(\Omega)$ satisfying boundary conditions (4.31), except of maybe at Γ_4. For any function $c \in C^\gamma(\mathbb{R}^2)$ such that $c(\mathbf{x}) \geq 1/2$, $c(\mathbf{x}) = 1$ in $\mathbb{R}^2 \setminus \Omega$ consider the solution $w_c(\mathbf{x}, \overline{s}) \in C^{2+\gamma}(\mathbb{R}^2 \setminus \{|\mathbf{x} - \mathbf{x}_0| < \theta\}), \forall \theta > 0$ of the problem (4.6), (4.7). Let $V_c(\mathbf{x}) = \overline{s}^{-2} \ln w_c(\mathbf{x}, \overline{s}) \in C^{2+\gamma}(\mathbb{R}^2 \setminus \{|\mathbf{x} - \mathbf{x}_0| < \theta\}), \theta > 0$ be the corresponding tail function and $V_{1,1}(\mathbf{x}, \overline{s}) \in C^2\left(\overline{\Omega}\right)$ be the initial tail function. Suppose that the cut-off pseudo frequency $\overline{s}$ is so large that the following estimates hold

$$\|V^*\|_{C^1(\overline{\Omega})} \leq \frac{\xi}{2}, \|V_{1,1}\|_{C^1(\overline{\Omega})} \leq \frac{\xi}{2}, \|V_c\|_{C^1(\overline{\Omega})} \leq \frac{\xi}{2}, \tag{4.63}$$

for any such function $c(\mathbf{x})$. Here $\xi \in (0, 1)$ is a sufficiently small number. Introduce the parameter $\beta := \overline{s} - \underline{s}$, which is the total length of the s-interval covered in our algorithm. Let α_0 be so small that it satisfies the corresponding condition of Theorem 4.1. Let $\alpha \in (0, \alpha_0)$ be the regularization parameter of the QRM. Assume that numbers h, σ, ξ, β, are so small that

$$h + \mu^{-1} + \sigma + \xi \leq \beta, \tag{4.64}$$

$$\beta \leq \frac{\sqrt{\alpha}}{136\overline{s}^2 (C^*)^2 C_1}, \tag{4.65}$$

where the number b_2 was introduced in Theorem 4.1 and the constant C_1 depends only on the domain Ω. We assume without loss of generality that $C_1 \in (1, C^*)$. Then the following estimates hold for all $\alpha \in (0, \alpha_0)$ and all $n \in [1, N]$

$$\|q_n\|_{H^5(\Omega)} \leq 3C^*, \tag{4.66}$$

$$\|q_n - q_n^*\|_{H^2(\Omega_\varkappa)} \leq 2C^* \alpha^{b_2}, \tag{4.67}$$

$$\|c_n - c^*\|_{C^1(\overline{\Omega}_\varkappa)} \leq 2C^* \alpha^{b_2}, c_n \geq \frac{1}{2} \text{ in } \Omega_\varkappa. \tag{4.68}$$

Remark 4.4. *1. Because of the term $\overline{s}^{-2}$ in inequalities (4.65), there is a discrepancy*

between these inequalities and (4.19). This discrepancy was discussed in detail in subsection 3.3 of [44] and in subsection 6.3 of [31], also see section 1.3. A new mathematical model proposed in these references allows the parameter ξ *in (4.63) to become infinitely small independently on the truncation pseudo frequency* $\overline{s}$*, also see discussion in the Introduction section 1.3. We point out that this mathematical model was verified on experimental data. Indeed, actually the derivatives* $\partial_{\overline{s}} V_{n,k}$ *instead of functions* $V_{n,k}$ *were used in the numerical implementation of [44], and this implementation was done prior experimental data were actually measured, see subsections 7.1 and 7.2 of [44]. It follows from (4.19) that one should expect that* $\left\|\partial_{\overline{s}} V_{n,k}\right\|_{C^2\left(\overline{\Omega}\right)} << \left\|V_{n,k}\right\|_{C^2\left(\overline{\Omega}\right)} = O\left(1/\overline{s}\right), \overline{s} \to \infty$*. Finally, we believe that, as in any applied problem, the independent verification on* blind *experimental data in [44] represents a valuable justification of this new mathematical model.*

2. In our definition "global convergence" means that, given the above new mathematical model, there is a rigorous guarantee that a good approximation for the exact solution can be obtained, regardless on the availability of a good first guess about this solution. Furthermore, such a global convergence analysis should be confirmed by numerical experiments. So, Theorem 4.2, complemented by our numerical results below, satisfies these requirements.

3. The assumption of the smallness of the parameter $\beta = \overline{s} - \underline{s}$ *is a natural one because equations (4.26) are actually generated by equation (4.20), which contains the nonlinearity in Volterra-like integrals. It is well known from the standard Ordinary Differential Equations course that solutions of nonlinear integral Volterra-like equations might have singularities on large intervals.*

Proof of Theorem 4.2: Denote $\widetilde{q}_{n,k} = q_{n,k} - q_n^*, \widetilde{V}_{n,k} = V_{n,k} - V^*$. By (4.63)

$$\left\|\widetilde{V}_{n,k}\right\|_{C^1\left(\overline{\Omega}\right)} \leq \xi. \tag{4.69}$$

This proof basically consists in estimating norms $\|\widetilde{q}_{n,k}\|_{H^i(\Omega_\varkappa)}$ from the above. Compared with proofs in [27, 31], the main difficulty here is that we have to analyze integral identities resulting from the QRM, instead of pointwise equations of [27, 31]. Hence, we use results of Theorem 4.1 here instead of the Schauder theorem of [27]. Recall that $(\cdot,\cdot)$ denotes the scalar product in $L_2(\Omega)$ and $[\cdot,\cdot]$ denotes the scalar product in $H^5(\Omega)$.

Since by (4.25) and (4.54) $q_0 \equiv q_0^* \equiv 0$, then (4.66) and (4.67) are true for $n = 0$. Assume that they are true for functions q_j with $j \leq n-1, n \geq 1$. Below we will prove them for $j := n$. Denote $Q_n^* = q_n^* - \Phi_n, Q_{n,k} = q_{n,k} - \Phi_n$. Below in this proof $v \in H^5(\Omega_n)$ is an arbitrary function satisfying (4.33). Let $G_{n,k}^*$ be the operator in the left hand side of (4.56). Let $H_{n,k}^*$ be the right hand side of (4.56). Substituting in (4.56) $q_n^* := Q_n^* + \Phi_n$, multiplying both sides by the function $G_{n,k}v$, integrating over Ω and then adding to both sides $\alpha[q_n^*, v]$, we obtain

$$\left(G_{n,k}^* Q_n^*, G_{n,k}v\right) + \alpha[Q_n^* + \Phi_n, v] = \left(H_{n,k}^* - G_{n,k}\Phi_n, G_{n,k}v\right) + \alpha[q_n^*, v]. \tag{4.70}$$

It follows from the proof of Lemma 4.3 that

$$(G_{n,k}Q_{n,k}, G_{n,k}v) + \alpha[Q_{n,k} + \Phi_n, v] = (H_{n,k} - G_{n,k}\Phi_n, G_{n,k}v). \tag{4.71}$$

Subtracting (4.70) from (4.71), we obtain

$$\left(G_{n,k}Q_{n,k} - G_{n,k}^* Q_n^*, G_{n,k}v\right) + \alpha[\widetilde{q}_{n,k}, v] = \left(H_{n,k} - H_{n,k}^*, G_{n,k}v\right) - \alpha[q_n^*, v], \tag{4.72}$$

Elementary calculations show that (4.72) is equivalent with

$$(G_{n,k}\widetilde{q}_{n,k}, G_{n,k}v) + \alpha[\widetilde{q}_{n,k}, v] = (P_{n,k}, G_{n,k}v) - \alpha[q_n^*, v]. \tag{4.73}$$

In addition, it follows from (4.60) that

$$\widetilde{q}_{n,k} \mid_{\Gamma_1} = \partial_z \widetilde{q}_{n,k} \mid_{\Gamma_1} = \partial_x \widetilde{q}_{n,k} \mid_{\Gamma_2} = \partial_x \widetilde{q}_{n,k} \mid_{\Gamma_3} = 0. \tag{4.74}$$

The function $P_{n,k}$ in (4.73) is

$$\begin{aligned} P_{n,k}(x) &= -A_{1,n}\left(h\sum_{j=1}^{n-1}\nabla\widetilde{q}_j - \widetilde{V}_{n,k}\right)\nabla q_n^* \\ &\quad -A_{2,n}\left(h\sum_{j=1}^{n-1}\nabla\widetilde{q}_j\right)\left(h\sum_{j=1}^{n-1}\left(\nabla q_j + \nabla q_j^*\right) - 2\nabla V_{n,k}\right) \\ &\quad +A_{2,n}\nabla\widetilde{V}_{n,k}\cdot\left(2h\sum_{j=1}^{n-1}\nabla q_j^* - \left(\nabla V_{n,k} + \nabla V^*\right)\right) - F_n. \end{aligned} \tag{4.75}$$

It follows from (4.63)-(4.65) as well as from (4.66) for $q_j, j \leq n-1$ that components of the vector function $a_{n,k}$ in the operator $G_{n,k}$ satisfy the corresponding condition of Theorem 4.1, $\left\|a_{n,k}^{(i)}\right\|_{C\left(\overline{\Omega}\right)} \leq 1, i = 1, 2$. Hence, Lemma 4.4 and Theorem 4.1, (4.52), (4.73) and (4.74) imply that

$$\left\|\widetilde{q}_{n,k}\right\|_{H^5(\Omega)} \leq \frac{\left\|P_{n,k}\right\|_{L_2(\Omega)}}{\sqrt{\alpha}} + C^*, \tag{4.76}$$

$$\left\|\widetilde{q}_{n,k}\right\|_{H^2(\Omega_\varkappa)} \leq C_1\frac{\left\|P_{n,k}\right\|_{L_2(\Omega)}}{\alpha^{b_1}} + \alpha^{b_2}C^*. \tag{4.77}$$

It follows from (4.76) and (4.77) that we now need to estimate the norm $\left\|P_{n,k}\right\|_{L_2(\Omega)}$ from the above. First, using (4.52), (4.59), (4.63), (4.64) as well as (4.66) and (4.67) for $q_j, j \leq n-1$, we obtain

$$\left\|-A_{1,n}\left(h\sum_{j=1}^{n-1}\nabla\widetilde{q}_j - V_{n,k}\right)\nabla q_n^*\right\|_{L_2(\Omega)} \leq 24\overline{s}^2\left(C^*\right)^2 C_1\beta. \tag{4.78}$$

Similarly we obtain

$$\left\| A_{2,n}\left(h\sum_{j=1}^{n-1}\nabla\widetilde{q}_j\right)\left(h\sum_{j=1}^{n-1}\left(\nabla q_j+\nabla q_j^*\right)-2\nabla V_{n,k}\right)\right\|_{L_2(\Omega)}\leq 80\overline{s}^2\left(C^*\right)^2C_1\beta. \quad (4.79)$$

Likewise,

$$\left\| A_{2,n}\nabla\widetilde{V}_{n,k}\cdot\left(2h\sum_{j=1}^{n-1}\nabla q_j^*-\left(\nabla V_{n,k}+\nabla V^*\right)\right)-F_n\right\|_{L_2(\Omega)}\leq 32\overline{s}^2C^*C_1\beta. \quad (4.80)$$

Summing up (4.78)-(4.80), we obtain $\|P_{n,k}\|_{L_2(\Omega)}\leq\left[136\overline{s}^2\left(C^*\right)^2C_1\right]\beta$. Hence, (4.65) implies that

$$\|P_{n,k}\|_{L_2(\Omega)}\leq\sqrt{\alpha}. \quad (4.81)$$

Hence, using (4.76), (4.77) and (4.81), we obtain

$$\|\widetilde{q}_{n,k}\|_{H^5(\Omega)}\leq 2C^*, \|\widetilde{q}_{n,k}\|_{H^2(\Omega_\varkappa)}\leq 2C^*\alpha^{b_2}. \quad (4.82)$$

The second inequality (4.82) proves (4.67). To prove (4.66), we use the first inequality (4.82) in $\|q_{n,k}\|_{H^5(\Omega)}\leq\|\widetilde{q}_{n,k}\|_{H^5(\Omega)}+\|q_n^*\|_{H^5(\Omega)}\leq 3C^*$. As soon as (4.66) and (4.67) are established, the proof of the first inequality (4.68) is straightforward. To do so, one needs to subtract (4.50) from (4.28) and then use (4.62), (4.66), (4.67), (4.27) and (4.54) in a straightforward manner. The second inequality (4.68) follows from (4.3) and the smallness condition imposed on the number α_0. □

4.6 A Simplified Mathematical Model of Imaging of Antipersonnel Plastics Land Mines

The first main simplification of our model is that we consider the 2-D instead of the 3-D case. Second, we ignore the air/ground interface, assuming that the governing PDE is valid on the entire 2-D plane. The third simplification is that we consider a plane wave instead of the point source in (4.1). This is because our current computer

code is designed only for the plane wave. As it is always the case of sophisticated computer codes, it takes quite an effort to re-design it for the case of a point source and this work is currently underway. The point source was considered above only for the convenience of analytical derivations due to Lemma 4.1.

Let the ground be $\{\mathbf{x} = (x, z) : z > 0\} \subset \mathbb{R}^2$. Suppose that a polarized electric field is generated by a plane wave, which is initialized at the point $(0, z^0), z^0 = -0.2 < 0$ at the moment of time $t = 0$. The following hyperbolic equation can be derived from Maxwell equations [32]

$$\varepsilon_r(\mathbf{x}) u_{tt} = \Delta u, \ (\mathbf{x}, t) \in \mathbb{R}^2 \times (0, \infty), \tag{4.83}$$

$$u(\mathbf{x}, 0) = 0, \ u_t(\mathbf{x}, 0) = \delta\left(z - z^0\right), \tag{4.84}$$

where the function $u(\mathbf{x}, t)$ is a component of the electric field. Recall that $\varepsilon_r(\mathbf{x})$ is the spatially distributed dielectric constant, see the beginning of section 4.1. We assume that the function $\varepsilon_r(\mathbf{x})$ satisfies the same conditions (4.3), (4.4) as the function $c(\mathbf{x})$. The Laplace transform (4.5) leads to the following analog of the problem (4.6), (4.7)

$$\Delta w - s^2 \varepsilon_r(\mathbf{x}) w = -\delta\left(z - z^0\right), \forall s \geq \underline{s}, \tag{4.85}$$

$$\lim_{|\mathbf{x}| \to \infty} (w - w_0)(\mathbf{x}, s) = 0, \forall s \geq \underline{s}, \tag{4.86}$$

where $w_0(z, s) = \exp(-s|z - z_0|)/(2s)$ is such a solution of equation (4.85) for the case $\varepsilon_r(\mathbf{x}) \equiv 1$ that $\lim_{|z| \to \infty} w_0(z, s) = 0$.

It is well known that the maximal depth of an antipersonnel land mine does not exceed about 10 cm=0.1 m. So, we model these mines as small squares with the 0.1 m length of sides, and their centers should be at the maximal depth of 0.1 m. We set $\Omega = \{\mathbf{x} = (x, z) \in (-0.3m, 0.3m) \times (0m, 0.6m)\}$. Consider dimensionless variables $\mathbf{x}' = \mathbf{x}/0.1, z^{0\prime} = z^0/0.1$. For brevity we keep the same notations both for

these variables and the new domain Ω,

$$\Omega = (-3,3) \times (0,6)\,. \tag{4.87}$$

We now use the values of the dielectric constant given at http://www.clippercontrols.com. Hence, $\varepsilon_r = 5$ in the dry sand and $\varepsilon_r = 22$ in the trinitrotoluene (TNT). We also take $\varepsilon_r = 2.5$ in a piece of wood submersed in the ground. Hence,

$$\frac{\varepsilon_r\,(\text{TNT})}{\varepsilon_r\,(\text{dry sand})} = \frac{22}{5} \approx 4.$$

Since the dry sand should be considered as a background outside of our domain of interest Ω, we introduce parameters $\varepsilon_r' = \varepsilon_r/5, s' = s \cdot 0.1 \cdot \sqrt{5}$, and again do not change notations. Then relations (4.85) and (4.86) are valid. Hence, we now can assume that the following values of this scaled dielectric constant

$$\varepsilon_r\,(\text{dry sand}) = 1, \varepsilon_r\,(\text{TNT}) = 4, \varepsilon_r\,(\text{piece of wood}) = 0.5. \tag{4.88}$$

In addition, centers of small squares modeling our targets should be in the rectangle

$$\{\mathbf{x} = (x,z) \in [-2.5,2.5] \times [0.5,1.0]\}\,. \tag{4.89}$$

The side of each of our small square should be 1, i.e. 10 cm. The interval $[0.5,1.0]$ in (4.89) corresponds to depths of centers between 5 cm and 10 cm and the interval $[-2.5,2.5]$ means that any such square is fully inside of Ω. Hence, an accurate image of the location of that small square as well as of the value of the coefficient $\varepsilon_r\,(\mathbf{x})$ both inside and outside of it would provide a useful information about the possible presence of a land mine and also might help to differentiate between mines and non-mines.

4.7 Numerical Studies

In this chapter we work only with the computationally simulated data. The data are generated by solving numerically equation (4.85) in the rectangle $R = [-4, 4] \times [-2, 8]$. By (4.87) $\Omega \subset R$. To avoid the singularity in $\delta(z - z^0)$, we actually solve in R the equation for the function $\widetilde{w} = w - w_0$ with zero Dirichlet boundary condition for this function, see (4.86). We solve the resulting Dirichlet boundary value problem via the FDM with the uniform mesh size $h_f = 0.0675$.

It is quite often the case in numerical studies, one should slightly modify the numerical scheme given by the theory, and so we did the same. Indeed, it is well known in computations that numerical results are usually more optimistic than analytical ones. We have modified our above algorithm via considering the function $\widetilde{v} = s^{-2} \cdot \ln(w/w_0)$. In other words, we have divided our solution w of the problem (4.85), (4.86) by the initializing plane wave w_0. This has resulted in an insignificant modification of equations (4.26). We have observed in our computations that the function w/w_0 at the measurement part $\Gamma_1 \subset \partial\Omega$ is poorly sensitive to the presence of abnormalities, as long as $s > 1.2$, see Figure 1-b). Hence, one should expect that the modified tail function for the function $\widetilde{v}$ should be small for $s > 1.2$, which is exactly what is required by the above theory. For this reason, we have chosen the truncation pseudo frequency $\overline{s} = 1.2$ and the initial tail function $V_{1,1} \equiv 0$.

4.7.1 Some details of the numerical implementation of the globally convergent method

We have generated the data for $s \in [0.5, 1.2]$ with the grid step size $h = 0.1$ in the s direction. Since the grid step size in the s-direction is $h = 0.1$ for $s \in [0.5, 1.2]$, then $\beta = 0.7$ and $N = 7$. Also, we took the number of iterations with respect to the tail $m_1 = m_2 = ... = m_N := m = 10$, since we have numerically observed the stabilization of functions $q_{n,k}, \varepsilon_r^{(n,k)}, V_{n,k}$ at $k = 10$, also, see section 4.3. In our computations we have relaxed the smoothness assumption in the QRM via taking in (4.32) the H^2-norm instead of the H^5-norm, see the first part of Remark 4.3.

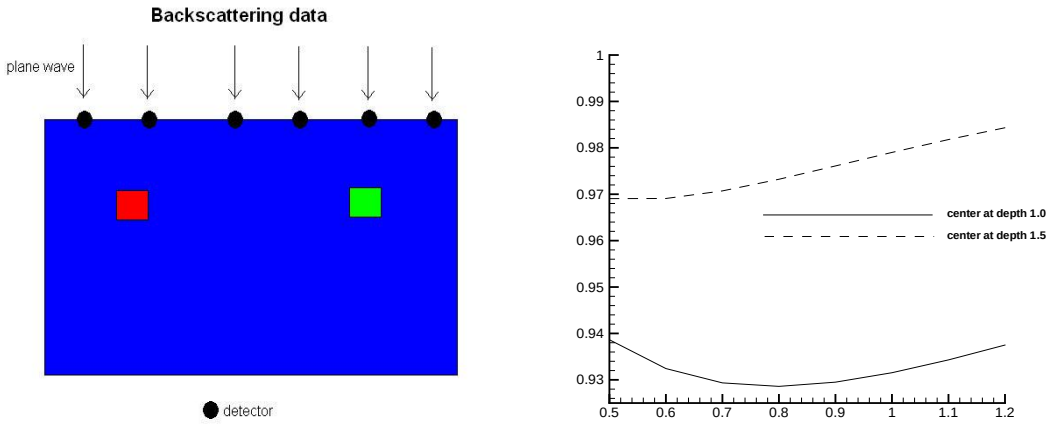

(a) (b)

Figure 4.1: (a) The schematic diagram of our data collection. The plane wave falls from the top and backscattering data are collected at the top side of this rectangle. (b) The "sensitivity" function $f(s) = w(0,0,s)/w_0(0,s)$, $s \in [0.5, 1.2]$ for two different centers $(0,1)$ and $(0,1.5)$ of mine-like targets, which correspond to 10 cm and 15 cm depths respectively.

Based on the experience of some earlier works on the QRM [4, 35] for linear ill-posed Cauchy problems, we have implemented the QRM via the FDM. Indeed, the FDM has allowed in [35] to image sharp peaks. On the other hand, the FEM of [4] did not let to image such peaks. So, we have written both terms under signs of norms of (4.32) in the FDM form. Next, to minimize the functional (4.32), we have used the conjugate gradient method. It is important that the derivatives with respect to the values of the unknown function at grid points should be calculated explicitly. This was done using the Kronecker symbol, see details in [35]. As soon as discrete values $\widetilde{\varepsilon}_r^{(n,k)}$ were computed, we have averaged each such value at the point (x_i, z_j) over nine (9) neighboring grid points, including the point (x_i, z_j) : to decrease the reconstruction error. The resulting discrete function was taken as $\varepsilon_r^{(n,k)}$.

We have used the 49×49 mesh in Ω. However, an attempt to use a finer 98×98 mesh led to a poor quality results. Most likely this is because the dimension of our above mentioned finite dimensional space was becoming too large, thus making it

"almost" infinitely dimensional, which would require to use in (4.32) the H^5-norm instead of the H^2-norm, see the first part of Remark 4.3. The regularization parameter in (4.32) was taken $\alpha = 0.04$.

We have made several sweeps over the interval $s \in [0.5, 1.2]$ as follows. Suppose that on the first s-sweep we have computed the discrete function $\varepsilon_r^{(1)}(\mathbf{x}) := \varepsilon_r^{(N,10)}(\mathbf{x})$, which corresponds to the last s-subinterval $[s_N, s_{N-1}] = [0.5, 0.6]$. Hence, we have also computed the corresponding discrete tail function $V^{(1)}(\mathbf{x})$. Next, we return to the first $s-$interval $[s_1, \overline{s}] = [1.1, 1.2]$, set $V_{1,1}^{(2)}(\mathbf{x}) := V^{(1)}(\mathbf{x})$ and repeat the algorithm of section 4.3. We kept repeating these $s-$sweeps p times until either the stabilization has was observed, i.e.

$$\|\varepsilon_r^{(p)} - \varepsilon_r^{(p-1)}\| \leq 10^{-5} \tag{4.90}$$

or an "explosion" of the gradient of the functional $J_{n,k}^{\alpha}$ on the sweep number p took place. "Explosion" means that

$$\|\nabla J_{n,k}^{\alpha}(q_{n,k}^{(p)})\| \geq 10^5, \tag{4.91}$$

for any appropriate values of indices n, k. Here and below $\|\cdot\|$ is the discrete $L_2(\Omega)-$norm. The stopping criterion (4.91) corresponds well with one of backbone principles of the theory of ill-posed problems. According to this principle, the iteration number can serve as one of regularization parameters, see pages 156 and 157 of [34].

Suppose that either (4.90) or (4.91) takes place. Then we work with the function $\varepsilon_r^{(p)}$. First, as it is usually done in imaging, we apply a truncation procedure. In this procedure we truncate to unity 85% of the $\max\left|\varepsilon_r^{(p)}(\mathbf{x})\right|$, see Figure 2. If we have several local maxima of $\left|\varepsilon_r^{(p)}(\mathbf{x})\right|$, then we apply the truncation procedure as follows. Let $\{\mathbf{x}_i\}_{i=1}^r \subset \Omega$ be points where those local maxima are achieved, and values of those maxima are respectively $\{a_i\}_{i=1}^r$. Consider certain circles $\{B(\mathbf{x}_i)\}_{i=1}^r \subset \Omega$ with the centers at points $\{\mathbf{x}_i\}_{i=1}^r$ and such that $\overline{B}(\mathbf{x}_i) \cap \overline{B}(\mathbf{x}_j) = \varnothing$ for $i \neq j$. In each circle

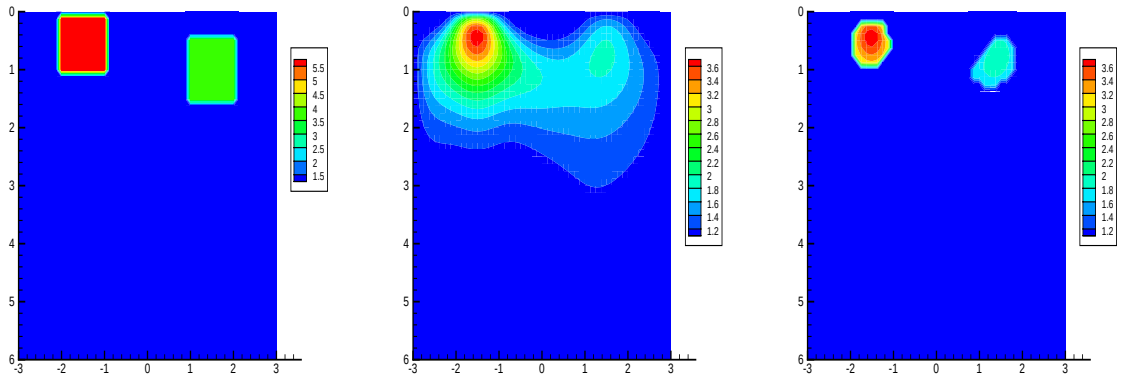

(a) (b) (c)

Figure 4.2: A typical example of the image resulting from the globally convergent stage. The rectangle is the domain Ω. This is the image of Test 4.1 (subsection 4.7.3). (a) The correct coefficient. Inclusions are two squares with the same size $d = 1$ of their sides, which corresponds to 10 cm in real dimensions. In the left square $\varepsilon_r = 6$, in the right one $\varepsilon_r = 4$and $\varepsilon_r = 1$ everywhere else, see (4.87) and (4.88). However, we do not assume knowledge of $\varepsilon_r(\mathbf{x})$ in Ω. Centers of these squares are at $(x_1^*, z_1^*) = (-1.5, 0.6)$ and $(x_2^*, z_2^*) = (1.5, 1.0)$. (b) The computed coefficient before truncation. Locations of targets are judged by two local maxima. So, locations are imaged accurately. However, the error of the computed values of the coefficient ε_r in them is about 40%. (c) The image of (b) after the truncation procedure, see the text.

$B(\mathbf{x}_i)$ set

$$\widetilde{\varepsilon}_r^{(p)}(\mathbf{x}) := \begin{cases} \varepsilon_r^{(p)}(\mathbf{x}) \text{ if } \left|\varepsilon_r^{(p)}(\mathbf{x})\right| \geq 0.85 a_i \\ 1, \text{ otherwise.} \end{cases}$$

Next, for all points $\mathbf{x} \in \Omega \setminus \cup_{i=1}^r B(\mathbf{x}_i)$, we set $\widetilde{\varepsilon}_r^{(p)}(\mathbf{x}) := 1$. As a result, we have obtained the truncated function $\widetilde{\varepsilon}_r^{(p)}(\mathbf{x})$. Finally we set $\varepsilon_r^{glob}(\mathbf{x}) := \widetilde{\varepsilon}_r^{(p)}(\mathbf{x})$ and go to Stage 2.

4.7.2 The second stage of our two-stage numerical procedure: a modified gradient method

Recall that this method is used on the second stage of our two-stage numerical procedure. Since this method is secondary to us and since we want to save space, we derive a modified gradient method only briefly here. A complete, although space

consuming derivation, including the rigorous derivation of Frechét derivatives, can be done using the framework developed in [40, 41]. We call our technique the "modified gradient method" because rather than following usual steps of the gradient method, we find zero of the Fréchet derivative of the Tikhonov functional via solving an equation with a contractual mapping operator.

Consider a wider rectangle $\Omega' \supset \Omega$, where $\Omega' = (-4, 4) \times (0, 6)$. We assume that both Dirichlet φ_0 and Neumann φ_1 boundary conditions are given on a wider interval $\Gamma_1' = \{z = 0\} \cap \overline{\Omega}'$, $\Gamma_1 \subset\subset \Gamma_1'$, i.e. similarly with (4.13)

$$\widetilde{w}(\mathbf{x}, s)|_{\Gamma_1'} = \widetilde{\varphi}_0(x, s), \tag{4.92}$$

$$\widetilde{w}_z(\mathbf{x}, s)|_{\Gamma_1'} = \widetilde{\varphi}_1(x, s) + e^{-s|z_0|}. \tag{4.93}$$

Also, we have observed in our computations that $\lim_{|\mathbf{x}|\to\infty} |\nabla \widetilde{w}(\mathbf{x}, s)| = 0$. Hence, we use

$$\partial_n \widetilde{w}_x \,|_{\partial\Omega' \setminus \Gamma_1'} = 0. \tag{4.94}$$

In addition, by (4.85)

$$\Delta \widetilde{w} - s^2 \varepsilon_r(\mathbf{x}) \widetilde{w} - s^2(\varepsilon_r(\mathbf{x}) - 1) w_0(z, s) = 0, \text{ in } \Omega'. \tag{4.95}$$

So, we now consider the solution of the boundary value problem (4.93)-(4.95), keeping the same notation. We want to find such a coefficient $\varepsilon_r(\mathbf{x})$, which would minimize the following Tikhonov functional

$$\begin{aligned} T(\varepsilon_r) &= \frac{1}{2} \int_a^b \int_{\Gamma_1'} (\widetilde{w}(x, 0, s) - \widetilde{\varphi}_0(x, s))^2 dx ds + \frac{\theta}{2} \left\| \varepsilon_r - \varepsilon_r^{glob} \right\|^2_{L_2(\Omega)} \\ &+ \int_a^b \int_{\Omega'} \lambda [\Delta \widetilde{w} - s^2 \varepsilon_r(\mathbf{x}) \widetilde{w} - s^2(\varepsilon_r(\mathbf{x}) - 1) w_0(z, s)] d\mathbf{x} ds, \end{aligned} \tag{4.96}$$

where $\theta > 0$ is the regularization parameter and $\lambda(\mathbf{x}, s)$ is the solution of the so-called "adjoint problem",

$$\begin{aligned} \Delta\lambda - s^2\varepsilon_r(\mathbf{x})\lambda &= 0, \text{ in } \Omega', & (4.97)\\ \lambda_z(x,0,s) &= \widetilde{w}(x,0,s) - \varphi_0(x,s),\ \partial_n\lambda|_{\partial\Omega'\setminus\Gamma_1'} = 0. & (4.98) \end{aligned}$$

If the coefficient $\varepsilon_r(\mathbf{x})$ is such that, in addition to (4.93)-(4.95), (4.92) is true, then $T(\varepsilon_r) = 0$, i.e. this coefficient provides the minimum value for the functional T. Because of (4.97), the second line in (4.96) equals zero. Although boundary value problems (4.93)-(4.95) and (4.97), (4.98) are considered in the domain Ω' with a non-smooth boundary, a discussion about existence of their solutions is outside of the scope of this chapter. We have always observed existence of numerical solutions with no singularities in our computations. Although, by the Tikhonov theory, one should consider a stronger H^k-norm of $\varepsilon_r - \varepsilon_r^{glob}$ in (4.96) [46], we have found in our computations that the simpler L_2-norm is sufficient. This is likely because we have worked computationally worked with not too many grid points. Using the framework of [40, 41], one can derive the following expression for the Fréchet derivative $T'(\varepsilon_r)$ of the functional T

$$T'(\varepsilon_r)(\mathbf{x}) = \theta\left(\varepsilon_r - \varepsilon_r^{glob}\right)(\mathbf{x}) - \int_a^b s^2\left[\lambda(\widetilde{w} + w_0)\right](\mathbf{x}, s)\, ds, \mathbf{x} \in \Omega.$$

Hence, to find a minimizer, one should solve the equation $T'(\varepsilon_r) = 0$. We solve it iteratively as follows

$$\varepsilon_r^n(\mathbf{x}) = \varepsilon_r^{glob}(\mathbf{x}) + \frac{1}{\theta}\int_a^b s^2\left[\lambda(\widetilde{w} + w_0)\right](\mathbf{x}, s, \varepsilon_r^{n-1})ds, \mathbf{x} \in \Omega, \quad (4.99)$$

where functions $\widetilde{w}(\mathbf{x}, s, \varepsilon_r^{n-1})$ and $\lambda(\mathbf{x}, s, \varepsilon_r^{n-1})$ are solutions of problems (4.93)-(4.95) and (4.97), (4.98) respectively with $\varepsilon_r(\mathbf{x}) := \varepsilon_r^{n-1}(\mathbf{x})$. One can easily prove that one can choose the number $(b-a)/\theta$ so small that the operator in (4.99) is contractual mapping. We have worked with such an operator in our computations. We have iterated in (4.99) until the stabilization has occurred, i.e. we have stopped iterations as soon as $\|\varepsilon_r^n - \varepsilon_r^{n-1}\|/\|\varepsilon_r^{n-1}\| \leq 10^{-5}$, where $\|\cdot\|$ is the discrete $L_2(\Omega)$ norm. Then we set that our computed solution is $\varepsilon_r^n(\mathbf{x})$. In our computations we took $a = 0.01, b = 0.05, \theta = 0.15$.

4.7.3 Numerical results

In our numerical tests we have introduced the multiplicative random noise in the boundary data using the following expression

$$w_\sigma(x_i, 0, s_j) = w(x_i, 0, s_j)[1 + \varsigma\sigma], \ i = 0, ..., M; \ , j = 1, .., N,$$

where $w(x_i, 0, s_j)$ is the value of the computationally simulated function w at the grid point $(x_i, 0) \in \Gamma_1'$ and at the value $s := s_j$ of the pseudo frequency, ς is a random number in the interval $[-1; 1]$ with the uniform distribution, and $\sigma = 0.05$ is the noise level. Hence, the random error is presented only in Dirichlet data but not in Neumann data.

Test 4.1. We test our numerical method for the case of two squares with the same size $d = 1$ of their sides. In the left square $\varepsilon_r = 6$, in the right one $\varepsilon_r = 4$ and $\varepsilon_r = 1$ everywhere else, see (4.88). Centers of these squares are at $(x_1^*, z_1^*) = (-1.5, 0.6)$ and $(x_2^*, z_2^*) = (1.5, 1.0)$. However, we do not assume *a priori* in our algorithm neither the presence of these squares nor a knowledge of $\varepsilon_r(\mathbf{x})$ at any point of the rectangle Ω. See Figure 2 for the globally convergent stage and Figure 3 for the final result.

Test 4.2. Consider now the case of imaging of a piece of wood, see (4.88). So, now our target is a square with the $d = 1$ size of its side. Inside of this square $\varepsilon_r = 0.5 < 1$

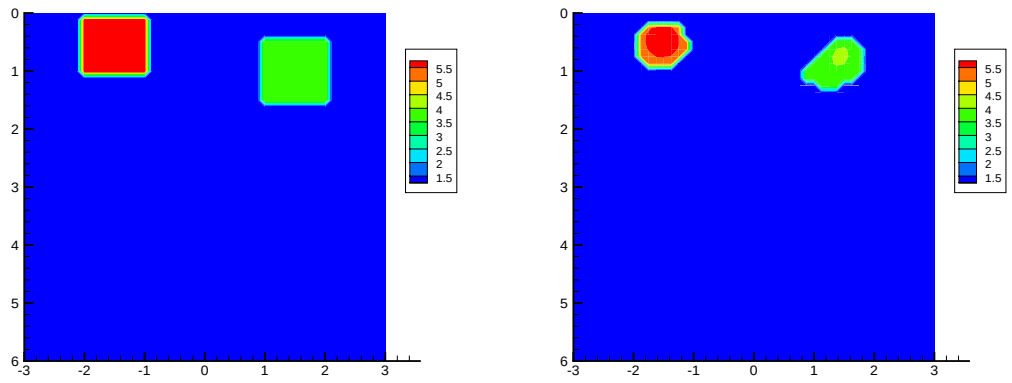

(a) (b)

Figure 4.3: Test 4.1. The image obtained on the globally convergent stage is displayed on Figure 4.2(c). (a) The correct image. Centers of small squares are at $(x_1^*, z_1^*) = (-1.5, 0.6)$ and $(x_2^*, z_2^*) = (1.5, 1.0)$ and values of the target coefficient are $\varepsilon_r = 6$ in the left square, $\varepsilon_r = 4$ in the right square and $\varepsilon_r = 1$ everywhere else. (b) The imaged coefficient $\varepsilon_r(\mathbf{x})$ resulting of our two-stage numerical procedure. Both locations of centers of targets and values of $\varepsilon_r(x)$ at those centers are imaged accurately. We have not used truncation on the second stage.

and $\varepsilon_r = 1$ outside. Figure 4 displays both this square and the reconstruction result.

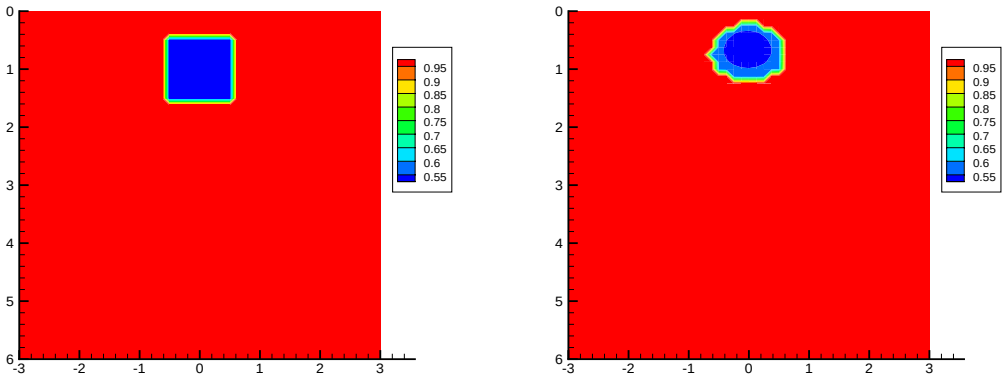

(a) (b)

Figure 4.4: Test 4.2. Imaging of a wooden-like targets: small square with the length of its side $d = 1$, see (a). Inside of this small square $\varepsilon_r = 0.5$ and $\varepsilon_r = 1$ outside of it.However, neither the presence of the small square nor the value of the unknown coefficient $\varepsilon_r(x)$ at any point of this rectangle Ω are not assumed to be known a priori in our algorithm. (b) The image computed after the two-stage numerical procedure. Location of the center of the small square and the value of $\varepsilon_r = 0.5$ at that center are imaged accurately. The value $\varepsilon_r = 1$ outside of the imaged small square is also accurately imaged.

REFERENCES

[1] M. Agranovsky and P. Kuchment, *Uniqueness of reconstruction and an inversion procedure for thermoacoustic tomography with variable sound speed*, *Inverse Problems*, 23, pp. 2089–2102, 2007.

[2] L. Bourgeois, *A mixed formulation of quasi-reversibility to solve the Cauchy problem for Laplace's equation*, *Inverse Problems*, 21, pp. 1087–1104, 2005.

[3] L. Bourgeois, *Convergence rates for the quasi-reversibility method to solve the Cauchy problem for Laplace's equation*, *Inverse Problems*, 22, pp. 413–430, 2006.

[4] C. Clason and M.V. Klibanov, *The quasi-reversibility method for thermoacoustic tomography in a heterogeneous medium*, *SIAM Journal on Scientific Computing*, 30, pp. 1–23, 2007.

[5] D. Finch, S. Patch and Rakesh, *Determining a function from its mean values over a family of spheres*, *SIAM Journal on Mathematical Analysis*, 35, pp. 1213–1240, 2004.

[6] V. Isakov, *Inverse Problems for Partial Differential Equations*, *Springer*, 2006.

[7] S.I. Kabanikhin and M.A. Bektemesov and D.V. Nechaev, *Numerical solution of the 2D thermoacoustic problem*, *Journal of Inverse and Ill-posed Problems*, 13, pp. 265–276, 2006.

[8] M.V. Klibanov and P.G. Danilaev, *On the solution of coefficient inverse problems by the method of quasi-inversion*, *Soviet Math. Doklady*, 41, pp. 83–87, 1990.

[9] M.V. Klibanov and P.G. Danilaev, *Estimates of initial conditions of parabolic equations and inequalities via lateral Cauchy data*, *Inverse problems*, 22, pp. 495–514, 2006.

[10] M.V. Klibanov and F. Santosa, *A computational quasi-reversibility method for Cauchy problems for Laplace's equation*, *SIAM Journal on Applied Mathematics*, 31, pp. 1653–1675, 1991.

[11] M. Kazemi and M.V. Klibanov, *Stability estimates for ill-posed problems involving hyperboilc equations and inequalities*, *SIAM Journal on Applied Mathematics*, 50, pp. 93–102, 1993.

[12] M.V. Klibanov and J. Malinsky, *Newton-Kantorovich method for 3-dimensional inverse scattering problem and stability of the hyperbolic Cauchy problem with time dependent data*, *Inverse Problems*, 7, pp. 577–595, 1991.

[13] M.V. Klibanov and Rakesh, *Numerical solution of a timelike Cauchy problem for the wave equation*, *Mathematical Methods in the Applied Sciences*, 15, pp. 559–570, 1992.

[14] M. V. Klibanov and A. Timonov, *Carleman Estimates for Coefficient Inverse Problems and Numerical Applications*, *VSP*, 2004.

[15] M.V. Klibanov, *Lipschitz stability for hyperbolic inequalities in octants with the lateral Cauchy data and refocusing in time reversal*, *Journal of Inverse and Ill-posed Problems*, 13, pp. 353–363, 2005.

[16] M.V. Klibanov, S.I. Kabanikhin and D.V. Nechaev, *Numerical solution of the problem of computational time reversal in a quadrant*, *Waves in Random and Complex Media*, 16, pp. 473–494, 2006.

[17] P. Kuchment and L. Kunyansky, *Mathematics of thermoacoustic tomography*, available at arXiv: 0704.0286v2, 2007.

[18] L. Kunyansky, *Explicit inversion formulae for the spherical mean Radon transform*, *Inverse Problems*, 23, pp. 373–383, 2007.

[19] M.M. Lavrent'ev, V.G. Romanov and S.P. Shishatskii, *Ill-Posed Problems of Mathematicl Physics and Analysis*, *AMS*, 1986.

[20] R. Lattes and J.-L. Lions, *The Method of Quasi-Reversibility. Applications to Partial Differential Equations*, *American Elsevier Publishing Co. Inc.*, 1969.

[21] Lop Fat Ho, *Observabilit'e frontier'e de l'equation des ondes*, *C.R. Acad. Sci. Paris*, 302, pp. 443–446, 1986.

[22] V.G. Romanov, *Integral Geometry and Inverse Problems for Hyperbolic Equations*, *Springer*, 1974.

[23] V.G. Romanov, *Carleman estimates for second order hyperbolic equations*, *Siberian Mathematical Journal*, 47, pp. 135–151, 2006.

[24] V.G. Romanov, *Stability estimates in inverse problems for hyperbolic equations*, *Milan Journal of Mathematics*, 74, pp. 357–385, 2006.

[25] R. Triggiani and P.F. Yao, *Carleman estimates with no lower order terms for general Riemann wave equations. Global uniqueness and observability in one shot*, *Applied Mathematics and Optimization*, 46, pp. 334–375, 2002.

[26] M. Xu, D. Feng, and L.V. Wang, *Time-domain reconstruction algorithms and numerical simulations for thermoacoustic tomography in various geometries*, *IEEE Trans. Biomed. Eng.*, 50, pp. 1086–1099, 2003.

[27] L. Beilina and M. V. Klibanov, *A globally convergent numerical method for a coefficient inverse problem*, *SIAM Journal on Scientific Computing*, 31, pp. 478–509, 2008.

[28] L. Beilina and M. V. Klibanov, *A globally convergent numerical method and the adaptivity technique for a hyperbolic coefficient inverse problem, Part I: analytical study*, available on-line at http://www.ma.utexas.edu/mp_arc/, 2009.

[29] L. Beilina and M. V. Klibanov, *A globally convergent numerical method and the adaptivity technique for a hyperbolic coefficient inverse problem, Part II: numerical studies*, available on-line at http://www.ma.utexas.edu/mp_arc/, 2009.

[30] L. Beilina and M. V. Klibanov, *Synthesis of global convergence and adaptivity for a hyperbolic coefficient inverse problem in 3D*, *Journal of Inverse and Ill-posed Problems*, 18, pp. 85–132, 2010.

[31] L. Beilina and M. V. Klibanov, *Synthesis of global convergence and adaptivity for a hyperbolic coefficient inverse problem in 3D*, *Journal of Inverse and Ill-posed Problems*, 18, pp. 85–132, 2010.

[32] M. Cheney and D. Isaacson, *Inverse problems for a perturbed dissipative half-space*, *Inverse Problems*, 11, pp. 865–888, 1995.

[33] P. G. Danilaev, *Coefficient Inverse Problems for Parabolic Type Equations and Their Applications*, *Inverse and Ill-Posed Problems Series*, 2001.

[34] H.W. Engl, M. Hanke and A. Neubauer, *Regularization of Inverse Problems*, *Kluwer Academic Publishers*, 2000.

[35] M.V. Klibanov, A.V. Kuzhuget, S.I. Kabanikhin and D.V. Nechaev, *A new version of the quasi-reversibility method for the thermoacoustic tomography and a coefficient inverse problem*, *Applicable Analysis*, 87, pp. 1227–1254, 2008.

[36] P. Sacks and F. Santosa, *A simple computational scheme for determining the sound speed of an acoustic medium from its surface impulse response*, *SIAM Journal on Scientific and Statistical Computing*, 8, pp. 501–520, 1987.

[37] M. Tadi and M. V. Klibanov and W. Cai, *An inversion method for parabolic equations based on quasireversibility*, *Computers and Mathematics with Applications*, 43, pp. 927–941, 2002.

[38] A.N. Tikhonov and V.Y. Arsenin, *Solutions of Ill-Posed Problems*, *Vh Winston*, 1977.

[39] J. Xin and M.V. Klibanov, *Numerical solution of an inverse problem of imaging of antipersonnel land mines by the globally convergent convexification algorithm*, *SIAM Journal on Scientific Computing*, 30, pp. 3170–3196, 2008.

[40] L. Beilina and M. V. Klibanov, *A posteriori error estimates for the adaptivity technique for the Tikhonov functional and global convergence for a coefficient inverse problem*, *Inverse Problems*, 26, 2010.

[41] L. Beilina and M. V. Klibanov and M.Yu. Kokurin, *Adaptivity with relaxation for ill-posed problems and global convergence for a coefficient inverse problem*, *Journal of Mathematical Sciences*, 167, pp. 279–325, 2010.

[42] B.A. Dubrovin, S.P. Novikov and A.T. Fomenko, *Modern Geometry Methods and Applications*, *Springer-Verlag*, 1985.

[43] D. Gilbarg and N.S. Trudinger, *Elliptic Partial Differential Equations of Second Order*, *Springer-Verlag*, 1983.

[44] M.V. Klibanov and M.A Fiddy and L. Beilina and N. Pantong and J. Schenk, *Picosecond scale experimental verification of a globally convergent algorithm for a coefficient inverse problem*, *Inverse Problems*, 26, 2010.

[45] V.G. Romanov and M. Yamamoto, *Recovering a Lam'e kernel in a viscoelastiv equation by a single boundary measurement*, *Applicable Analysis*, 89, pp. 377–390, 2010.

[46] A.N. Tikhonov, A.V. Goncharsky, V.V. Stepanov and A.G.Yagola, *Recovering a Lam'e kernel in a viscoelastiv equation by a single boundary measurement*, *Kluwer Academic Publishers*, 1995.

[47] M. Haltmeier, O. Scherzer, P. Burgholzer and G. Paltauf, *Thermoacoustic computed tomography with large planar receivers*, *Inverse Problems*, 20, pp. 1663–1673, 2004.

[48] A.V. Kuzhuget, M.V. Klibanov, *Global convergence for a 1-D inverse problem with application to imaging of land mines*, *Applicable Analysis*, 89, pp. 125–157, 2010.

[49] A.V. Kuzhuget, M.V. Klibanov, L.Beilina, V.G. Romanov, *Global convergence and quasireversibility for a coefficient inverse problem with backscattering data*, submitted for publication to SIAM Journal on Mathematical Analysis.